One-dimensional two-phase analytical models applied to closed-loop reservoir management

By

A. van Harmelen

in partial fulfillment of the requirements for the degree of

Master of Science
in Applied Mathematics

at the faculty of EEMCS of Delft University of Technology,
to be defended publicly on September 9th 2016.

Student number:	1512315	
Supervisor:	Prof. dr. ir. J.D. Jansen,	TU Delft
Thesis committee:	Prof. dr. ir. A.W. Heemink,	TU Delft
	Dr. J.L.A. Dubbeldam,	TU Delft

TU Delft Delft University of Technology

Abstract

Reservoir characteristics such as size and permeability are often non-trivial, which is why sophisticated yet often time-intensive numerical models are commonly used in the Closed-Loop Reservoir Management of subsurface reservoirs in order to maximize profit from oil production. For certain reservoirs, however, simple analytical models can accurately compete with such numerical models at lower computational efforts. Analytical linear and radial displacement models as well as various pressure models are derived and combined in this thesis, and are shown to be accurate approximations of one- and two-dimensional two-phase flow in a multi-layered, rectangular, and horizontal reservoir. Assuming among other that each layer is operated by a single injector-producer pair as well as that each layer is homogeneous and isolated from other layers, simplifies the equations and prevents cross-layer flow. If cross-layer flow does occur, however, then the considered analytical models are unable to accurately describe the reservoir flow.

Acknowledgments

This master thesis project has been an eventful and interesting time to say the least and I look back with joy on the time spent, but without certain people it wouldn't have been possible.

First and foremost, I would like to thank Prof. dr. ir. Jan-Dirk Jansen and Prof. dr. ir. Arnold Heemink for supervising me and for making this project available to me. Moreover, their critical thinking, eye for detail, practicality, enthusiasm and patience have been invaluable to me. Also their willingness to let me pause my thesis such that I could go to America for a research internship was greatly appreciated. Additionally, I would like to thank dr. Johan Dubbeldam for being part of the graduation committee.

Second, I would like to thank my immediate family for supporting me during this graduation project. A special thanks goes to my parents as their unending support, trust and believe in me made my entire education so far not only possible, but also easier and enjoyable.

Last but not least, I am also grateful to my close friends and fellow students for reminding me to take some time off every now and then, as well as for discussing my progress from time to time and putting everything in perspective.

Arnaud van Harmelen
September 9th, 2016, Delft

Contents

List of Figures

List of Tables

List of Abbreviations

BoReP	- pressure model for two-phase flow in a bounded reservoir
CLRM	- Closed-Loop Reservoir Management
Li-BoReP	- model combining Linear displacement model with BoReP pressure description
NPV	- Net Present Value: today's value of future money
RaLiRa	- displacement model consisting of Radial-Linear-Radial flow regimes consecutively
RaLiRa-BoReP	- model combining RaLiRa displacement and BoReP pressure description
RelPerm	- relative permeability

1 Introduction

When a production well in a reservoir can no longer produce sufficient amounts of oil on its own because the subsurface pressure is too low to push oil to the surface, a phase such as liquid water can be injected into the reservoir by means of an injector well. The idea behind this part of the oil production process, known as secondary recovery, is that the injected phase increases the reservoir pressure such that the oil production rates increase and more oil is extracted from the reservoir.

Although secondary recovery leads to an increased amount of produced oil and, more importantly, to more profit, injecting a phase such as liquid water into a reservoir also costs money. Moreover, at some point in the life span of the reservoir, the injected water will reach the producer well and be produced alongside oil and thus slow the increase of profit over time. Consequently, maximizing profit is not simply achieved by injecting as much water as required to replace all the oil in the reservoir with water. The amount of water produced alongside the oil will additionally increase over time, resulting in a significant drop in the oil production rate. Hence, the financial benefits of injecting into the reservoir decrease and it becomes evermore costly to continue doing so. Therefore, at a certain time it is no longer profitable to inject water into the reservoir.

Smart management of the reservoir is required in order to maximize profit. This entails taking into account, for example, reservoir properties, pressure measurements in the injector and producer, estimates of the remaining oil in the reservoir, and of course a function that relates the costs and profit of injecting water into and producing oil and water from the reservoir. Controlling the reservoir in such a way in order to maximize profit is known as Closed-Loop Reservoir Management.

1.1 Problem description

The Closed-Loop Reservoir Management (CLRM) in this thesis comprises three main pillars and is depicted in Figure 1.1. The first is known as the Virtual Asset, because it generates synthetic production data using Sintef's Matlab Reservoir Simulation Toolbox (MRST). MRST has to be provided with reservoir properties, boundary conditions as well as well locations and properties, after which it functions as a black box. Well pressures and/or flowrates are its only controllable input, and it subsequently calculates the resulting flow inside the reservoir. Consequently, saturation levels and pressures change over time. A (white Gaussian) noise is then added to the well pressures and the resulting pressures are labeled as the measured pressures.

One or more models then attempt to approximate the 'true' reservoir state by assimilating these measured pressures. This data assimilation step (i.e. updating the models) is, in this thesis, limited to estimating saturations and pressures in the reservoir as well as the reservoir permeability.

Next, an optimization algorithm uses the updated model in order to determine new optimal control settings (e.g. well pressures, injection rates) that maximizes future profit predictions. This

optimal configuration then serves as input to the virtual asset as well as the analytical model, which closes the loop of smart management of the reservoir.

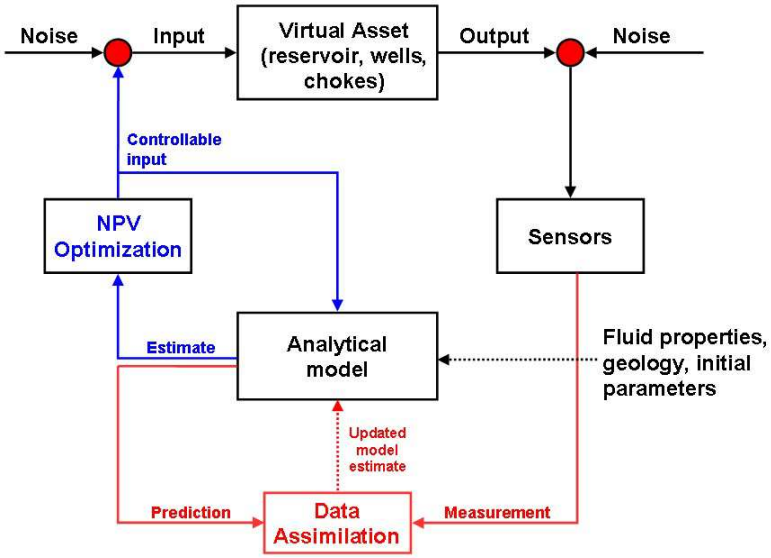

Figure 1.1 - Closed-Loop Reservoir Management

Maximizing profit with CLRM therefore greatly depends on the model choice and its accuracy in approximating the 'true' reservoir. In order to choose between complex and simplistic models, one has to consider their tradeoff, which foremost lies in accuracy and required computation time. For example, analytical models allow for fast computing but may be too simplistic and inaccurate under certain conditions, while more complex models might be more accurate but at the same time require more computation time.

1.2 Research objective

Little research was found on the use of one-dimensional analytical models during Closed-Loop Reservoir Management, although Weijermars et al. (2016) showed that analytical models of reservoir flow can produce results nearly identical to those of sophisticated numerical simulators. The analytical model, used to prevent premature water breakthrough, considered in that study was a two-dimensional two-phase (with equal viscosities and no relative permeability influences) description of reservoir flow between a direct-line-drive of injectors and producers.

A first objective was to familiarize myself with MRST in an autodidactic fashion. Secondly, I had to implement the analytical displacement model in Matlab in order to fulfill the main research objective.

The main research objective of this thesis is to assess the applicability and accuracy of various one-dimensional two-phase analytical models, whilst including relative permeability influences and non-equal viscosities, in approximating the (true) one- and two-dimensional reservoir flow during Closed-Loop Reservoir Management.

In this assessment two types of well orientations will be tested. The first concerns horizontal injector and producer wells that span the full width of the reservoir and are located at opposing sides halfway the height of the reservoir. The second considers vertical wells spanned across the height of the reservoirs, located halfway the width of the reservoir at again opposing sides.

1.3 Thesis outline

In order to fulfill the main research objective, this thesis starts with considering relevant aspects of reservoir flow. To this end the basic (differential) equations and (analytical) solutions thereof are derived in chapter 2. At the end of chapter 2, the two analytical solutions are combined to form a new and slightly more sophisticated analytical model.

Chapter 3 treats the derivation of reservoir pressure drop models and briefly describes choke valve pressure drop models, which are to be used conjointly with the displacement models of chapter 2. Chapter 3 also considers one of the reservoir pressure drop models for controlling two-dimensional flow, and additionally briefly investigates asymptotic flowrate and pressure behavior of an analytical pressure drop model.

Next, chapter 4 introduces the key-aspects of CLRM and looks into the behavior of the virtual asset, both at maximum as well as below maximum flowrate conditions. Subsequently, chapter 4 shows CLRM results for horizontal as well as vertical well orientations using the models treated in the preceding chapters.

Conclusions and discussion then follow in chapter 5, which leads to the chapter concerning recommendations (chapter 6). References regarding the for this thesis relevant literature, as well as an appendix with additional but less relevant CLRM results, are given at the end of this thesis

2 Reservoir flow & analytical solutions

This chapter covers the theoretical background of the necessary equations for reservoir flow. In section 2.1 the relevant concepts of phase flow through a porous medium are explained and are subsequently combined in section 2.2 into the well-known Buckley-Leverett equation. Next, the method of characteristics is employed and a solution to the Buckley-Leverett equation is given for one-dimensional (linear) displacement in the *x*-direction. Section 2.4 briefly touches upon the flow equations and the solution to the Buckley-Leverett equation for radial flow in a circular reservoir. Lastly, in section 2.5, the two Buckley-Leverett solutions are combined into a model describing one-dimensional radial-linear-radial flow along the (straight) inter-well axis.

2.1 General equations

The following subsections contain six important general concepts of phase flow. First, a general mass balance equation is derived, describing the flow in and out of a control volume in terms of mass flowrates. Next Darcy's law, an expression relating a phase's flowrate to its mobility and pressure, is shown. Thirdly phase mobility is explained, describing its dependency on viscosity as well as on absolute and relative permeability. Subsequently relative permeability, specifically the (modified) Brooks-Corey model, is treated. Next to last, capillary pressure is discussed; linking a difference in phase pressure to relative permeability. Lastly, the concept of state equations is briefly mentioned.

2.1.1 Mass balance

The assumption of total mass balance is one of the important concepts in the derivation below. Given a rectangular control volume, multiple phases can flow in and out over time and change the total mass inside. To maintain mass balance for each phase, the difference in a phase's mass rate at the boundaries of a control volume over a small time period Δt should equal the control volume's change in mass over the same time.

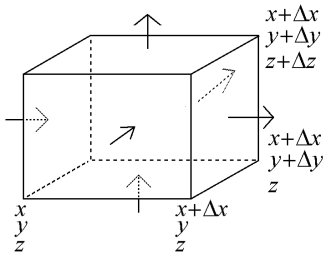

Figure 2.1 - Control volume

Using q_α to denote the phase volumetric flowrate with unit [$m^3 s^{-1}$], ρ_α the phase density [kg m^{-3}], ϕ the control volume's porosity [-] and S_α the phase saturation [-], a three-dimensional mass balance of the control volume depicted above leads to the following equation:

$$\underbrace{\left[\left((q_\alpha\rho_\alpha)_x-(q_\alpha\rho_\alpha)_{x+\Delta x}\right)+\left((q_\alpha\rho_\alpha)_y-(q_\alpha\rho_\alpha)_{y+\Delta y}\right)+\left((q_\alpha\rho_\alpha)_z-(q_\alpha\rho_\alpha)_{z+\Delta z}\right)\right]}_{\text{mass rates at the boundaries of the control volume}}\cdot\Delta t$$
$$=\underbrace{\Delta x\cdot\Delta y\cdot\Delta z\cdot\left((\phi S_\alpha\rho_\alpha)_{t+\Delta t}-(\phi S_\alpha\rho_\alpha)_t\right)}_{\text{Change in mass over time }\Delta t}. \tag{2.1.1}$$

The phase saturation is a number between 0 and 1, representing the percentage of the control volume occupied by that phase. Of course, the sum of all saturations should equal one:

$$\sum_\alpha S_\alpha = 1 \tag{2.1.2}$$

Recognizing that the influx at each of the control volume's boundaries is equal to the flow velocity times the cross-sectional area at the boundary, that is $q_\alpha = \widetilde{q_\alpha}\cdot A$, the left hand side of equation (2.1.1) can be written as

$$\left[\left(\Delta y\Delta z\widetilde{q_\alpha}\rho_\alpha\right)_x-\left(\Delta y\Delta z\widetilde{q_\alpha}\rho_\alpha\right)_{x+\Delta x}+\left(\Delta x\Delta z\widetilde{q_\alpha}\rho_\alpha\right)_y-\left(\Delta x\Delta z\widetilde{q_\alpha}\rho_\alpha\right)_{y+\Delta y}+\ldots\right.$$
$$\left.\left(\Delta x\Delta y\widetilde{q_\alpha}\rho_\alpha\right)_z-\left(\Delta x\Delta y\widetilde{q_\alpha}\rho_\alpha\right)_{z+\Delta z}\right]\cdot\Delta t. \tag{2.1.3}$$

Substituting (2.1.3) in (2.1.1), dividing by Δx, Δy, Δz, Δt, and taking the limit as Δx, Δy, Δz and Δt all tend to zero, results in

$$-\frac{\partial\widetilde{q_\alpha}\rho_\alpha}{\partial x}-\frac{\partial\widetilde{q_\alpha}\rho_\alpha}{\partial y}-\frac{\partial\widetilde{q_\alpha}\rho_\alpha}{\partial z}=\frac{\partial\phi S_\alpha\rho_\alpha}{\partial t}. \tag{2.1.4}$$

A source term can be added to equation (2.1.4), which is written in a more compact form as

$$-\nabla\cdot\dot{\mathbf{m}}_\alpha+q_{s\alpha}=\frac{\partial m_\alpha}{\partial t}, \tag{2.1.5}$$

where $\dot{\mathbf{m}}_\alpha=\rho_a\widetilde{\mathbf{q}_a}$ is the three-component (x, y, z) mass flux vector with unit [kg m^{-2} s^{-1}], $m_\alpha=\phi S_\alpha\rho_\alpha$ the mass per unit volume [kg m^{-3}], and $q_{s\alpha}$ the source term [kg m^{-3} s^{-1}]. The source term simply adds ($q_{s\alpha}>0$) or subtracts ($q_{s\alpha}<0$) mass from the reservoir.

2.1.2 Darcy's law

A standard expression that relates a phase's flowrate to its mobility and its pressure gradient is Darcy's law. Derived through experiments and published by Henry Darcy in 1856, the equation describes the conservation of momentum for flow through a porous medium. Inertia effects cause deviations from Darcy's law to occur at higher velocities, however due the low velocities in a porous medium these effects are small and can be ignored (Bear, 1972). If high velocities are encountered, one way of dealing with those effects is adding an inertial term, called the Forchheimer term. However, including the Forchheimer term is outside of the scope of this thesis and will therefore be neglected.

Neglecting the previously mentioned inertial effects, Darcy's law reads:

$$\widetilde{\mathbf{q}_\alpha}=-\boldsymbol{\lambda}_\alpha(\nabla p_\alpha-\rho_\alpha g\nabla h). \tag{2.1.6}$$

Or, for one-dimensional flow with a constant cross-section A,

$$q_\alpha=-\lambda_\alpha A(\nabla p_\alpha-\rho_\alpha g\nabla h), \tag{2.1.7}$$

where λ_α is the phase mobility [m^2 Pa^{-1} s^{-1}], p_α the pressure [Pa], g the gravitational constant [m s^{-2}] and h the height of the reservoir [m].

Darcy's law basically states that a higher mobility, pressure gradient and/or cross-section leads to a higher outflow.

2.1.3 Phase mobility

The phase mobility introduced in the previous subsection describes the ease with which a phase moves through the reservoir. The two main concepts of mobility are viscosity and permeability, which are respectively a phase's resistance to flow and how well fluids can flow through the reservoir. Phase mobility is defined by the its viscosity μ_α [Pa s^{-1}] and relative permeability $k_{r\alpha}$ [-], as well as the reservoir's absolute permeability matrix $\mathbf{k}$ [m^2]:

$$\lambda_\alpha = \frac{k_{r\alpha}}{\mu_\alpha}\mathbf{k}. \tag{2.1.8}$$

Often it is possible to align the coordinate system with the geological layering of the reservoir, which turns $\mathbf{k}$ into a diagonal matrix (Jansen, 2013).

Equation (2.1.8) expresses that a higher permeability of the phase or reservoir leads to a higher mobility of the phase. On the other hand, there is an inverse relationship between mobility and viscosity: the less viscous a phase is, the more mobile it is.

2.1.4 Relative permeability

The (dimensionless) relative phase permeability mentioned in the previous subsection is usually modeled through the experimentally derived (modified) Brooks-Corey model, which is given by

$$k_{r\alpha} = k_{r\alpha,0} S_{\alpha,eff}^{n_\alpha}, \tag{2.1.9}$$

where $k_{r\alpha,0}$ is the phase end-point relative permeability, n_α the Corey exponent and $S_{\alpha,eff}$ the effective saturation of phase α.

The reason for introducing the effective saturation is that in practice it may be impossible to completely extract certain phases, leaving behind immovable residuals $S_{\alpha r}$. The effective saturation is simply the real saturation scaled on the movable saturation, meaning it takes on values between 0 and 1. The value 0 is attained at a phase's residual saturation ($S_\alpha = S_{\alpha r}$), whereas 1 is attained at a phase's maximum saturation ($S_\alpha = 1 - \sum_{\beta \neq \alpha} S_{\beta r}$):

$$S_{\alpha,eff} = \frac{S_\alpha - S_{\alpha r}}{1 - \sum_\beta S_{\beta r}} \tag{2.1.10}$$

2.1.5 Capillary pressure

Capillary pressure is defined as the difference in pressure between a wetting and a non-wetting phase, i.e. $p_c = p_{nw} - p_w$, and often has a strong effect on very low wetting phase saturations and a weak effect on higher saturations. When water is used to displace oil (called imbibition), water is the wetting face. Just as pressure depends on saturation, so does capillary pressure. Therefore the question arises if it is possible to characterize capillary pressure as a function of wetting phase saturation explicitly. One well known model is the empirical Brooks-Corey capillary pressure model (Brooks and Corey, 1966), but over the years also theoretical models have been derived.

Li (2004b) reports that many natural porous media are fractals (e.g. reservoir rock) and thus can be modeled with a fractal model. An example of a fractal model, is the relationship between the number of pores and the radius of the pores (Li, 2010). According to Li, other authors "*have derived the empirical Brooks-Corey capillary pressure model theoretically from fractal modeling of a porous medium*" (Li, 2010), but Li derived a new and more general capillary pressure and relative permeability model. For details on the derivation, see for instance Li (2004a,b) and Li (2010). The capillary pressure model reads

$$p_c = \left[p_{\max}^{-\lambda} - \left(p_{\max}^{-\lambda} - p_e^{-\lambda} \right) S_{w,eff} \right]^{\frac{-1}{\lambda}}, \tag{2.1.11}$$

where $S_{w,eff}$ is the effective wetting phase saturation, p_{max} is the capillary pressure at the injected phase's maximum saturation, p_e is the entry capillary pressure, i.e. the pressure when the injected phase is at its residual saturation level, and λ is the pore size distribution index.

The pore size distribution index is a number that characterizes the heterogeneity of the pore size. In the case of drainage, if $\lambda > 0$ and $p_{\max} \to \infty$, (2.1.11) reduces to the Brooks-Corey capillary pressure model:

$$p_c = p_e (S_{w,eff})^{\frac{-1}{\lambda}}. \tag{2.1.12}$$

When considering an imbibition process expression (2.1.11), with $\lambda > 0$ but this time $p_e \to \infty$, simplifies to the empirical Li-Horne capillary pressure model suggested by Li and Horne (2001):

$$p_c = p_{\max} (1 - S_{w,eff})^{\frac{-1}{\lambda}}. \tag{2.1.13}$$

Obviously when introducing a new, or in this case more generalized, model it should be validated with experimental data. Li and Horne (2006) reported that the general capillary pressure model can match the experimental data obtained from various rock core samples, therefore validating their model.

Linking capillary pressure and relative permeability

Burdine (1953) suggested a method for inferring relative permeability from capillary pressure data for wetting as well as non-wetting phases:

$$\begin{aligned} k_{rw} &= (S_{w,eff})^2 \frac{\int_0^{S_w} \mathrm{dS_w} / (p_c)^2}{\int_0^1 \mathrm{dS_w} / (p_c)^2} \\ k_{rnw} &= (S_{nw,eff})^2 \frac{\int_{S_w}^1 \mathrm{dS_w} / (p_c)^2}{\int_0^1 \mathrm{dS_w} / (p_c)^2} \end{aligned} \tag{2.1.14}$$

Following Li (2004b), combining (2.1.11) with the above Burdine model this results in

$$\begin{aligned} k_{rw} &= (S_{w,eff})^2 \frac{1 - (S_{we})^{\frac{2+\lambda}{\lambda}}}{1 - \alpha^{\frac{2+\lambda}{\lambda}}} \\ k_{rnw} &= (1 - S_{w,eff})^2 \frac{(S_{we})^{\frac{2+\lambda}{\lambda}} - \alpha^{\frac{2+\lambda}{\lambda}}}{1 - \alpha^{\frac{2+\lambda}{\lambda}}} \end{aligned} \tag{2.1.15}$$

where $\alpha = (p_e / p_{\max})^{-\lambda}$ and $S_{we} = 1 - (1 - \alpha) S_{w,eff}$.

Under the same conditions that resulted in (2.1.12) (i.e. the Brooks-Corey capillary pressure model), the Burdine model for relative permeabilities (2.1.15) reduces to

$$k_{rw} = (S_{w,eff})^2\left[(S_{w,eff})^{\frac{2+\lambda}{\lambda}}\right]$$
$$k_{rnw} = (1-S_{w,eff})^2\left[1-(S_{w,eff})^{\frac{2+\lambda}{\lambda}}\right] \tag{2.1.16}$$

The relative permeability model (2.1.16) is well known as the Brooks-Corey relative permeability model. When $p_e = p_{max}$, (2.1.15) is reduced to the modified Brooks-Corey model with $n_\alpha = 3$

$$k_{r\alpha} = S_{\alpha,eff}^3. \tag{2.1.17}$$

2.1.6 Equations of state

In the first three subsections the density, permeability, viscosity and porosity all played a part in the equations and just as fluid flow is dependent on pressure, these parameters themselves are dependent on pressure. Even more so, some of these parameters can also be dependent on temperature. Equations describing the relationship between these parameters and pressure and temperature are commonly known as equations of state. Certain assumptions, however, render these parameters constant, which is why the equations of state will receive no further consideration.

2.2 Reservoir flow equations

As the, for this thesis, most important concepts of fluid flow have been addressed, this next section focuses on combining all subsections of section 2.1 into a single equation that describes two phase flow. A sketch of the reservoir considered is shown below in Figure 2.2.

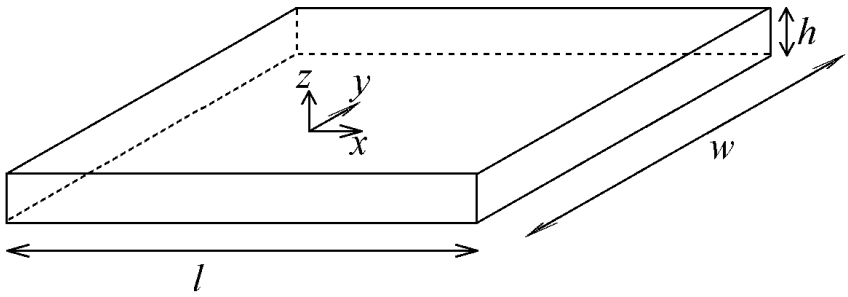

Figure 2.2 - Reservoir model

2.2.1 Reservoir characteristics and assumptions

As the reservoir, the phases and the flow that have to be modeled have certain characteristics, it is important to incorporate them into the model. This subsection lists the characteristics and assumptions.

The reservoir is considered to be:

- horizontal with constant height h
- thin enough, i.e. small h, such that it is reasonable to assume a constant saturation over the reservoir height
- rectangular shaped with length $l >> h$ and width $w >> h$, meaning the cross-section is constant
- perforated by an injector at $x = 0$ and a producer at $x = l$
- incompressible
- homogeneous
- isotropic

The displacement is considered to be:

- one-dimensional
- immiscible
- laminar

Each phase is assumed to be:

- incompressible
- homogeneous
- isothermal

2.2.2 Mass balance & total flowrate

The assumption of horizontal flow reduces the three-dimensional mass balance equation (2.1.4) to the one-dimensional form

$$-\frac{\partial \widetilde{q_\alpha}\rho_\alpha}{\partial x} = \frac{\partial \phi S_\alpha \rho_\alpha}{\partial t}, \tag{2.1.18}$$

where $\widetilde{q_\alpha}$ is the phase flowrate in [m s^{-1}].

Due to the assumption of a constant cross-section the above equation can also be written as

$$-\frac{\partial q_\alpha \rho_\alpha}{\partial x} = A \cdot \frac{\partial \phi S_\alpha \rho_\alpha}{\partial t} \tag{2.1.19}$$

where $q_\alpha = \widetilde{q_\alpha} \cdot A$ is the volumetric flow in [m^3 s^{-1}].

Since each phase is assumed to be incompressible, homogeneous and isothermal, both the density and viscosity of each phase are constant, i.e. $\rho_\alpha(T, p) = \rho_\alpha$ and $\mu_\alpha(T, p) = \mu_\alpha$. The assumptions of an incompressible, homogeneous and isotropic reservoir imply that the porosity ϕ and absolute permeability k are constant. These assumptions lead to a simplification of equation (2.1.19):

$$-\rho_\alpha \cdot \frac{\partial q_\alpha}{\partial x} = A \cdot \phi \cdot \rho_\alpha \frac{\partial S_\alpha}{\partial t} \tag{2.1.20}$$

or

$$-\frac{\partial q_\alpha}{\partial x} = A \cdot \phi \cdot \frac{\partial S_\alpha}{\partial t} \tag{2.1.21}$$

As stated in equation (2.1.2), an obvious though important equation is that the sum over all saturations is constant over space and time. Moreover, this means that the change in saturation over time is equal to zero:

$$\sum_\alpha S_\alpha = 1 \quad \text{and} \quad \sum_\alpha \frac{\partial S_\alpha}{\partial t} = 0. \tag{2.1.22}$$

Summing over all phases in equation (2.1.21) and using (2.1.22) reveals the important property of constant total flow q_t:

$$-\frac{\partial q_t}{\partial x} = -\sum_\alpha \frac{\partial q_\alpha}{\partial x} = A \cdot \phi \cdot \sum_\alpha \frac{\partial S_\alpha}{\partial t} = 0 \tag{2.1.23}$$

This is, of course, in agreement with the incompressibility assumption of each of the phases and the reservoir. However, it is important to note that q_t is only constant in the spatial dimension and therefore does not need to be constant in time.

2.2.3 Fractional flow

Another key-feature is that liquid water is used to displace the oil in the reservoir. Therefore the type of displacement considered is that of imbibition, i.e. a non-wetting phase (oil in this case) is displaced by a wetting phase (water).

Continuing from equation (2.1.21) and using (2.1.23), write the left-hand side as

$$-\frac{\partial q_\alpha}{\partial x} = -\frac{\partial\left(q_\alpha \frac{q_t}{q_t}\right)}{\partial x} = -q_t \frac{\partial f_\alpha}{\partial x}, \tag{2.1.24}$$

where $f_\alpha \coloneqq q_\alpha / q_t$ is the (dimensionless) fractional flow.

Since f_α is only dependent on q_α, which in turn depends only on S_α, the right-hand side of (2.1.24) can be rewritten. Substitution into equation (2.1.21) yields

$$-q_t \frac{\mathrm{d}f_\alpha}{\mathrm{d}S_\alpha}\frac{\partial S_\alpha}{\partial x} = A \cdot \phi \cdot \frac{\partial S_\alpha}{\partial t} \tag{2.1.25}$$

As there are only two phases in the reservoir, the choice is made to write all the equations in terms of water saturation. The next step is rewriting f_w such that it no longer depends on q_w, for which the first step is using the one-dimensional form of Darcy's law (see (2.1.7)). The use of Darcy's law is congruent with the assumption of laminar flow. Since additionally the reservoir is thin and quite stretched out, gravity effects are considered negligible. Using Darcy's law leads to the expression

$$f_w \coloneqq \frac{q_w}{q_t} = \frac{q_t - q_o}{q_t} = 1 + \frac{1}{q_t}\lambda_o A \frac{\partial p_o}{\partial x}. \tag{2.1.26}$$

Recalling that the capillary pressure is defined as the pressure difference of the non-wetting and wetting phase, that is $p_c = p_o - p_w$, expression (2.1.26) is rewritten to

$$\begin{aligned} f_w &= 1 + \frac{1}{q_t}\lambda_o A \frac{\partial (p_c + p_w)}{\partial x} \\ &= 1 + \frac{1}{q_t}\lambda_o A\left(\frac{\partial p_c}{\partial x} - \frac{q_w}{\lambda_w A}\right) \\ &= 1 + \frac{1}{q_t}\lambda_o A \frac{\partial p_c}{\partial x} - f_w \frac{\lambda_o}{\lambda_w} \end{aligned} \tag{2.1.27}$$

Using that the total mobility is given by $\lambda_t = \lambda_o + \lambda_w$, rewriting (2.1.27) leads to

$$f_w = \frac{\lambda_w}{\lambda_t}\left(1 + \frac{1}{q_t}\lambda_o A \frac{\partial p_c}{\partial x}\right). \tag{2.1.28}$$

Or alternatively, as the capillary pressure depends only on water saturation,

$$f_w = \frac{\lambda_w}{\lambda_t}\left(1 + \frac{1}{q_t}\lambda_o A \frac{\mathrm{d}p_c}{\mathrm{d}S_w}\frac{\partial S_w}{\partial x}\right). \tag{2.1.29}$$

Substitution of the previous expression for the fractional water flow into equation (2.1.25) with $\alpha = w$ results in

$$-q_t \frac{\mathrm{d}}{\mathrm{d}S_w}\left(\frac{\lambda_w}{\lambda_t}\left(1 + \frac{1}{q_t}\lambda_o A \frac{\mathrm{d}p_c}{\mathrm{d}S_w}\frac{\partial S_w}{\partial x}\right)\right)\frac{\partial S_w}{\partial x} = A \cdot \phi \cdot \frac{\partial S_w}{\partial t} \tag{2.1.30}$$

2.3 Buckley-Leverett - linear displacement

This section will simplify (2.1.30) further and subsequently solve the resulting Buckley-Leverett equation. In the last subsection, the concept of a shock front is used to obtain saturation profiles.

2.3.1 The Buckley-Leverett equation

In order to derive the Buckley-Leverett equation another assumption is required, namely that of zero capillary pressure:

$$p_c \coloneqq p_o - p_w = 0. \tag{2.1.31}$$

This assumption simplifies (2.1.29) to

$$f_w = \frac{\lambda_w}{\lambda_t} \tag{2.1.32}$$

and therefore (2.1.30) to

$$-q_t \frac{\mathrm{d}}{\mathrm{d}S_w}\left(\frac{\lambda_w}{\lambda_t}\right)\frac{\partial S_w}{\partial x} = A \cdot \phi \cdot \frac{\partial S_w}{\partial t}, \tag{2.1.33}$$

or,

$$-q_t \frac{\mathrm{d}f_w}{\mathrm{d}S_w}\frac{\partial S_w}{\partial x} = A \cdot \phi \cdot \frac{\partial S_w}{\partial t}. \tag{2.1.34}$$

This last equation is known as the Buckley-Leverett equation, named after the authors who were first to present and analyze it (Buckley and Leverett, 1942).

For this hyperbolic partial differential equation, initial and boundary conditions need to be specified. The residual water saturation level is chosen as the initial condition, denoted by S_{wi}. Residual water saturation is also known as connate water saturation (S_{wc}), however throughout this thesis S_{wi} is used. The initial condition thus reads

$$S_w(x,0) = S_{wi} \tag{2.1.35}$$

This means that initially the reservoir is completely filled with oil, minus some residual water.

The boundary condition will be specified at the injector location ($x = 0$), as this is the only place in the reservoir where the water saturation can be explicitly controlled. The saturation level will be the maximum water saturation possible, because the only injected phase is water and a smaller value would mean that also oil is injected into the reservoir. The boundary condition thus reads

$$S_w(0,t) = 1 - S_{or} \tag{2.1.36}$$

2.3.2 Saturation propagation

Because equation (2.1.34) is a hyperbolic equation it is possible to use the method of characteristics to find relationships between independent variables for which the dependent ones do not change. In equation (2.1.34) the independent variables are x and t, whereas the dependent variable is S_w. In order to find a level of constant saturation, $S_w = \widehat{S_w}$, the material derivative of saturation should equal zero, i.e.

$$\left.\frac{\mathrm{d}S_w}{\mathrm{d}t}\right|_{S_w=\widehat{S_w}} = \left.\frac{\partial S_w}{\partial x}\right|_{S_w=\widehat{S_w}} \left.\frac{\mathrm{d}x}{\mathrm{d}t}\right|_{S_w=\widehat{S_w}} + \left.\frac{\partial S_w}{\partial t}\right|_{S_w=\widehat{S_w}} = 0 \tag{2.1.37}$$

Rewriting equation (2.1.37) leads to an equation that describes the propagation speed for a specific saturation level:

$$\left.\frac{\mathrm{d}x}{\mathrm{d}t}\right|_{S_w=\widehat{S_w}} = -\frac{\left.\frac{\partial S_w}{\partial t}\right|_{S_w=\widehat{S_w}}}{\left.\frac{\partial S_w}{\partial x}\right|_{S_w=\widehat{S_w}}} \tag{2.1.38}$$

By combining equations (2.1.38) and (2.1.34), the propagation speed can be expressed as

$$\frac{\mathrm{dx}}{\mathrm{dt}}\Big|_{S_w=\widehat{S_w}} = \frac{q_t}{A\cdot\phi}\frac{\mathrm{d}f_w}{\mathrm{dS}_w}\Big|_{S_w=\widehat{S_w}} \tag{2.1.39}$$

Integrating this equation results in an expression for the position of a saturation level

$$x(t)\big|_{S_w=\widehat{S_w}} = \frac{\int_0^t q_t(\tilde{t})d\tilde{t}}{A\cdot\phi}\frac{df_w}{dS_w}\Big|_{S_w=\widehat{S_w}} \tag{2.1.40}$$

Dividing (2.1.40) by the total length of the reservoir, l, results in the dimensionless expression

$$x_D(t_D)\big|_{S_w=\widehat{S_w}} = t_D\frac{df_w}{dS_w}\Big|_{S_w=\widehat{S_w}}, \tag{2.1.41}$$

where $x_D(t) = \frac{x(t)}{l}$ and $t_D = \frac{V_i(t)}{V_p} = \frac{\int_0^t q_t(\tilde{\mathrm{t}})\mathrm{d}\tilde{\mathrm{t}}}{A\cdot l\cdot\phi}$.

In this notation $V_i(t)$ is the total injected volume (with unit [m^3]) at time t and V_p is the pore volume, i.e. the volume of the reservoir that is available for flow.

Expression (2.1.41) formulates the dimensionless position of a certain saturation value for every dimensionless time. While originally the phase saturation was a function of position and time, now position is a function of saturation and time.

An example of the fractional flow derivative is given below in Figure 2.3, for which the corresponding parameters are given in Table 2.1. Part of calculating the fractional flow derivative is calculating phase and total mobility, both of which are for the most part determined by the underlying relative permeability model. The relative permeability model used in this thesis is the Brook-Corey relative permeability model (see (2.1.9)).

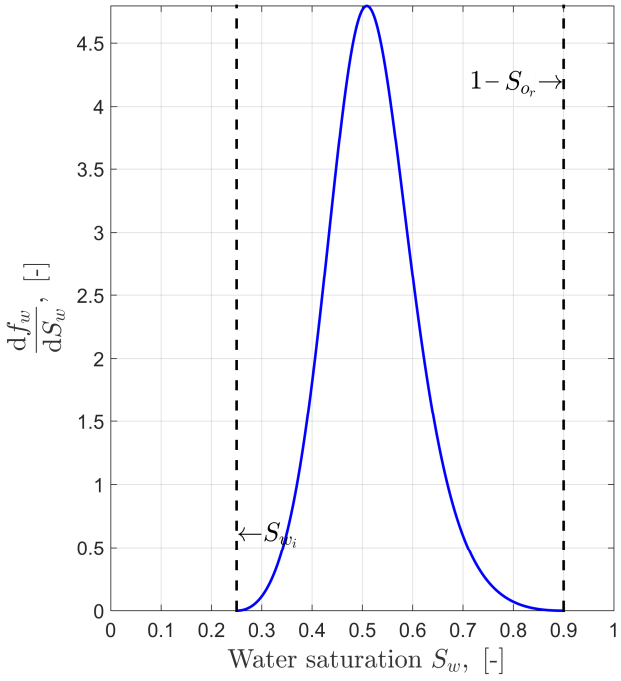

Figure 2.3 - Fractional flow derivative

Parameter	Symbol	Value	SI unit
Initial water saturation	S_{wi}	0.25	-
Residual oil saturation	S_{or}	0.1	-
End-point water rel perm[1]	$k_{rw,0}$	0.5	-
End-point oil rel perm	$k_{ro,0}$	0.9	-
Corey exponent water	n_w	3	-
Corey exponent oil	n_o	3	-
Viscosity water	μ_w	0.35	cp
Viscosity oil	μ_o	1.9	cp
Permeability	k	300	mD

Table 2.1 - Parameters for Figure 2.3

2.3.3 Shock front solution

From Figure 2.3 it becomes clear that a new problem has arisen: for all except one of the fractional flow derivative's possible values, there are two saturation values. This means that for any given point in space and time (see (2.1.41)), there are two corresponding saturation values. This physical impossibility is a consequence of the zero capillary pressure assumption. In practice capillary pressure creates a quick increase of water saturation when the saturation level is still low. In other words, capillary pressure attains higher values for lower saturations.

The quick increase can be emulated through a shock front. Buckley and Leverett (1942) came up with the idea of a front formed by a real and imaginary solution, the existence of which was subsequently proven by Terwilliger et al. (1951). They proved that a discontinuity exists between a zone in front of the shock front where all saturations move with the same speed and a zone behind the shock front where all saturations have a different speed that is lower than that of the shock front.

The question that remains, is what the saturation value of the shock front is. Welge (1952) proposed a procedure where the speed of the front is assumed to be proportional to the slope of a tangent to the fractional flow curve f_w. The tangent goes through the point $(S_{wi}, 0)$ and touches the fractional flow curve at the point $(S_{wf}, f_w(S_{wf}))$ where S_{wf} is the shock front saturation. The tangent must have the largest possible gradient, as the change in saturation is the biggest at the shock front where the saturation level jumps from the initial level to a certain higher saturation level.

If $y(S_w) = a(S_w + b)$ is the aforementioned tangent, then the first criteria, $y(S_{wi}) = 0$, reduces the expression to $y(S_w) = a(S_w - S_{wi})$. The second criteria implies that $y(S_{wf}) = f_w(S_{wf})$ and thus the formula of the tangent is

$$y(S_w) = \frac{f_w(S_{wf})}{(S_{wf} - S_{wi})}(S_w - S_{wi}). \tag{2.1.42}$$

Since the slope of the tangent $y(S_w)$ should be the maximum possible value, the shock front saturation hence is given by

$$S_{wf} := \left\{ S_w \,|\, \max_{S_w} \frac{f_w(S_w)}{(S_w - S_{wi})} \right\} \tag{2.1.43}$$

[1] The term 'rel perm' is an abbreviation for relative permeability

Moreover, the slope of the tangent and the slope of the f_w curve are the same at the shock front saturation:

$$\left.\frac{\mathrm{d}f_w}{\mathrm{dS_w}}\right|_{S_w=S_{wf}} = \frac{f_w(S_{wf})}{(S_{wf}-S_{wi})} \tag{2.1.44}$$

Hence, the front saturation might also be found by solving the equation below (where $S_{wi} < S_w < 1-S_{or}$):

$$\frac{\mathrm{d}f_w}{\mathrm{dS_w}} = \frac{f_w(S_w)}{(S_w-S_{wi})}. \tag{2.1.45}$$

The shock front solution to equation (2.1.41) can now be expressed for all saturation values:

$$x_D(t_D,S_w) = \begin{cases} t_D \dfrac{\mathrm{d}f_w}{\mathrm{d}S_w} & , \quad S_{wf} \le S_w \le 1-S_{or} \\ t_D \left.\dfrac{\mathrm{d}f_w}{\mathrm{d}S_w}\right|_{S_w=S_{wf}} & , \quad S_{wi} \le S_w \le S_{wf} \end{cases} \tag{2.1.46}$$

Figure 2.4 illustrates that (2.1.43) as well as (2.1.45) could be used to determine the shock front saturation. Also shown below is an example of a Buckley-Leverett profile and its propagation through time, where dimensionless values are used for both the spatial and temporal dimensions. The parameters corresponding to these two figures can be found in Table 2.2. The dimensional time between profiles is 50 days and since the water injection rate is also constant (750 m^3/day), the shock front propagates at a constant pace through the reservoir.

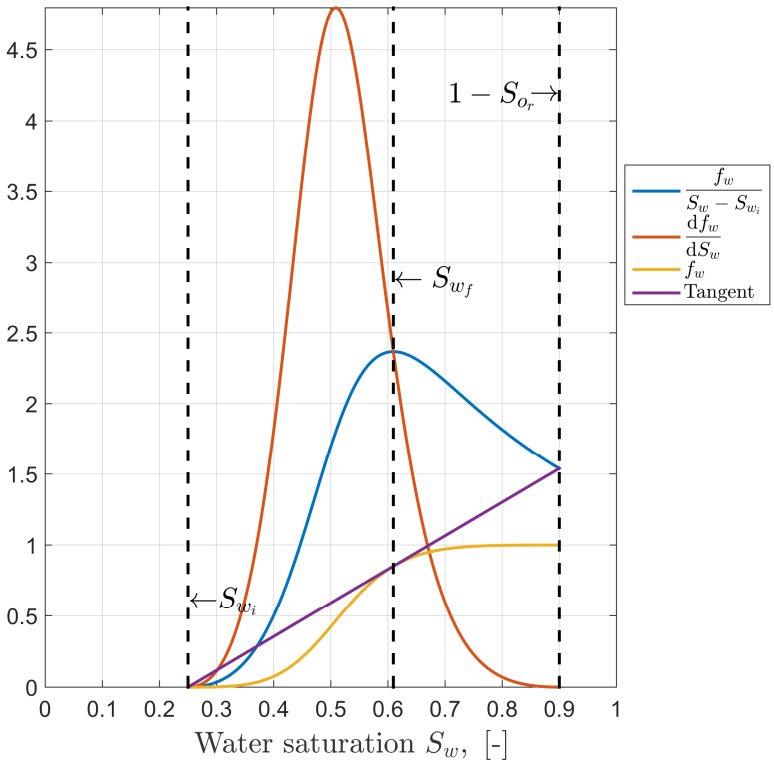

Figure 2.4 - Determining shock front saturation

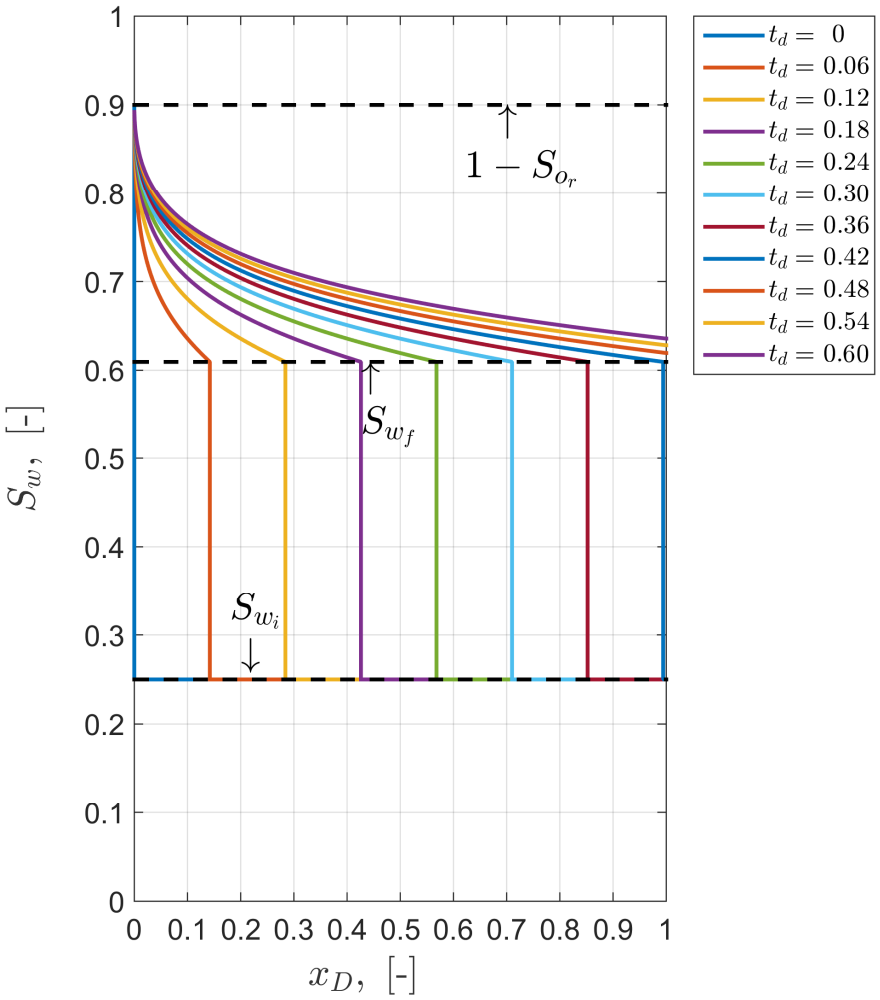

Figure 2.5 - Buckley-Leverett profiles

Parameter	Symbol	Value	Unit
Initial water saturation	S_{wi}	0.25	-
Residual oil saturation	S_{or}	0.1	-
End-point water rel perm	$k_{rw,0}$	0.5	-
End-point oil rel perm	$k_{ro,0}$	0.9	-
Permeability	k	300	m^2
Corey exponent water	n_w	3	-
Corey exponent oil	n_o	3	-
Viscosity water	μ_w	0.35	cp
Viscosity oil	μ_o	1.9	cp
Reservoir length	l	1000	m
Reservoir width	w	250	m
Reservoir height	h	10	m
Porosity	ϕ	0.25	-
Injection rate	q_t	750	m^3/day
Total time	t	500	days

Table 2.2 - Parameters for Figure 2.4 and Figure 2.5

2.4 Buckley-Leverett - Radial displacement

In case of radial flow, such as in a circular reservoir with a vertical injector or producer at its centre (Figure 2.6), the derivation of the flow equations is similar to those in the preceding three sections and has been considered before by many authors (among others Matthews and Russell (1967), and more recently by Ling (2015)). Therefore, this section only explains the most relevant equations.

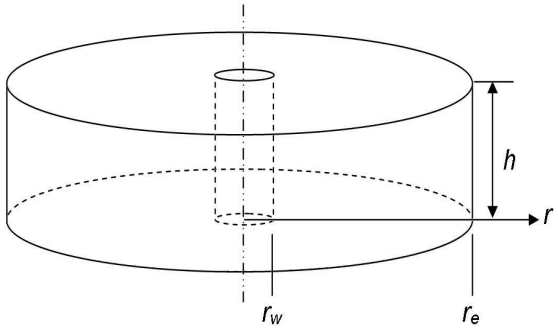

Figure 2.6 - Circular reservoir with a well at the centre

More specifically, fractional flow equation (2.1.32) remains the same. The only two differences in equation (2.1.34) are that the dimensional derivative is taken with respect to radial coordinate r instead of x and that the cross-section A is dependent on r as it is cylindrical (instead of rectangular). Measuring the radius r positive in the direction of the flow, equation (2.1.34) for an injector well becomes:

$$\begin{aligned} -q_t \frac{\mathrm{d}f_w}{\mathrm{d}S_w}\frac{\partial S_w}{\partial r} &= A\cdot\phi\cdot\frac{\partial S_w}{\partial t} \\ &= 2\pi r h\cdot\phi\cdot\frac{\partial S_w}{\partial t}. \end{aligned} \tag{2.1.47}$$

Hence, equation (2.1.39) similarly changes to

$$\left.\frac{\mathrm{d}r}{\mathrm{d}t}\right|_{S_w=\widehat{S_w}} = \frac{q_t}{2\pi r h\cdot\phi}\left.\frac{\mathrm{d}f_w}{\mathrm{d}S_w}\right|_{S_w=\widehat{S_w}} \tag{2.1.48}$$

or,

$$\left.\frac{\mathrm{d}\left(0.5r(t)^2\right)}{\mathrm{d}t}\right|_{S_w=\widehat{S_w}} = r\left.\frac{\mathrm{d}r}{\mathrm{d}t}\right|_{S_w=\widehat{S_w}} = \frac{q_t}{2\pi h\cdot\phi}\left.\frac{\mathrm{d}f_w}{\mathrm{d}S_w}\right|_{S_w=\widehat{S_w}} \tag{2.1.49}$$

Integrating over time yields

$$\int_0^t \left.\frac{\mathrm{d}\left(0.5r(\tilde{t},S_w)^2\right)}{\mathrm{d}\tilde{t}}\right|_{S_w=\widehat{S_w}} d\tilde{t} = \int_0^t \frac{q_t}{2\pi h\cdot\phi}\left.\frac{\mathrm{d}f_w}{\mathrm{d}S_w}\right|_{S_w=\widehat{S_w}} d\tilde{t} \tag{2.1.50}$$

The solution for an injector well, employing that at $t=0$ each saturation level is located at the well location (i.e. $r(0,\widehat{S_w}) = r_w$), is therefore given by

$$r(t,\widehat{S_w}) = \sqrt{r_w^2 + \int_0^t q_t d\tilde{t}\,\frac{1}{\pi h\cdot\phi}\left.\frac{\mathrm{d}f_w}{\mathrm{d}S_w}\right|_{S_w=\widehat{S_w}}} \tag{2.1.51}$$

For a producer well with its centre at the origin, however, the direction of flow is inwards towards the well and the radius is measured positive in opposite direction of the flow. Considering that at $t=0$ each saturation level is still at the external radius of the radial flow regime (i.e. $r(0,\widehat{S_w}) = r_e$), the derivation results in

$$r(t,\widehat{S_w}) = \sqrt{r_e^2 - \int_0^t q_t d\tilde{t}\,\frac{1}{\pi h\cdot\phi}\left.\frac{\mathrm{d}f_w}{\mathrm{d}S_w}\right|_{S_w=\widehat{S_w}}} \tag{2.1.52}$$

Note that $q_t \geq 0$ *in all.*

Lastly, since the fractional flow expression is unchanged, the shock front saturation can again be found as described in section 2.3.3.

2.5 Buckley-Leverett - Combining radial and linear displacement

While some reservoirs might be governed (and sufficiently described) by one-dimensional linear or radial flow, others can be governed by two-dimensional flow in a rectangular reservoir. Figure 2.7a below depicts such a rectangular reservoir with two wells: an injection well located at the left side of the reservoir and a producer well located at the right side of the reservoir. Consequentially, when neglecting gravity and assuming equal injection over the height of the reservoir, the fluid flow is two-dimensional and flows along streamlines such as shown in Figure 2.7b (adapted from Jansen (2016)). The lines tangential to the streamlines are equipotential lines of equidistant magnitude, i.e. lines along which the pressure is constant (i.e. *equipotential*) and between which the pressure change is constant (*equidistant magnitude*).

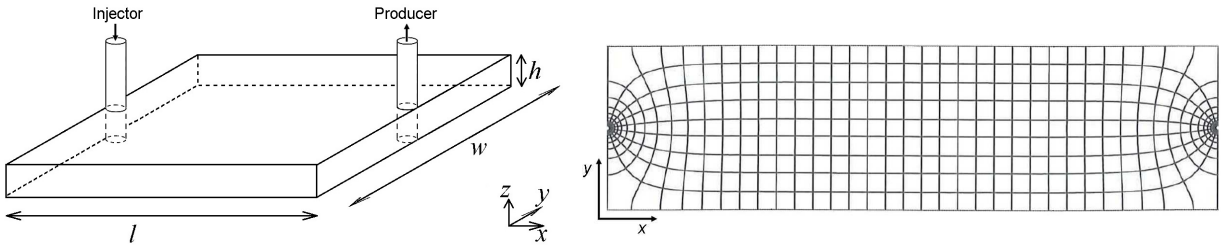

Figure 2.7 - Schematic representation of two-dimensional flow

a) rectangular reservoir with vertical injector and producer.

b) streamlines and equipotential lines for figure a.

Both representations are not to scale.

The middle part of Figure 2.7b indicates that reservoirs with a very small width (w) or large length to width ratio (l/w) are predominantly governed by linear flow in the x-direction. For such reservoirs the saturation distribution is given by equation (2.1.40).

On the other hand, near both wells (Figure 2.7b) the streamlines and equipotential lines display radial flow characteristics, which means that reservoirs with a relatively small length are more strongly influenced by radial flow.

Between the radial flow regime and the linear flow regime, there is an area in which the streamlines have to converge from radial to linear flow (near the injector) and vice versa (near the producer). The convergence is strongest near the reservoir's front and back ($y = 0$ and $y = w$), where streamlines need to make an almost 90° angle. Hence the convergence is considered weakest along the inter-well axis (i.e. $y = w/2$) as the streamline that coincides with it does not need to make any angle. Therefore it can be considered that this specific streamline, as an approximation, only experiences radial and linear displacement. This consideration gives rise to idea of Radial-Linear-Radial (*RaLiRa*) flow at the inter-well axis, where the saturation displacement changes at a certain x,y-coordinate (x_{ra}, $w/2$) from a radial to a linear regime and at another x,y-coordinate (x_{ar}, $w/2$) back to a radial regime.

The first step in finding coordinates x_{ra} and x_{ar} is realizing that for the symmetric reservoir in question (Figure 2.7a) there is a simple relation between the two coordinates, i.e. $x_{ar} = l - x_{ra}$. Secondly, in order

to maintain continuity of the displacement, the time-derivative in (2.1.39) and (2.1.48) have to be equal to each other at these coordinates:

$$\frac{q_t}{2\pi x_{ra} h \cdot \phi} \frac{\mathrm{d}f_w}{\mathrm{d}S_w}\bigg|_{S_w=\widehat{S_w}} = \frac{\mathrm{dr}}{\mathrm{dt}}\bigg|_{r=x_{ra},\, S_w=\widehat{S_w}} = \frac{\mathrm{dx}}{\mathrm{dt}}\bigg|_{x=x_{ra},\, S_w=\widehat{S_w}} = \frac{q_t}{wh \cdot \phi} \frac{\mathrm{d}f_w}{\mathrm{d}S_w}\bigg|_{S_w=\widehat{S_w}} \tag{2.1.53}$$

Hence, the left radial regime ends at $x_{ra} = w/(2\pi)$ and the right radial regimes starts at $x_{ra} = l - w/(2\pi)$. The entire saturation distribution for $\widehat{S_w} \geq S_{wf}$ along the inter-well axis then follows from combining expressions (2.1.40), (2.1.51) and (2.1.52).

Firstly, the location of saturation levels in the left radial regime is given by

$$x(t, \widehat{S_w}) = \sqrt{x_w^2 + \int_0^t q_t d\tilde{t} \, \frac{1}{\pi h \cdot \phi} \frac{\mathrm{d}f_w}{\mathrm{d}S_w}\bigg|_{S_w=\widehat{S_w}}}, \quad \text{for all } \widehat{S_w} \text{ s.t. } \int_0^t q_t d\tilde{t} \leq V_{p,ra}(\widehat{S_w}) \tag{2.1.54}$$

where $V_{p,ra}(\widehat{S_w}) = \pi h \phi (x_{ra}^2 - x_w^2) \,/\, f_w'(\widehat{S_w})$ is the injected pore volume required to displace saturation level $\widehat{S_w}$ from the injector well to x_{ra} (i.e. from x_w to $w/(2\pi)$).

Secondly, for the linear regime, the location of a saturation level can be expressed as

$$x(t, \widehat{S_w}) = x_{ra} + \frac{\int_0^t q_t d\tilde{t} - V_{p,ra}(\widehat{S_w})}{wh \cdot \phi} \frac{\mathrm{d}f_w}{\mathrm{d}S_w}\bigg|_{S_w=\widehat{S_w}}, \quad \text{for all } \widehat{S_w} \text{ s.t. } V_{p,ra}(\widehat{S_w}) \leq \int_0^t q_t d\tilde{t} \leq V_{p,ar}(\widehat{S_w}) \tag{2.1.55}$$

where $V_{p,ar}(\widehat{S_w}) = V_{p,ra}(\widehat{S_w}) + (l - 2x_{ra}) wh\phi \,/\, f_w'(\widehat{S_w})$ is the injected pore volume required to displace saturation level $\widehat{S_w}$ from the x_w to $l - x_{ra}$.

Lastly, the saturations in the right radial regime are given by

$$x(t, \widehat{S_w}) = l - \sqrt{x_{ra}^2 - \frac{\int_0^t q_t d\tilde{t} - V_{p,ar}(\widehat{S_w})}{\pi h \cdot \phi} \frac{\mathrm{d}f_w}{\mathrm{d}S_w}\bigg|_{S_w=\widehat{S_w}}}, \quad \text{for all } \widehat{S_w} \text{ s.t. } V_{p,ar}(\widehat{S_w}) \leq \int_0^t q_t d\tilde{t} \leq V_{p,\mathrm{end}}(\widehat{S_w}) \tag{2.1.56}$$

where $V_{p,\mathrm{end}}(\widehat{S_w}) = V_{p,ar}(\widehat{S_w}) + V_{p,ra}(\widehat{S_w})$ is the injected pore volume required to displace saturation level $\widehat{S_w}$ from the x_w to $l - x_w$ (i.e. from injector to producer).

It is important to note that the presented flow solution is devised for the inter-well axis only. Consequently, the model can be expected to be more accurate in determining the moment of water breakthrough in comparison to using only the linear displacement model. On other hand, the actual water saturation value at the producer well (after water breakthrough has occurred) is always lower than that of the RaLiRa model, because all other streamlines -along which it takes more time for the water to reach the producer- are not taken into account by the RaLiRa model.

3 Pressure drop models

This chapter covers models for pressure drop between the injector to producer wells, for which the general concept is treated in the first section. The second section introduces choke valves as a means to regulate the flowrate or pressure drop between the wells. The third section details the derivation of various formulae for pressure drop in the reservoir and additionally treats the numerical integration technique that is used to evaluate this pressure drop. Next to last, controllability of flowrates with the linear displacement model and associated pressure drop model is investigated. Lastly, section 3.5 briefly investigates asymptotic behavior of the simplest pressure drop model.

3.1 The reservoir model and pressure drop

The Buckley-Leverett model enabled computation of the saturation distribution in the reservoir through time. A more interesting case where this model can be used is a multi-layered reservoir. The amount of Buckley-Leverett models needed is equal to the number of layers in the reservoir, though the basic model does not change: water still propagates from the left to the right (i.e. from injector to producer). Figure 3.1 below, which visualizes two types of reservoirs, shows the j^{th} layer of the reservoir as well as the injector and producer running along the edge the reservoir.

The first type that Figure 3.1 depicts is a vertical cross section of a layered reservoir where the layers, separated by thin *horizontal* impermeable layers, lie on top of one another in the z-dimension. In this case the (vertical) injector and producer are located halfway the width of the reservoir (i.e. $y = w/2$). For the linear displacement model it is assumed that the injected water is immediately equally distributed over the width of the reservoir, which is reasonable for narrow reservoirs. Furthermore, the assumption on the permeability of the pressure drop model has not changed: each layer has a constant permeability k.

The second type concerns a horizontally layered reservoir, where Figure 3.1 depicts the top-view of the reservoir whose layers, separated by thin *vertical* impermeable layers, lie next to one another along the width of the reservoir. The (horizontal) injector and producer are located halfway the height of the reservoir (i.e. $h/2$) and run along the entire width of the reservoir. Injected water is assumed to be immediately equally distributed over the height of the reservoir and the permeability k within the pressure drop model is again assumed constant per layer.

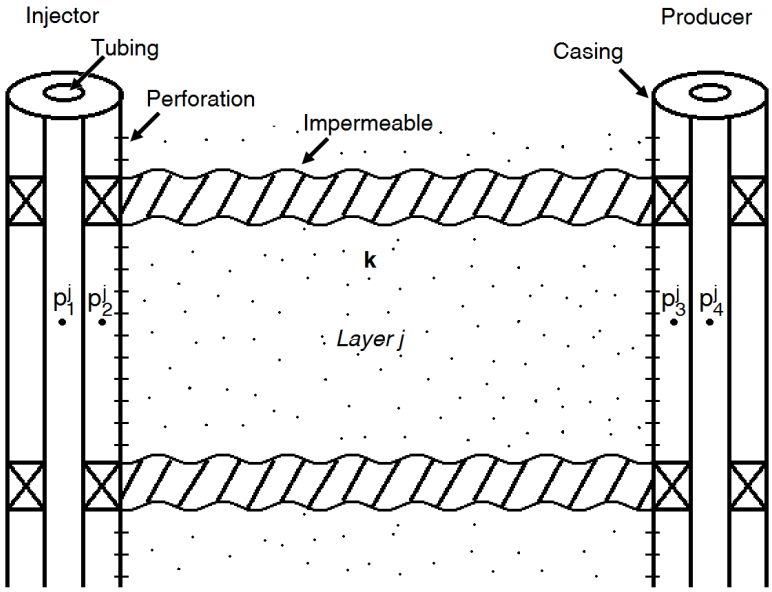

Figure 3.1 - Multi-layered reservoir: four pressure locations per layer

Water that flows from inside the injector into the reservoir pushes oil (and after breakthrough also water) into the producer and consequently changes the pressure distribution over time. In order to facilitate this flow, the injector and producer need to be supplied with a flowrate and/or pressure. However, a pressure assigned to a well may not necessarily be the same as that which the reservoir experiences just on the outside of that well because of a local loss of pressure. Choke valves (introduced in the next section) can mimic this behavior and at the same time provide a means to control flowrates. Therefore, choke valve models are used as inflow control valves (ICV). The pressure drop for layer j (Δp^j) from injector to producer, i.e. $p_1^j - p_4^j$, is then given by

$$\Delta p^j = \Delta p_{chl}^j + \Delta p_{res}^j + \Delta p_{chr}^j \tag{3.1.1}$$

In (3.1.1), the reservoir pressure drop ($p_2^j - p_3^j$) is denoted by p_{res}^j, while the choke valve pressure drop on the left ($p_1^j - p_2^j$) and on the right ($p_3^j - p_4^j$) are respectively denoted by Δp_{chl}^j and Δp_{chr}^j.

3.2 Choke valve pressure drop

This section shortly touches upon flow through restrictions (e.g. a choke valve) and contains excerpts from chapter 5 of the book by Jansen (2016). A restriction in the production process is there either on purpose or not and a can be classified as either a fixed-size or variable-size restriction. When a fixed-size restriction needs to be replaced by another one, the production cycle needs to be either partly or completely halted. Variable-size restrictions, on the other hand, are restrictions that, as the name suggests, can vary in size without halting the production. An example of a variable-size restriction is a choke valve and it deliberately, yet in a controlled fashion, causes a change in flowrate and/or pressure drop. Additionally, a restriction can be used to measure flowrates.

When considering the pressure drop as a result of the left choke valve, there is only a single and (assumed to be) incompressible fluid flowing through it: water. A semi-empirical expression for the pressure drop in incompressible single-phase liquid flow through a (sudden) restriction such as a choke valve is given by the expression

$$\Delta p_{chl}^j = \frac{\rho_w}{2} \frac{(q_t^j)^2}{A_{chl,j}^2} \frac{1}{C_d^2} \tag{3.2.1}$$

where $A_{chl,j} = \pi r_{chl,j}^2$ is the throat area, and C_d is an empirical discharge coefficient often supplied by the manufacturer of the restriction. Note that $q_{t,j}$ is used instead of q_t^j as the incompressibility assumption lead to a spatially constant flowrate (see (2.1.23)).

Equation (3.2.1) can be modified to allow for two-phase flow through the restriction, resulting in a description for the pressure drop due to the choke valve at the producer side:

$$\Delta p_{chr}^j = \frac{1}{2}\frac{(q_{w,j}\rho_w + q_{o,j}\rho_o)}{q_{t,j}}\frac{(q_t^j)^2}{A_{chr,j}^2}\frac{1}{C_d^2} \tag{3.2.2}$$

Or, in terms of fractional flow:

$$\Delta p_{chr}^j = \frac{(f_{w,j}\rho_w + f_{o,j}\rho_o)}{2}\frac{(q_t^j)^2}{A_{chr,j}^2}\frac{1}{C_d^2} \tag{3.2.3}$$

Using the Buckley-Leverett fractional flow model for f_w, expression (3.2.3) can also be expressed in terms of water saturation.

Note that even though C_d is usually not determined for two-phase flow, this parameter is assumed to be the same for two-phase flow as it is for single phase flow.

3.3 Reservoir pressure drop models

In order to find the pressure distribution in the reservoir (or more specifically the pressure drop between the injector and producer well), a reservoir pressure drop formula is derived in this section. Due to the assumption of zero capillary pressure, oil pressure equals water pressure (p_o = p_w) and therefore the subscripts *o* and *w* are dropped when considering pressure.

Starting with the fundamental theorem of calculus, the pressure in the reservoir for time *t* and location *x* can be expressed as follows:

$$\begin{aligned} p^j(x,t) &= p^j(x_{inj},t) - \Delta p_{res}^j(x,t) \\ &= p^j(x_{inj},t) + \int_{x_{inj}}^{x} \frac{\partial p^j}{\partial \hat{x}}\,\mathrm{d}\hat{x}. \end{aligned} \tag{3.3.1}$$

3.3.1 Linear displacement model associated pressure drop

Using Darcy's law for the water phase (equivalently the oil phase could have been used), (3.3.1) for (one-dimensional) linear displacement can be written as

$$p^j(x,t) = p^j(x_{inj},t) + \int_{x_{inj}}^{x} \frac{-q_w^j}{\lambda_{w,j} wh}\,\mathrm{d}\hat{x}. \tag{3.3.2}$$

As q_t is independent of the spatial dimension x, multiplying the integrand with q_t/q_t and using the fractional flow expression from equation (2.1.32) yields

$$p^j(x,t) = p^j(x_{inj},t) - \frac{q_t^j}{wh}\int_{x_{inj}}^{x} \frac{1}{\lambda_{t,j}}\,\mathrm{d}\hat{x} \tag{3.3.3}$$

The integral in (3.3.3) cannot be calculated analytically: while $\lambda_{t,j}$ is a function of saturation and this in turn is a function of *x* (and *t*), the Buckley-Leverett solution (2.1.46) gives *x* as a function of saturation (and *t*). As this is may not be an invertible relation, the integral has to be evaluated numerically through the use of a numerical integration technique, which will be discussed in section 3.3.4.

However, since there is a discontinuity at the shock front, the above formula for pressure has to be manipulated further before it can be integrated numerically. The first and most crucial step is to split the integral in two: one calculating the pressure drop behind and the other ahead of the shock front (x_f). This results in:

$$p^j(x,t) = p^j(x_{inj},t) - \frac{q_t^j}{wh}\left(\int_{x_{inj}}^{\min(x,x_f)} \frac{1}{\lambda_{t,j}}\mathrm{d}\hat{x} + \int_{\min(x,x_f)}^{x} \frac{1}{\lambda_{t,j}}\mathrm{d}\hat{x}\right) \tag{3.3.4}$$

Remembering that the water saturation ahead of the shock front is at initial conditions, meaning λ_t is a constant and equal to $\widehat{\lambda_o}$ (i.e. oil mobility for $S_w = S_{wi}$), the pressure drop can be reformulated as follows:

$$p^j(x,t) = p^j(x_{inj},t) - \frac{q_t^j}{wh}\left(\int_{x_{inj}}^{\min(x,x_f)} \frac{1}{\lambda_{t,j}}\mathrm{d}\hat{x} + (x - \min(x,x_f))\frac{1}{\widehat{\lambda_{o,j}}}\right) \tag{3.3.5}$$

Hence the reservoir pressure drop for layer j is given by

$$\Delta p_{res}^j(t) = \begin{cases} \dfrac{q_t^j}{wh}\left(\displaystyle\int_{x_{inj}}^{x_f} \frac{1}{\lambda_{t,j}}\mathrm{d}\hat{x} + (x_{prod} - x_f)\frac{1}{\widehat{\lambda_{o,j}}}\right), & \text{if } x_f \le x_{prod} \\ \dfrac{q_t^j}{wh}\displaystyle\int_{x_{inj}}^{x_{prod}} \frac{1}{\lambda_{t,j}}\mathrm{d}\hat{x}, & \text{otherwise} \end{cases} \tag{3.3.6}$$

Using the dimensionless coordinate $x_D = \dfrac{\hat{x} - x_w}{l - 2x_w}$, with $x_{inj} = x_w$ and $x_{prod} = l - x_w$, leads to:

$$\Delta p_{res}^j(t) = \begin{cases} \dfrac{q_t^j(l-2x_w)}{wh}\left(\displaystyle\int_0^{x_{Df}} \frac{1}{\lambda_{t,j}}\mathrm{d}x_D + (1 - x_{Df})\frac{1}{\widehat{\lambda_{o,j}}}\right), & \text{if } x_{Df} \le 1 \\ \dfrac{q_t^j(l-2x_w)}{wh}\displaystyle\int_0^1 \frac{1}{\lambda_{t,j}}\mathrm{d}x_D, & \text{otherwise} \end{cases} \tag{3.3.7}$$

3.3.2 Radial-Linear-Radial displacement model associated pressure drop

An approximation for two-dimensional saturation propagation along the inter-well axis has been given in section 2.5 and therefore the pressure (drop) model derived in the previous subsection needs to be adapted to the RaLiRa displacement model.

First of all, Darcy's law as used in the previous section to describe the pressure change is still applicable, though over a smaller interval:

$$\frac{\mathrm{d}p}{\mathrm{d}x} = \frac{-q_t}{\lambda_t wh}, \quad \text{for } x_{ra} \le x \le l - x_{ra} \tag{3.3.8}$$

Secondly, the radial form of Darcy's law for an injector located at x,y-coordinate $(0,w/2)$ is needed. Assuming the radius direction is measured positive in the direction of the flow, means that the pressure change is negative. Since only pressure drop over the inter-well axis is considered, the radial coordinate r is reduced to the coordinate x and hence Darcy's law reads:

$$\frac{\mathrm{d}p}{\mathrm{d}x} = \frac{-q_t}{\lambda_t 2\pi h x}, \quad \text{for } x_w \le x \le x_{ra} \tag{3.3.9}$$

The radial form of Darcy's law is also required for a producer located at $(l,w/2)$. At the inter-well axis, the pressure change is still negative for increasing x and therefore Darcy's law is easily found to be:

$$\frac{\mathrm{d}p}{\mathrm{d}x} = \frac{-q_t}{\lambda_t 2\pi h(l-x)}, \quad \text{for } l - x_{ra} \le x \le l - x_w \tag{3.3.10}$$

Note that in (3.3.8), (3.3.9) and (3.3.10) $q_t \geq 0$ and that the pressure derivatives are continuous at the x-coordinates x_{ra} and l - x_{ra}.

The pressure can now be expressed, following the same procedure as before, as follows:

$$p^j(x,t) = p^j(x_w,t) - \frac{q_t^j}{2\pi h}\int_{x_w}^{\min(x,x_{ra})} \frac{1}{\lambda_{t,j}\hat{x}}\,d\hat{x} - \frac{q_t^j}{wh}\int_{x_{ra}}^{\max(\min(x,l-x_{ra}),x_{ra})} \frac{1}{\lambda_{t,j}}\,d\hat{x} - \frac{q_t^j}{2\pi h}\int_{l-x_{ra}}^{\max(x,l-x_{ra})} \frac{1}{\lambda_{t,j}(l-\hat{x})}\,d\hat{x} \quad (3.3.11)$$

Splitting each of the integrals to account for the location of the shock front results in the expression:

$$\begin{aligned} p^j(x,t) = p^j(x_w,t) &- \frac{q_t^j}{2\pi h}\left(\int_{x_w}^{\min(\min(x,x_f),x_{ra})} \frac{1}{\lambda_{t,j}\hat{x}}\,d\hat{x} + \int_{\min(\min(x,x_f),x_{ra})}^{\min(x,x_{ra})} \frac{1}{\lambda_{t,j}\hat{x}}\,d\hat{x}\right) \\ &- \frac{q_t^j}{wh}\left(\int_{x_{ra}}^{\max(\min(\min(x,x_f),l-x_{ra}),x_{ra})} \frac{1}{\lambda_{t,j}}\,d\hat{x} + \int_{\max(\min(\min(x,x_f),l-x_{ra}),x_{ra})}^{\max(\min(x,l-x_{ra}),x_{ra})} \frac{1}{\lambda_{t,j}}\,d\hat{x}\right) \\ &- \frac{q_t^j}{2\pi h}\left(\int_{l-x_{ra}}^{\max(\min(x,x_f),l-x_{ra})} \frac{1}{\lambda_{t,j}(l-\hat{x})}\,d\hat{x} + \int_{\max(\min(x,x_f),l-x_{ra})}^{\max(x,l-x_{ra})} \frac{1}{\lambda_{t,j}(l-\hat{x})}\,d\hat{x}\right) \end{aligned} \quad (3.3.12)$$

Since the saturation level in each of the right integrals is equal to the initial water saturation, the term λ_t is constant in those integrals and hence the integrals can be analytically evaluated. As the x-coordinate of the producer is $x = l - x_w$, the pressure drop model for the RaLiRa displacement is:

$$\begin{aligned} \Delta p_{res}^j(t) &= p^j(x_w,t) - p^j(l-x_w,t) \\ &= \frac{q_t^j}{2\pi h}\left(\int_{x_w}^{\min(x_f,x_{ra})} \frac{1}{\lambda_{t,j}\hat{x}}\,d\hat{x} + \frac{1}{\widehat{\lambda_{o,j}}}\ln\left(\frac{x_{ra}}{\min(x_f,x_{ra})}\right)\right) \\ &+ \frac{q_t^j}{wh}\left(\int_{x_{ra}}^{\max(\min(x_f,l-x_{ra}),x_{ra})} \frac{1}{\lambda_{t,j}}\,d\hat{x} + \frac{1}{\widehat{\lambda_{o,j}}}(l - x_{ra} - \max(\min(x_f,l-x_{ra}),x_{ra}))\right) \\ &+ \frac{q_t^j}{2\pi h}\left(\int_{l-x_{ra}}^{\max(x_f,l-x_{ra})} \frac{1}{\lambda_{t,j}(l-\hat{x})}\,d\hat{x} + \frac{1}{\widehat{\lambda_{o,j}}}\ln\left(\frac{l-\max(x_f,l-x_{ra})}{x_w}\right)\right) \end{aligned} \quad \text{for } x_f \leq l - x_w \quad (3.3.13)$$

Just as in (3.3.6), the remaining integrals have to be evaluated numerically (see section 3.3.4).

3.3.3 Analytical pressure for a bounded reservoir: a multi-phase approach

While the RaLiRa displacement model of section 2.5 and the associated pressure drop model (3.3.13) might be an improvement for describing (along the inter-well axis) two-dimensional two-phase flow and pressure drop for a reservoir setup as shown in Figure 2.7b, an alternative to (3.3.13) comes from an analytical model for two-dimensional single-phase pressure that accounts for two no-flow boundaries.

Adapting the derivation in Jansen (2016, chapter 7) to the situation depicted in Figure 2.7b, the single-phase pressure in an oil reservoir with a producer well (located at coordinate (l,w/2)) and no-flow boundaries at $y = 0$ and $y = w$ is given by

$$p(x,y,t) = c_0 + \frac{\mu_o q}{k}\frac{1}{4\pi h}\ln\left(\cosh\left(2\pi\frac{x-l}{w}\right) - \cos\left(2\pi\frac{y-\frac{w}{2}}{w}\right)\right) \quad (3.3.14)$$

where $q > 0$ and c_0 is a constant that can be used to define the reservoir pressure.

Since (3.3.14) is a solution of the Laplace equation (a differential equation that is both linear and homogeneous), the principle of linear superposition is applicable and an injection well (located at coordinate (0,w/2)) can simply be added. Hence, (3.3.14) becomes:

$$
\begin{aligned}
p(x,y,t) &= c_0 + \frac{\mu_o q}{k}\frac{1}{4\pi h}\ln\left(\cosh\left(2\pi\frac{x-l}{w}\right)-\cos\left(2\pi\frac{y-\frac{w}{2}}{w}\right)\right) \\
&\quad -\frac{\mu_o q}{k}\frac{1}{4\pi h}\ln\left(\cosh\left(2\pi\frac{x}{w}\right)-\cos\left(2\pi\frac{y-\frac{w}{2}}{w}\right)\right) \\
&= c_0 + \frac{\mu_o q}{k}\frac{1}{4\pi h}\ln\left(\frac{\cosh\left(2\pi\frac{x-l}{w}\right)-\cos\left(2\pi\frac{y-\frac{w}{2}}{w}\right)}{\cosh\left(2\pi\frac{x}{w}\right)-\cos\left(2\pi\frac{y-\frac{w}{2}}{w}\right)}\right)
\end{aligned}
\tag{3.3.15}
$$

Note that when calculating the pressure drop between two coordinates, c_0 will cancel out and hence is of no importance.

Taking the derivative of (3.3.15) with respect to x and simplifying the result, yields an expression that looks similar to the one-dimensional (linear) single-phase form of Darcy's law:

$$
\frac{\mathrm{d}p}{\mathrm{d}x} = -\frac{\mu_o q}{k}\frac{1}{wh}\,f(x,y) \tag{3.3.16}
$$

In (3.3.16) the function $f(x,y)$ is given by

$$
f(x,y) = \frac{1}{2}\left(\frac{\sinh\left(2\pi\frac{x}{w}\right)}{\cosh\left(2\pi\frac{x}{w}\right)-\cos\left(2\pi\frac{y-\frac{w}{2}}{w}\right)} - \frac{\sinh\left(2\pi\frac{x-l}{w}\right)}{\cosh\left(2\pi\frac{x-l}{w}\right)-\cos\left(2\pi\frac{y-\frac{w}{2}}{w}\right)}\right) \tag{3.3.17}
$$

Therefore, for two-dimensional two-phase flow (3.3.16) can be written as

$$
\frac{\mathrm{d}p_\alpha}{\mathrm{d}x} = -\frac{q_\alpha}{\lambda_\alpha}\frac{1}{wh}\,f(x,y) \tag{3.3.18}
$$

Equation (3.3.18) can be interpreted as a modified one-dimensional Darcy law that accounts for the influence of no-flow boundaries on the pressure change in a reservoir with two wells (i.e. see Figure 2.7a). When used in the derivation of the fractional flow expression (equation (2.1.29)), it yields the same fractional flow formula $f_w = \lambda_w/\lambda_t$ (while, importantly, still assuming zero capillary pressure). Hence, also the linear displacement model and RaLiRa displacement model are left unaltered. Consequently, the pressure drop over the (one-dimensional) inter-well axis becomes

$$
\begin{aligned}
\Delta p_{res}^{j}(t) &= \frac{q_t^j}{wh}\int_{x_w}^{l-x_w}\frac{1}{\lambda_{t,j}}\,f\left(x,\frac{w}{2}\right)\mathrm{d}\hat{x} \\
&= \frac{q_t^j}{wh}\left(\int_{x_w}^{\min(x_f,\,l-x_w)}\frac{1}{\lambda_{t,j}}\,f\left(x,\frac{w}{2}\right)\mathrm{d}\hat{x} + \frac{1}{\widehat{\lambda_{o,j}}}\int_{\min(x_f,\,l-x_w)}^{l-x_w} f\left(x,\frac{w}{2}\right)\mathrm{d}\hat{x}\right) \\
&= \frac{q_t^j}{wh}\left(\int_{x_w}^{\min(x_f,\,l-x_w)}\frac{1}{\lambda_{t,j}}\,f\left(x,\frac{w}{2}\right)\mathrm{d}\hat{x} + \frac{-1}{\widehat{\lambda_{o,j}}}\frac{w}{4\pi}\left[\ln\left(\frac{\cosh\left(2\pi\frac{x-l}{w}\right)-1}{\cosh\left(2\pi\frac{x}{w}\right)-1}\right)\right]_{x=\min(x_f,\,l-x_w)}^{l-x_w}\right)
\end{aligned}
\tag{3.3.19}
$$

Obviously, the accurateness of (3.3.19) depends on the accuracy of the estimated displacement, i.e. on the accuracy of the (one-dimensional) linear displacement model and the (one-dimensional) RaLiRa displacement model.

3.3.4 Numeric integration

Because the integrands of the preceding pressure drop models can not be integrated analytically, a numeric integration technique has to be used. Calculating an integral numerically means that the

integrand has to be evaluated at certain points (abscissas) along the *x*-dimension. Preferably a high accuracy is achieved with as few function evaluations (ordinates) as possible.

Classical techniques

Classical techniques such as the trapezoidal rule, Simpson's rule, the five point Newton-Cotes formula, etc. are intuitive in the sense that the integrand is evaluated at equally spaced abscissas. Additionally, if the integrand is a polynomial, exact solutions of degree *n* may exist but often require *n* or *n-1* ordinates. However the integrand in (3.3.7) is not a polynomial and therefore a small number of ordinates would not be sufficient to achieve an accurate approximation of the expression.

The reason that a small number of ordinates are insufficient is that the specified abscissas are not necessarily distributed in an optimal way. Optimally determined abscissas and associated weights (with which ordinates are to be multiplied), often include irrational numbers. Hildebrand (1987) gives, at the start of chapter 8, reasons for using methods that determine optimal abscissas over the classical methods, especially since the advent of computers.

Another consideration while determining which numerical integration technique is to be used to evaluate the reservoir pressure drop is that classical techniques often are closed type formulas, which means they use the endpoints of the integration interval (e.g. the five point Newton-Cotes formula). Up to the moment of breakthrough one of the endpoints of the integration interval in (3.3.7) is the shock front location x_f, where the water saturation is discontinuous. Since the integrand is integrated over x (and thus over the water saturation with a discontinuity at x_f), selecting a method that uses this endpoint x_f could potentially increase the error in calculating the integral. This is circumvented by choosing a method which does not use the endpoints of the integration interval.

Legendre-Gauss Quadrature

As mentioned in the previous section, a numerical integration technique is needed that does not make use of an interval's endpoints. Moreover, it is preferable if no large amount of abscissas and ordinates are required by the method while still being accurate. Only the bare essentials regarding the chosen numerical integration technique are reviewed here (for a detailed derivation see Hildebrand (1987), chapters 7 & 8).

A Gaussian quadrature of order l attempts, by picking l optimally located abscissas, to obtain the best approximation of the integral through means of a weighted average. For an arbitrary function f and for a weight function w it is possible to write:

$$\int_a^b w(x) f(x) \mathrm{dx} = \sum_{n=1}^{l} w_n f(x_n) + E \tag{3.3.20}$$

where x_n is the n^{th} optimally located abscissas, w_n the corresponding weight and E the error.

The Legendre-Gauss Quadrature is a Gaussian quadrature over the interval $[-1,1]$, with the constant weighting function $w(x) = 1$. The abscissas for a quadrature of order l are the roots of the l^{th} Legendre polynomial, $P_l(x)$, for which the following differential recurrence formula holds (Szego, 1967)

$$(1-x^2)P_l'(x) = -lxP_l(x) + lP_{l-1}(x) = (l+1)xP_l(x) - (l+1)P_{l+1}(x) \tag{3.3.21}$$

It follows from (3.3.21) that, since $P_l(x_n) = 0$,

$$(1-x_n^2)P_l'(x_n) = lP_{l-1}(x_n) = -(l+1)P_{l+1}(x_n). \tag{3.3.22}$$

The weights for the Legendre-Gauss Quadrature are given by

$$w_n = -\frac{2}{(l+1)P_{l+1}(x_n)P_l'(x_n)} = \frac{2}{lP_{l-1}(x_n)P_l'(x_n)}, \tag{3.3.23}$$

Using (3.3.22), expression (3.3.23) can be modified to, among others, the following forms

$$w_n = \frac{2}{(1-x_n^2)P_l'(x_n)^2} = \frac{2(1-x_n^2)}{(l+1)^2P_{l+1}(x_n)^2}. \tag{3.3.24}$$

The error term in (3.3.20), though not further considered in this thesis, is given by

$$E = \frac{2^{2l+1}(l!)^4}{(2l+1)[(2l)!]^3} f^{(2l)}(\xi), \tag{3.3.25}$$

Matlab implementation

In determining the abscissas, an initial guess is used as a starting point after which the abscissas are approximated with Newton-Raphson's iterative procedure:

$$x_{j+1} = x_j - \frac{f(x_j)}{f'(x_j)}, \tag{3.3.26}$$

Alternatively, in terms of abscissas x_n and the l^{th} Legendre polynomial:

$$x_{n,j+1} = x_{n,j} - \frac{P_l(x_{n,j})}{P_l'(x_{n,j})}. \tag{3.3.27}$$

Given the first two Legendre polynomials, $P_0 = 1$ and $P_1 = x$, with initial guess $x_{n,0}$, the iterative loop continues until the absolute difference between two consecutive iterations is less than or equal to a preset value. An initial guess for the n^{th} root of the l^{th} Legendre polynomial, which results in fast convergence (Davis and Rabinowitz, 1975) of Newton-Raphson's iterative procedure, is given by

$$x_{n,0} = \cos\left(\pi \frac{n-0.25}{l+0.5}\right) \tag{3.3.28}$$

The l^{th} polynomial value for each of the abscissas $x_{n,j}$ is determined by rewriting the right-hand side equality of (3.3.21) in terms of Legendre polynomials of lower degree. Manipulation of this equality, i.e. $-lxP_l(x) + lP_{l-1}(x) = (l+1)xP_l(x) - (l+1)P_{l+1}(x)$, results in the relationship

$$P_l(x_{n,j}) = \frac{(2l-1)x_{n,j}P_{l-1}(x_{n,j}) - (l-1)P_{l-2}(x_{n,j})}{l} \tag{3.3.29}$$

Additionally, reformulating the left-hand side equality of (3.3.21) yields an expression for $P_l'(x_{n,j})$:

$$P_l'(x_{n,j}) = \frac{-lx_{n,j}P_l(x_{n,j}) + lP_{l-1}(x_{n,j})}{(1-x_{n,j}^2)}. \tag{3.3.30}$$

Combining (3.3.27) with (3.3.28), (3.3.29) and (3.3.30), a new approximate value for each of the abscissas ($x_{n,j+1}$) is iteratively calculated until the convergence criteria, $|x_{n,j+1} - x_{n,j}| \leq \varepsilon$, has been met.

As the Legendre-Gauss quadrature is a Gaussian quadrature over the interval $[-1,1]$, all abscissas lie in the interval $(-1,1)$, whereas this should be (a, b). The values a and b depend on the model in question, the shock front position and on the dimensional/dimensionless formulation. For example for the dimensional formulation of the RaLiRa displacement model: $a = x_w$ and $b = \min(l - x_w, x_f)$. The correct abscissas can be found by using the linear transformation

$$x_n^* = a + \frac{(x_n+1)}{2} \cdot (b-a) \tag{3.3.31}$$

The weights are calculated through use of the left-hand side equality of (3.3.24). Since the weighting function w is equal to one, its integral equals the interval's length and therefore also the sum of the weights w_n should equal the length of the interval. The length of the interval is determined by a and b, hence and the correct formulation of (3.3.24) is

$$w_n = \frac{b-a}{(1-x_n^{*2})P_l'(x_n^*)^2}. \tag{3.3.32}$$

3.3.5 Preliminary results

In this subsection a simulation is carried out to showcase the behavior of the flowrates and the reservoir pressure drop over time. The case considered is that of a two layered reservoir with horizontal wells, where the permeability of one of the layers is twice the permeability of the other (see Table 3.1 for parameters). There are two subcases investigated, *subcase a* and *b*, with *subcase a* using specified total flowrates (per layer) and *subcase b* using a specified reservoir pressure drop. Implementation of both subcases in Matlab is visualized below in Figure 3.2.

For *subcase a*, the total flowrate for each layer is specified upfront and there are no pressure drop constraints imposed. Consequentially, it is always known where the shock front will be and therefore also what the reservoir pressure drop is.

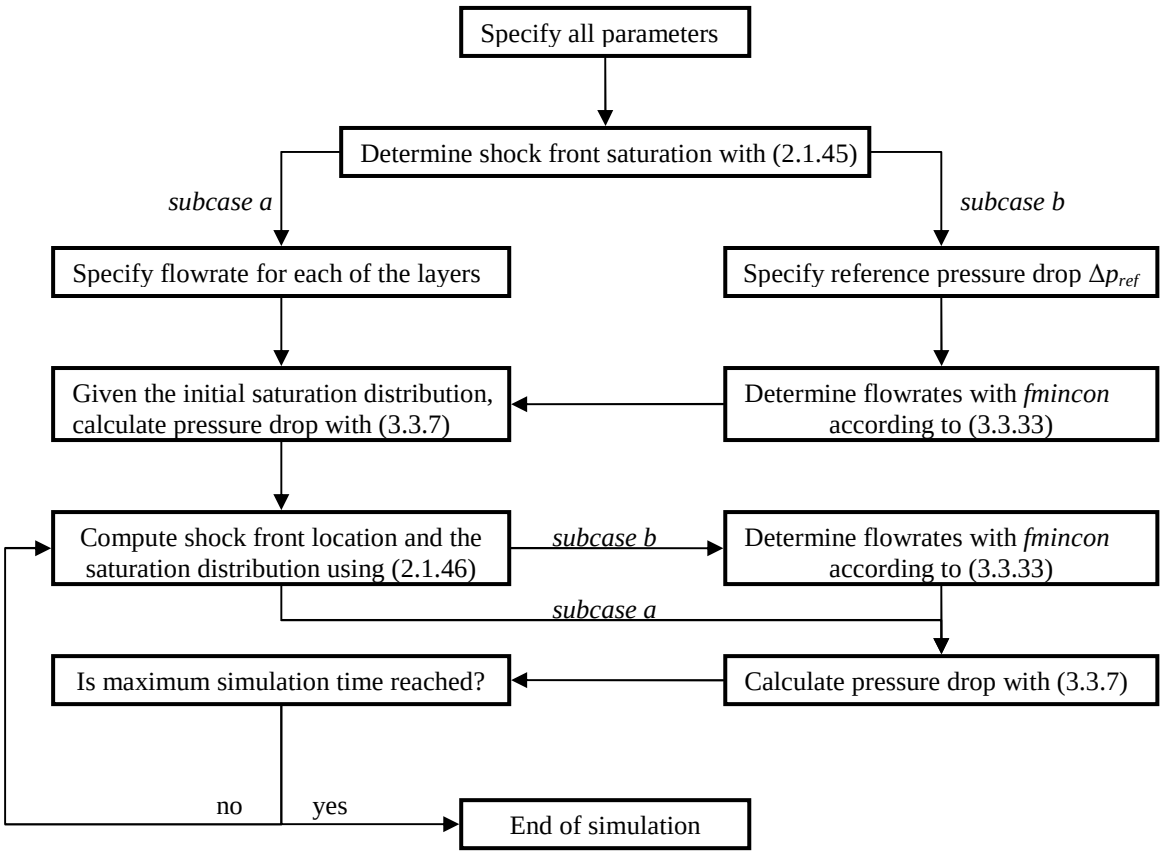

Figure 3.2 - Matlab computational flowchart for the analytical model

In the solution structure for *subcase b* an additional step is required as it assumes that a reservoir pressure drop, dubbed the reference pressure drop (Δp^{ref}), has been specified. At the beginning of each

time step, taking the current saturation distribution into account, flowrates are calculated such that the reservoir pressure drop in each layer at that specific moment satisfies $\Delta p_{res} = \Delta p^{ref}$.

However, since there is only one injector and one producer, also only one injector pressure and one producer pressure can be specified in reality. This in turn implies that the pressure drop of each layer should equal its neighbor's. Alternatively, given the injector pressure, this also means the producer pressures of the layers should be equal to one another. In this reactive approach to the fixed pressures, the flowrates are obtained through Matlab's minimization routine *fmincon*, with aid of its build-in interior-point algorithm. The Euclidean norm is used as the objective function to be minimized.

Furthermore, since it is impossible to inject infinite amounts of water into the reservoir, a condition is added to the minimization problem stating that the sum of the flowrates is not allowed to exceed a certain value. Additionally, to prevent possible cross flow (i.e. flow from producer to injector), each of the flowrates has to be non-negative. Using $\Delta p^0 = \Delta p^{ref}$, the minimization problem for a reservoir consisting of n layers mathematically comes down to

$$\begin{aligned} &\min_{q_t,\,j} \sqrt{\sum_{j=1}^{n} \left(\Delta p^{\,j} - \Delta p^{\,j-1}\right)^2} \\ &\textit{with} \quad \sum_{j=1}^{n} q_t^j \le q_{t,\max} \\ &\textit{and} \quad\quad q_t^j \ge 0 \;\forall j \end{aligned} \tag{3.3.33}$$

Parameter	Symbol	Value	Unit
Initial water saturation	S_{wi}	0.25	-
Residual oil saturation	S_{or}	0.1	-
End-point water rel perm	$k_{rw,0}$	0.5	-
End-point oil rel perm	$k_{ro,0}$	0.9	-
Permeability	k	[600;300]	mD
Corey exponent water	n_w	3	-
Corey exponent oil	n_o	3	-
Viscosity water	μ_w	0.35	cp
Viscosity oil	μ_o	1.9	cp
Reservoir length	l	1000	m
Reservoir width	w	500	m
Reservoir height	h	10	m
Porosity	ϕ	0.25	-
Time step size	dt	100	days
Total time	t	1000	days
# Legendre-Gauss abscissas	-	100	-
Subcase a			
Injection rate	q_t	1500	m^3/day
Injection rate layer j	q_t^j	750	m^3/day
Subcase b			
Pressure drop reference	Δp^{ref}	20	MPa
Maximum total injection rate	$q_{t,max}$	2000	m^3/day
Minimum injection rate layer j	$q_{t,j,min}$	0	m^3/day

Table 3.1 - Preliminary case: parameters

Subcase a - constant flowrates

For the parameters displayed in the table above, the resulting saturation profiles and reservoir pressure drop are shown in Figure 3.3 and Figure 3.4. Since a constant injection rate (750 m^3/day per layer, each 250m wide) is considered, the advance of the saturation profiles is constant over time. Moreover, as in both layers the water is injected at the same rate, the saturation profiles of both layers are identical.

The pressure drop, on the contrary, is neither constant over time (because of the constant injection rate) nor the same for both layers. First of all, the pressure drop is not the same for both layers because the permeability of layer 1 is twice the permeability of layer 2 and because the injection rates are equal. Therefore, the reservoir pressure drop of layer 1 is exactly half the pressure drop of layer 2 (see expression (3.3.7)).

Secondly, the pressure drop is linear over time up to the point of breakthrough (Figure 3.4) because of the constant water injection and the consequentially linear progression of the shock front. After breakthrough has occurred, however, the amount of water in the reservoir no longer increases linearly because evermore water is being produced which causes the pressure drop to no longer be linear. Moreover, as less and less of the lower water saturation values are attained (see Figure 3.3), the reciprocal of the total mobility attains less and less of its higher values, causing the pressure drop to decrease non-linearly over time once breakthrough has occurred.

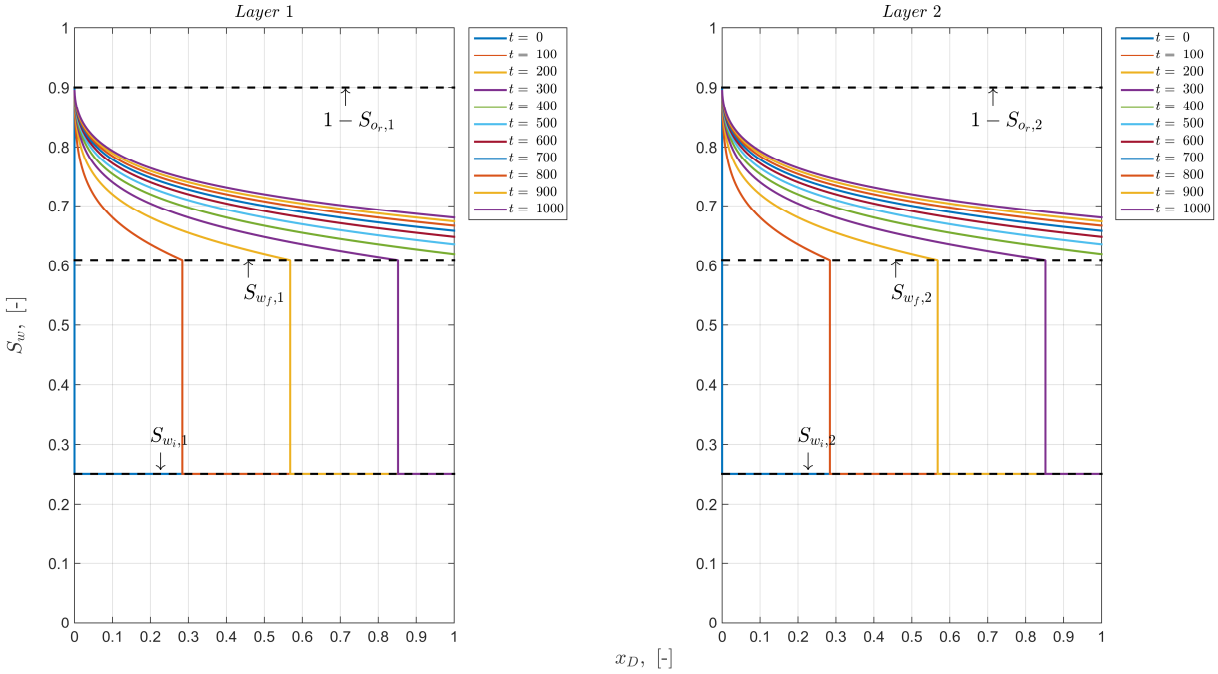

Figure 3.3 - Preliminary case *subcase a*: Saturation profiles over time (in days)

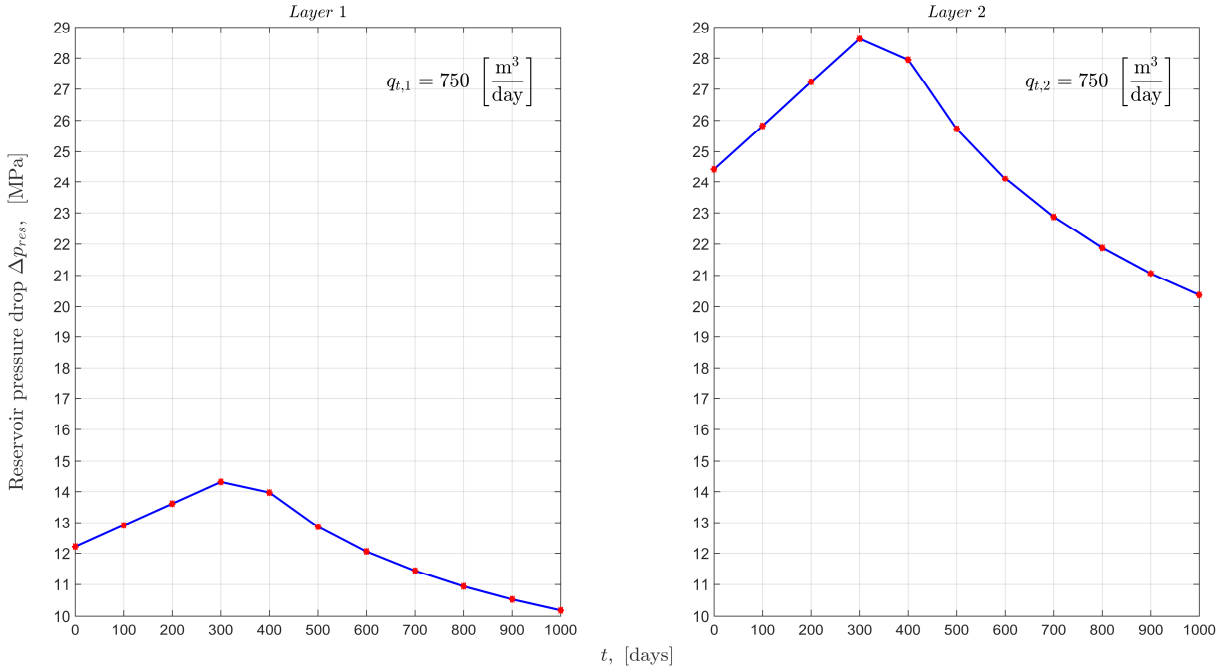

Figure 3.4 - Preliminary case *subcase a*: Reservoir pressure drop

Subcase b - prescribed pressure drop

The key aspect of this subcase is that a reference pressure drop is prescribed as well as that there exists a maximum total flowrate. In order to see the complete behavior of the model (i.e. (2.1.46) and (3.3.7) in combination with (3.3.33)) the values for Δp_{res} and $q_{t,max}$ are conveniently chosen, respectively 20MPa and 2000m^3/day.

The saturation profiles (Figure 3.6) are no longer identical between layers, because the flowrates are different per layer. Moreover, as the flowrate of each layer is no longer constant, the saturation profiles move at different speeds over time. As the permeability of the two layers differ by a factor two, it comes as no surprise that water breakthrough times also differ by a factor two (± 500 days and ± 250 days).

Coincidentally, the maximum total flowrate of 2000m^3/day is reached just after the second water breakthrough. Once this rate has been reached at around 600 days, the seemingly best way to keep the pressure drop of both layers equal (in accordance with (3.3.33)) is to keep the flowrates constant (see Figure 3.5). In *subcase a* the pressure drop behavior for constant flowrates was already investigated: after breakthrough the pressure drop starts decreasing non-linearly. This indeed happens once the maximum total flowrate is reached and the flowrates are kept constant. Moreover, the pressure drop, while equal for both layers, drops almost 25% in 400 days.

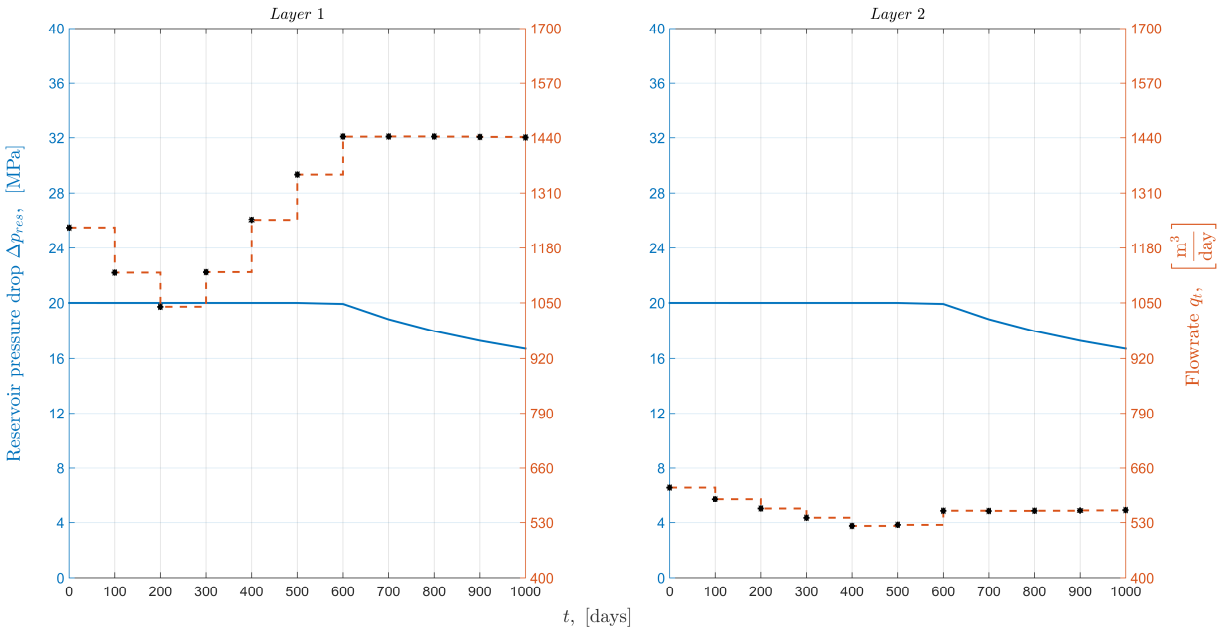

Figure 3.5 - Preliminary case *subcase b*: Reservoir pressure drop and flowrates

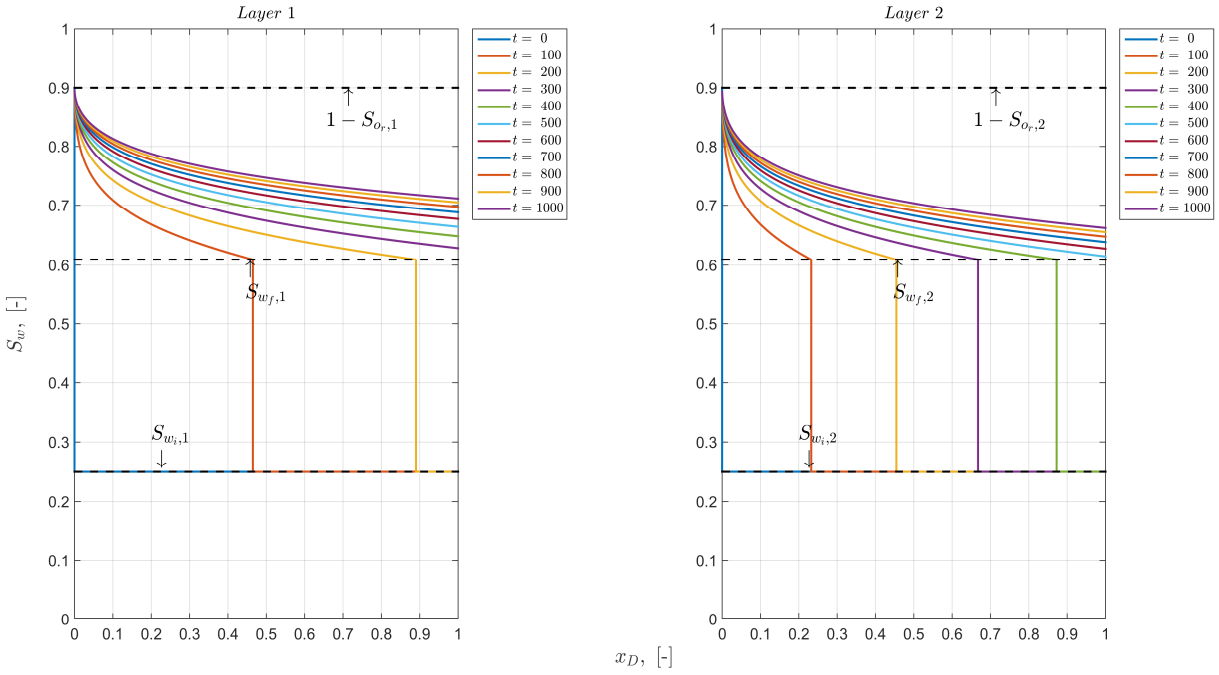

Figure 3.6 - Preliminary case *subcase b*: Saturation profiles over time (in days)

3.4 Controlling two-dimensional flow with the linear displacement model

A prominent question in the use of the linear displacement and pressure model is how useful they are for describing and controlling flow in a reservoir that is being operated with two horizontal wells with flow occurring between the layers. Of course when the real reservoir consists of separate layers of (approximately) constant permeability, the models will work adequately as they were derived for just such a reservoir. Moreover, even if the permeability of a layer strongly varies in the *x*-dimension (i.e. the length of the reservoir) the models can still be used, as the water propagation model is one-dimensional and therefore does not depend on the permeability. The reservoir pressure model, on the other contrary, does depend on the permeability and relies on an accurate estimate of it.

Consider therefore a reservoir existing of n isotropic layers that allow flow between the layers. As the flow in the reservoir is for the most part determined by the pressures p_2^j and p_3^j (see Figure 3.1), it is the linear reservoir pressure drop model (i.e. without choke valve pressure drop) that warrants further investigation. Therefore a wide range of reservoir configurations is tested by varying key parameters to see if two-dimensional flow between layers can be controlled with the (one-dimensional) linear model.

The general parameter investigated is of course the flowrate and for each layer j a distinction is made between the *simulated* flowrate and the *measured* flowrate. The simulated flowrate is defined as the injection rate and the measured flowrate is defined as the production rate at the producer side of the reservoir. The measured flowrate, equal to the simulated flowrate in the eyes of the linear model, are different for the real reservoir as flow between layers occurs. The (beta) ratio of the measured and simulated flowrates (or the production and injection rates), is defined as

$$\beta = \frac{q_{t,1meas}}{q_{t,2\text{meas}}} \Big/ \frac{q_{t,1\text{sim}}}{q_{t,2\text{sim}}} \tag{3.4.1}$$

3.4.1 Permeability

Starting off the analysis is one of the most important and non-controllable aspects of reservoir flow: the reservoir's absolute permeability. The real reservoir, simulated with Sintef's MRST, is assumed to be as simplistic as possible: it exists out of two layers, each with its own constant isotropic permeability that allows flow into the other layer. Another simplification is that each layer is modeled with only one grid cell in the y- and z-dimension. Almost all parameters of Table 3.1 stay the same; those changed or new are displayed in Table 3.2 below.

Parameter	Symbol	Value	Unit
Time step size	dt	10	days
Injection rate layer j	$q_{t,j}$	1000	m^3/day
Number of grid cells in x-direction	nx	500	-
Number of grid cells in y-dimension	ny	2	-
Number of grid cells in z-dimension	nz	1	-
Absolute permeability in all directions [layer 1; layer 2]			
Scenario 1	k	[600;100]	mD
Scenario 2	k	[600;120]	mD
Scenario 3	k	[600;150]	mD
Scenario 4	k	[600;200]	mD
Scenario 5	k	[600;300]	mD
Scenario 6	k	[600;600]	mD
Scenario 7	k	[600;1200]	mD
Scenario 8	k	[600;2400]	mD

Table 3.2 - Permeability analysis parameters

The beta ratio, which simplifies to the ratio of *measured* flowrates because the *simulated* flowrate is equal for both layers, corresponding to the table above is shown in Figure 3.7 from which four phases can be identified.

First of all, the beta ratio in the early production stage is more or less equal to the permeability ratio. Considering that inside the real reservoir a pressure balance is maintained and that in the early production stage there is mostly oil in the reservoir, a production ratio roughly equal to the permeability ratio is congruent with (3.3.7).

Secondly, when the high permeability layer is about to experience water breakthrough, that layer is experiencing a stronger pressure buildup. Consequentially, this causes a drop in the production rate of that layer and therefore a decrease (if $k_1/k_2 > 1$) or an increase (if $k_1/k_2 < 1$) in the beta ratio.

Thirdly, after water breakthrough has occurred in the first layer, the water flows in the direction of least resistance which is the high permeable layer. As more and more water flows in that direction, the beta ratio increases again (decreases if $k_1/k_2 < 1$) and surpasses the initial beta ratio value. More noticeable is that this increase (or decrease) is approximately linear.

Lastly, water breakthrough in the second layer occurs, causing the beta ratio to decreasingly decrease ($k_1/k_2 > 1$) or increase ($k_1/k_2 < 1$). The beta ratios also start heading towards an equilibrium value. In particular, each curve slowly converges back towards its initial value. The reason for this is that if the reservoir is produced for an infinite amount of time, then all the oil will be replaced by water. Consequentially, there is no difference in relative permeability throughout the reservoir, meaning the only difference in flowrates at the producer side is caused by absolute permeability differences.

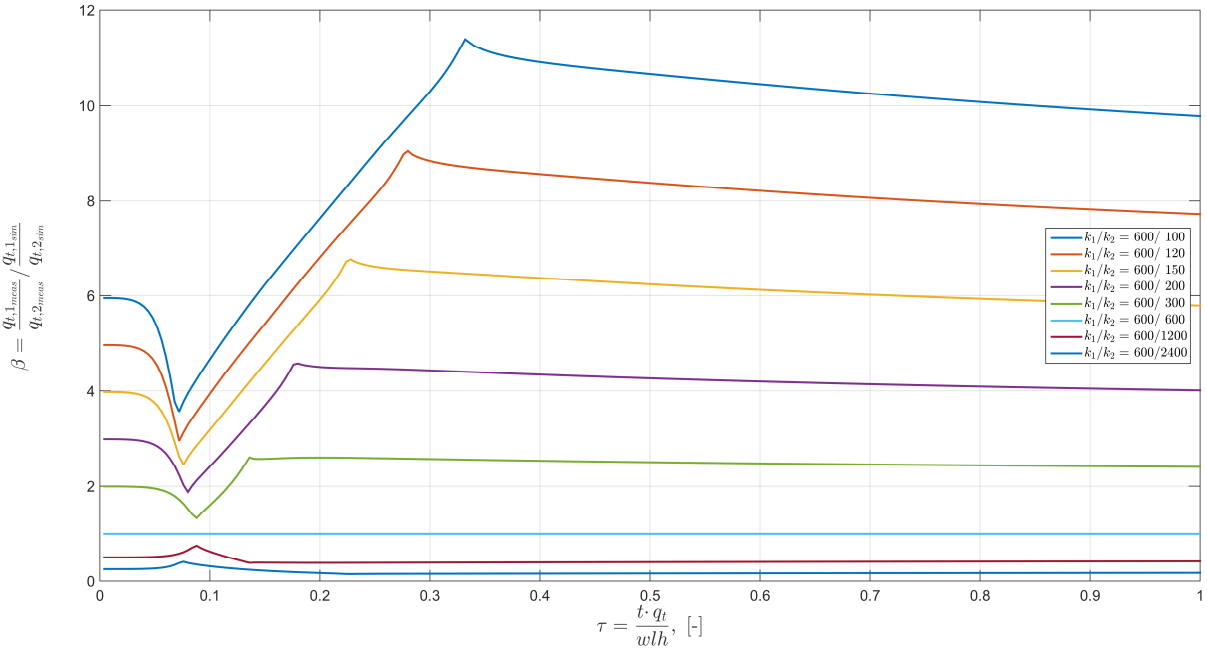

Figure 3.7 - Beta ratio versus dimensionless time for varying permeability ratios

Additionally, the water breakthrough times in Figure 3.7 as well as the time between breakthroughs are different for different permeability ratios. This makes sense when considering that fluid in the low permeability layer flows into the high permeability layer and the stronger the permeability ratio, the stronger this effect. Moreover, as can be seen by comparing permeability ratios 600/300 and 600/1200, breakthrough times are the same for two permeability ratios that are each others reciprocal.

While one might suspect a linear relationship between the permeability ratio and the beta ratio, especially during the early production stage, this is not the case. The figure below exemplifies that

only during the early production process (blue curve) there is a linear relation ship between the two ratios. Once water injection has been going on for quite a while (e.g. 1000 days), that linear relationship is no more.

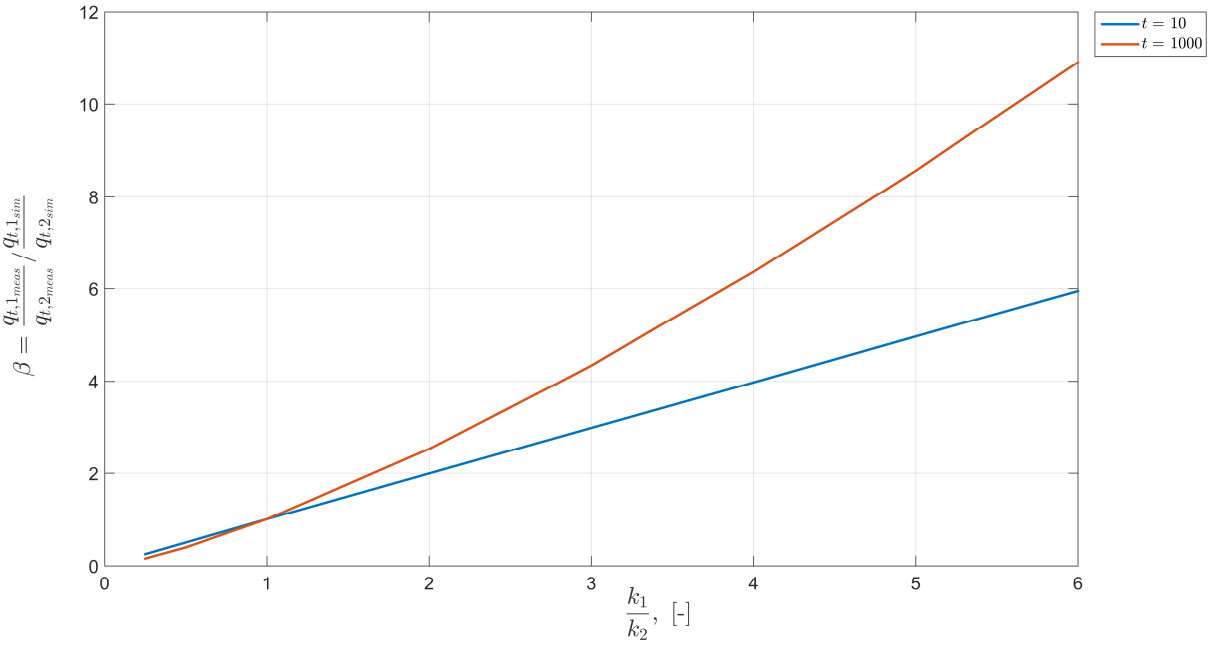

Figure 3.8 - Beta ratio versus permeability ratio

For the remainder of section 3.4, the permeability of the two layers are respectively 600mD and 300mD.

3.4.2 Reservoir length & width

The reservoir considered in the previous subsection was rectangular with width w = 500m and length l = 1000m. The next parameter considered is the reservoir length-to-width ratio, by varying l from 100m to 2500m with increments of 400m. The result is shown below in Figure 3.9.

For a reservoir with length-to-width ratio $l/w << 1$, the beta ratio (with *simulated* flowrate ratio of 1, i.e. equal injection rates per layer) is close to 1. On the other hand, for l/w values larger than 1.4 the beta ratio starts of close to 2, just as one would expect based on the permeability ratio and Figure 3.7. For these larger values the same pattern as before emerges: there is a drop in the beta ratio when approaching the first water breakthrough, whereas between breakthroughs it swiftly increases again up to the point of second breakthrough. After the second breakthrough the beta ratio will slowly go back towards its initial value, though it will require an infinite amount of time.

The difference in results for small and large length-to-width ratios can be explained in a simple way: the larger values, i.e. small values for w and/or large values for l, imply that the layer volume is relatively small compared to the cross-sectional area between the layers, which means that there is ample opportunity for fluid to flow from one layer to another.

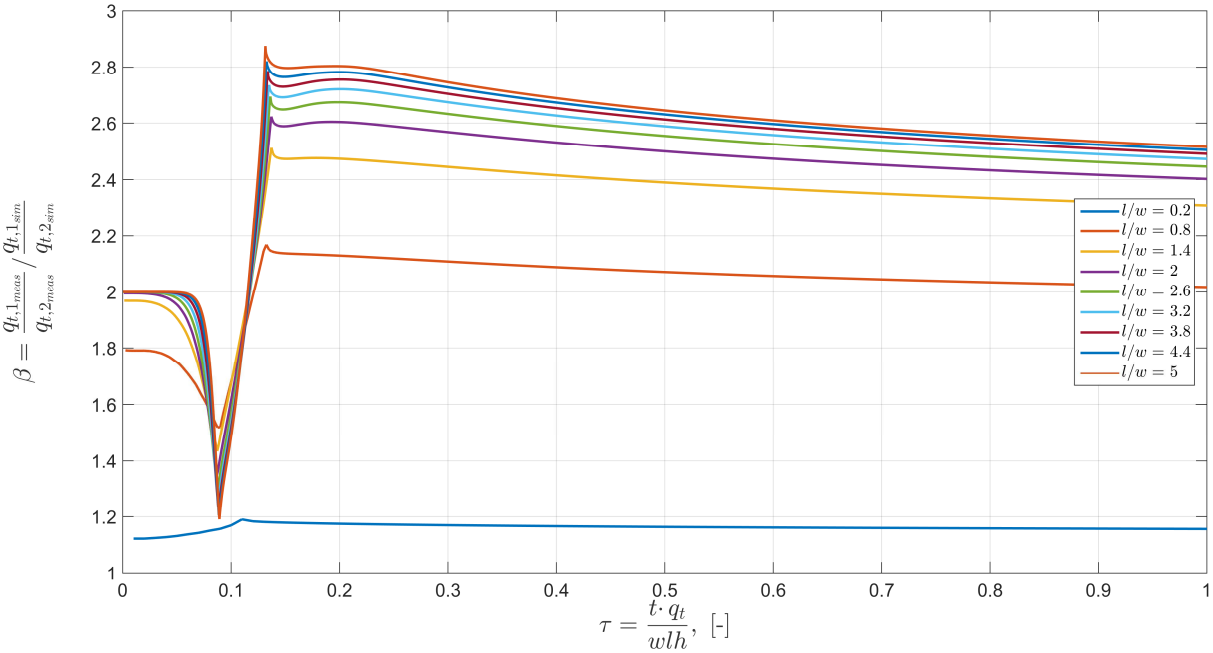

Figure 3.9 - Beta ratio versus dimensionless injected pore volume for length-to-width ratios

While the lower values of the length-to-width ratio in Figure 3.9 above already displayed a non-linear behavior, this is also true for the higher values as can be seen in the figure below. Figure 3.10 below shows the beta ratio for early and late production stages. While in the early stage (10 days) the beta ratio is constant for length-to-width ratios larger than 2, this is no longer the case in the late stage (25.000 days) nor is it linear.

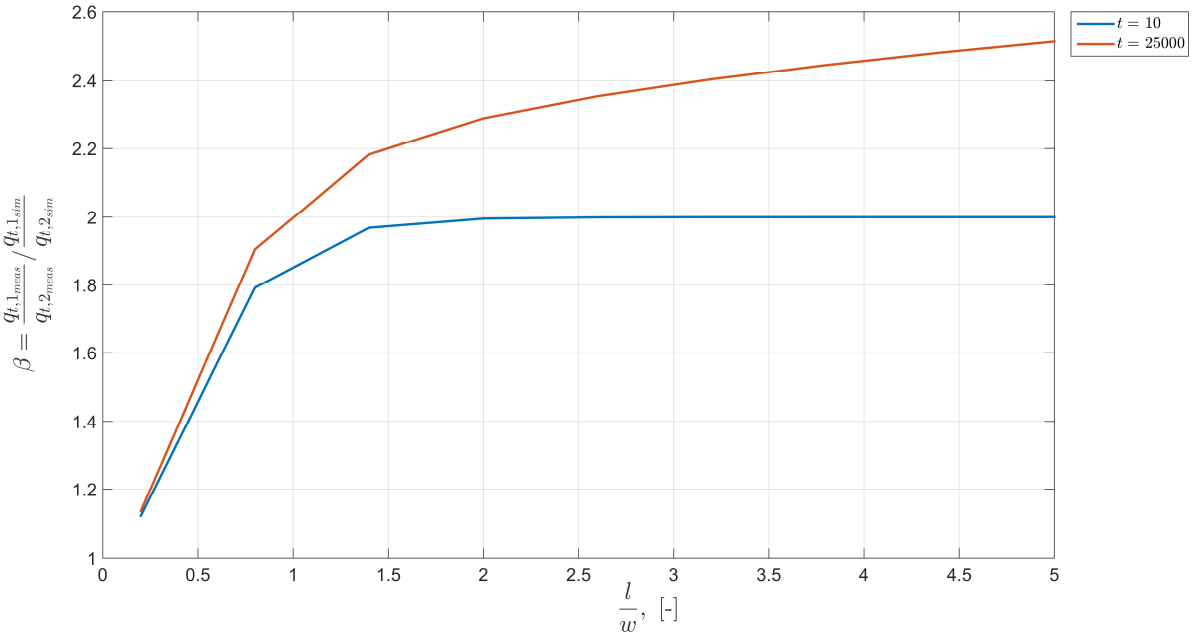

Figure 3.10 - Production ratio versus length-to-width ratios for early and late production stage

3.4.3 Injection rates

Another important, but this time controllable, concept of reservoir flow is the injection rates. In the previous subsection it was held at the arbitrarily chosen value of 1000m^3/day per layer. The general idea is to see if changing this value has any effect on the beta ratio)shown below in Figure 3.11). However, it is no surprise that injecting a different but still equally distributed amount of water has no

effect on the permeability ratio, as it only changes the speed with which the water is injected and distributed over the reservoir.

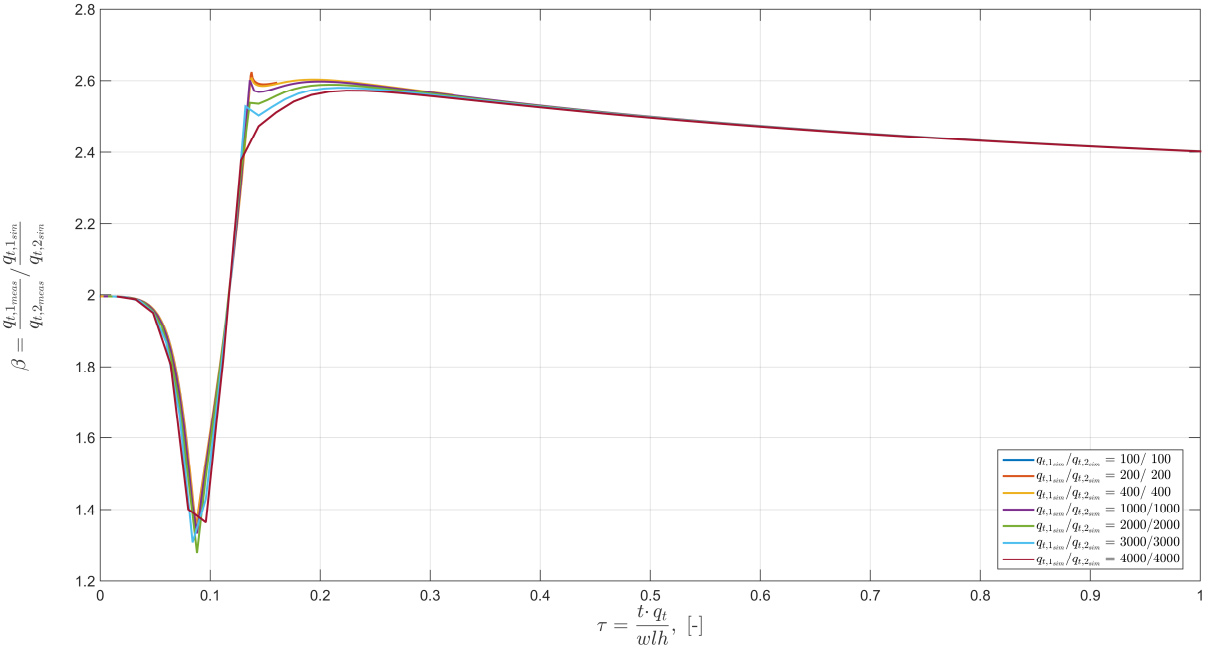

Figure 3.11 - Beta ratio versus dimensionless time for a variety of equal injection rates

A logical extension in trying to understand the flow behavior inside a reservoir, while still focusing on the injection rates, is to keep the injection rate of one layer constant while varying the other (the result of which is shown in Figure 3.12 below). The curve with equal injection rates (purple) starts off at a beta ratio of 2, due to the permeability ratio (see also Figure 3.11). All other curves are a linear scaling of the purple curve due to the different *simulated* flowrate ratios, meaning that different injection rates barely have an effect on the production rates $q_{t,1meas}$ and $q_{t,2meas}$. Hence, varying the injection rates per layer also does not provide control the reservoir's interior.

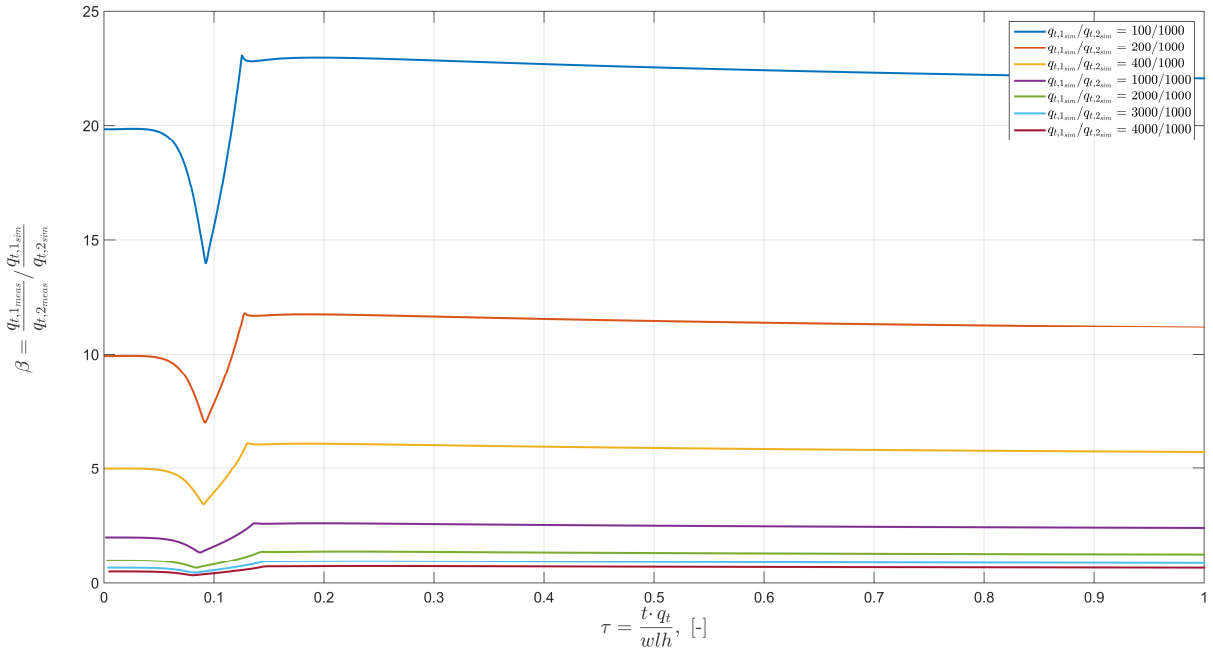

Figure 3.12 - Beta ratio versus dimensionless time for a variety of injection rates

3.4.4 Reservoir pressure drop - Linear displacement

Since choke valves are ignored for the moment, the entire production process is controlled by specifying injection/production rates and/or pressures. Therefore, while keeping the permeabilities of layer 1 and 2 at respectively 600mD and 300mD, the reservoir pressure drop is the next controllable parameter to be analyzed by keeping it at constant levels.

As observed earlier, a constant pressure drop leads to injection rates that are no longer constant over time. Since the flowrates into and out of the reservoir will therefore be different not only over time but also from each other, the focus shifts to the production ratio $q_{t,1meas}/q_{t,2meas}$ (which can be seen as a beta ratio with equal injection rates) in order to keep the analysis as simple as possible.

The figure below shows the production ratio for different levels of constant pressure drop. Comparison with Figure 3.11 reveals that the production ratio is the same in shape as the beta ratio with equal injection rates. The only real difference is in the values attained around and after the second breakthrough (i.e. at $\tau \approx 0.15$).

Because the production ratio is similar for different pressure drop levels, fixing the reservoir pressure drop does not provide control over the flow in the reservoir. Since different flowrates also did not give control over flow inside the reservoir, there is no way to control what happens inside the reservoir while the injector and producer allow flow into and out of every layer in the reservoir. If there is control over which injector/producer sections allow fluid flow, then control over flow in the reservoir becomes possible (e.g. by incorporating ICV's or on-off switches, see Brouwer (2004)).

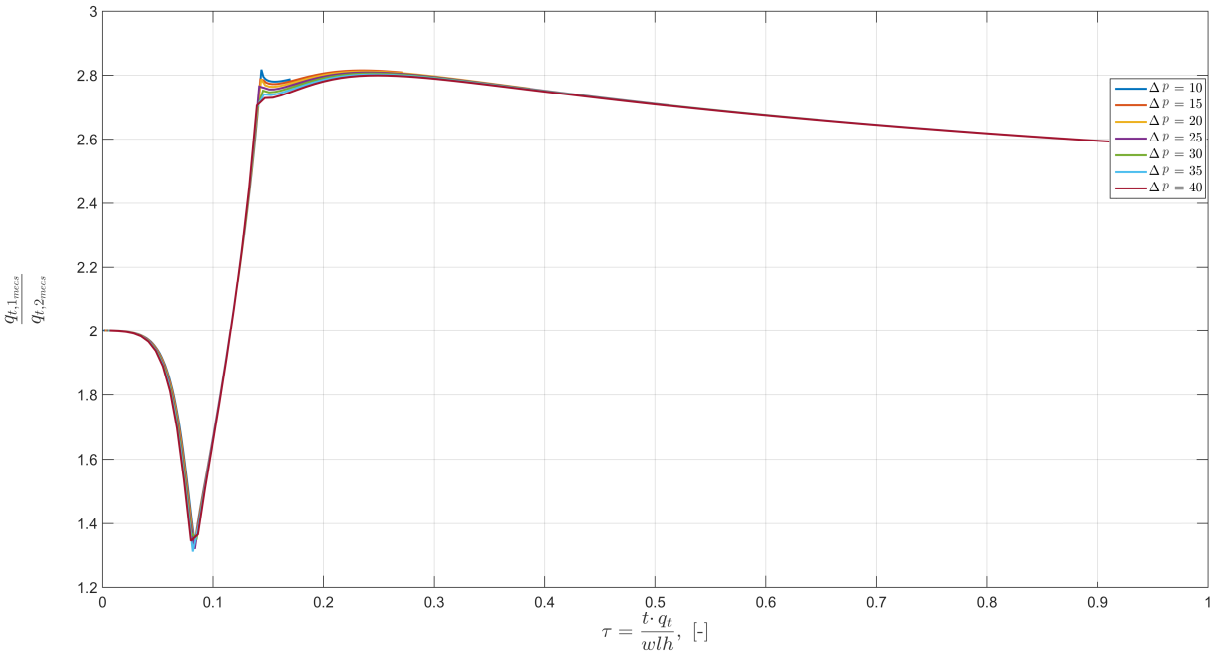

Figure 3.13 - Production ratio versus dimensionless injected pore volume for a variety of pressure drops

3.5 Analysis of the pressure drop model for linear displacement

The previous section focused on the reservoir pressure drop model and concluded in Subsection 3.4.4 that the reservoir pressure drop model does not provide control over flow inside the reservoir. The aim of this section is to briefly analyze the (entire) pressure drop model described in Sections 3.1, 3.2 and 3.3. In the first subsection an analytical formula is derived for the flowrates by assuming a prescribed reference pressure drop. The second subsection derives the asymptotic flowrate for the linear

displacement and pressure model and visualizes the asymptotic behavior of the flowrates and the pressures.

3.5.1 Analytical flowrates

In Subsection 3.3.5 (*subcase b*), a reference pressure drop was supplied and Matlab's *fmincon* determined the appropriate flowrate for each layer. However, if the maximum total flowrate ($q_{t,max}$) has not yet been reached, then these numerically determined flowrates can also be obtained analytically. Alternatively, the analytically determined flowrates can serve as initial guess for the numerical solver.

Starting from (3.1.1) and using (3.2.1), (3.2.3) and (3.3.7), the pressure drop for the j^{th} layer is given by (considering linear displacement and pressure drop):

$$\Delta p^j = \frac{\rho_w}{2}\frac{(q_t^j)^2}{A_{chl,j}^2}\frac{1}{C_d^2} + \frac{q_t^j l}{A_j}\left(\int_0^{\min(1,x_{Df,j})}\frac{1}{\lambda_{t,j}}dx_{D,j} + (1-\min(1,x_{Df,j}))\frac{1}{\widehat{\lambda_{o,j}}}\right) + \frac{(f_{w,j}\rho_w + f_{o,j}\rho_o)}{2}\frac{(q_t^j)^2}{A_{chr,j}^2}\frac{1}{C_d^2} \quad (3.5.1)$$

Every time when new flowrates are to be calculated, all elements of (3.5.1) are already known. This in turn, since the pressure drop has to equal the reference pressure drop (i.e. $\Delta p^j = \Delta p^{ref}$), makes equation (3.5.1) a quadratic equation in q_t^j and therefore easy to solve. However, as the solution will look rather tedious the exact solution is left out of the thesis.

It is important to remark that once $q_{t,\max}$ is reached, one must choose to either keep the flowrates constant (which was the result of the previously mentioned *subcase b*) or to rely again on a numerical solver such as Matlab's *fmincon* routine.

While keeping flowrates constant seems a good way to keep equal pressure drop between layers, it only works when considering reservoir pressure drop. If one or multiple choke valve pressure drop models at the producer side or other complex models are used, then keeping the flowrates constant will most likely not result in nearly identical pressure drops between injector and producer. Hence one might want to use a numerical solver once more. Though it may not be the ideal flowrate guess, since there might no longer be an analytical flowrate solution at this point in the simulation, one could opt to use the previous' iteration flowrates as initial guess for the numerical solver.

3.5.2 Asymptotic pressure and flowrate limit

Producing all the oil from a reservoir (with the exception of the irreducible oil) will take an infinite mount of time because the maximum water saturation ($1-S_{or}$) has zero velocity (see (2.1.46)), making it economically unwise to produce a reservoir ad infinitum. Nevertheless, a still interesting question is what the flowrate of each layer would be ad infinitum.

Assuming that the reservoir is completely filled with water means that the total mobility in the integrand in equation (3.5.1) is constant, i.e. $\lambda_t = \widehat{\lambda_w}$. Additionally, the fractional water flow f_w in the expression equals one, further simplifying it to yet again a quadratic equation in q_t^j:

$$(q_t^j)^2\left(\frac{\rho_w}{2}\frac{1}{A_{chl,j}^2}\frac{1}{C_d^2} + \frac{\rho_w}{2}\frac{1}{A_{chr,j}^2}\frac{1}{C_d^2}\right) + q_t^j\frac{l}{A_j\widehat{\lambda_{w,j}}} - \Delta p^{ref} = 0 \quad (3.5.2)$$

The parameters shown below in Table 3.3 replace some of and are supplementary to the parameters of Table 3.1. Figure 3.14 below shows the oil and water production through the lifetime of the reservoir

and Figure 3.15 displays the pressures from injector to producer, with the injector pressure set at 30MPa and the producer pressure set at 20MPa.

Parameter	Symbol	Value	Unit
Water density	ρ_w	1014	kg m^{-3}
Oil density	ρ_o	859	kg m^{-3}
Discharge coefficient	C_d	0.7	-
Left choke throat area	$A_{chl,j}$	$\pi(0.01/2)^2$	m^2
Right choke throat area	$A_{chr,j}$	$\pi(0.01/2)^2$	m^2
Time step size	dt	10	days
Total time	t	1.000.000	days

Table 3.3 - Asymptotical case: parameters

Breakthrough occurs in the early production stage and causes the oil production rate in Figure 3.14 to drop early on. Correspondingly, the water production rate increases rapidly in the early production stage. However, at one tenth of the total simulation time (i.e. at 100.000 days) both layers are already strongly saturated with water, causing the increase of the water production rate to decrease significantly. Another striking observation is that, due to including choke valve pressure models, the layer limits of water production are close to one another and do not differ by a factor 2, which would be the case if only the reservoir pressure drop model was taken into account.

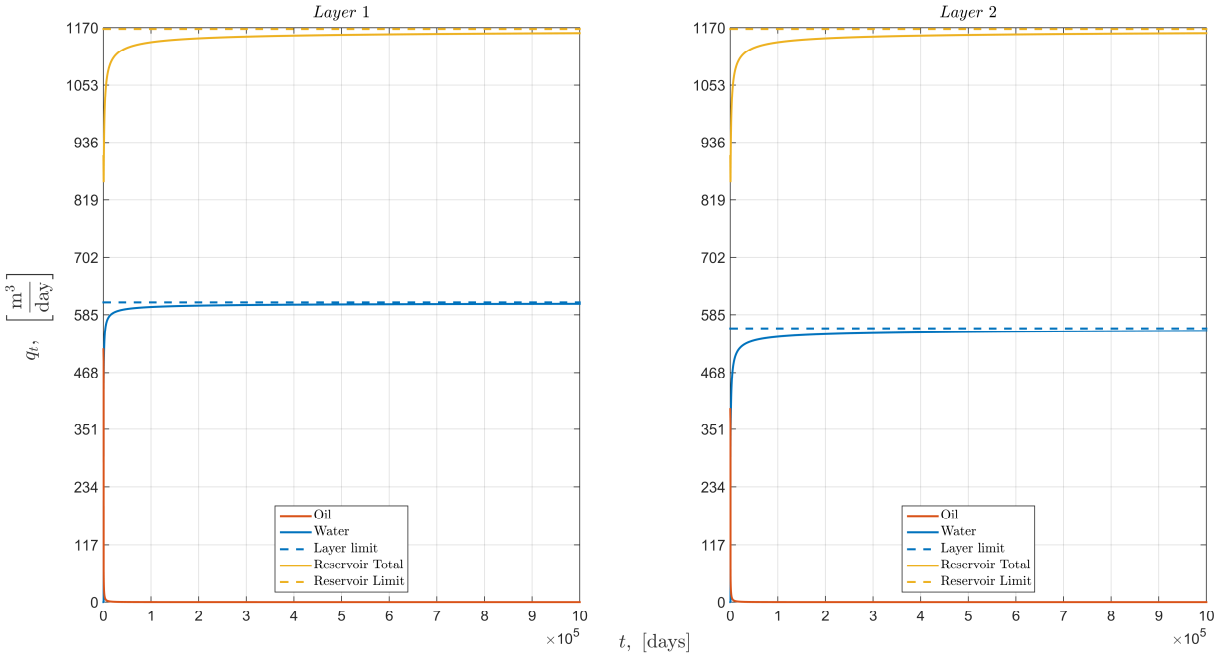

Figure 3.14 - Asymptotical case: production rates

When in *subcase b* the maximum total flowrate of 2000m^3/day was reached, the reservoir pressure drop consequentially declined (see Figure 3.5). In the new setup (i.e. with choke valve pressure models included, see Figure 3.1), however, the reference pressure drop of 10MPa is maintained in each of the layers during the entire simulation which additionally lasts 1000 times longer (Figure 3.15). The reason that reference pressure drop is now maintained, is that the maximum total flowrate of 2000m^3/day is not reached because the incorporated choke valve pressure drop models capture large portions of the prescribed reference pressure drop.

As the water flowrates quickly increased towards their equilibrium in the early simulation time, also the reservoir pressure drop and both the choke valve pressure drops swiftly approach their equilibrium. Moreover, in each layer the asymptotical choke valve pressure drops are equal as their throat areas and discharge coefficients are equal (see (3.5.2)). Lastly, one can conclude from Figure 3.15 below that the reservoir pressure drop decreases asymptotically.

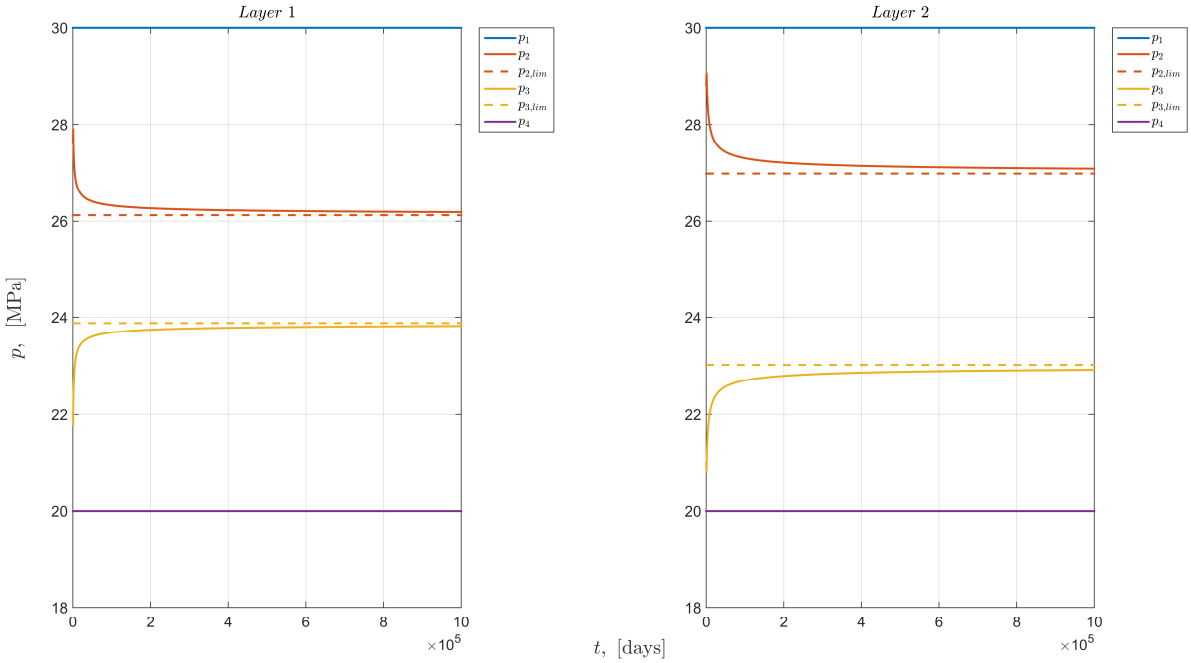

Figure 3.15 - Asymptotical case: pressures

4

Closed-Loop Reservoir Management

In this chapter the analytical propagation and pressure drop models are used during the Closed-Loop Reservoir Management (CLRM) of a reservoir. In the first section CLRM is introduced and briefly explained. The second section investigates the behavior of pressures in the reservoir (i.e. the virtual asset), whereas sections 4.3 up to 4.7 show results for a varying array of CLRM simulations. The last section briefly touches upon computation times.

4.1 Introduction

This section discusses the main concepts of CLRM consecutively: first the virtual asset is treated, followed by data assimilation and finished by net present value optimization.

4.1.1 Virtual asset

The first pillar in CLRM (Figure 1.1) is the measurement of state parameters (e.g. flowrates, pressures). Since no field production data is available, such measurements need to be generated by simulating a real reservoir with Sintef's MRST, i.e. a virtual asset is used to generate measurements. The virtual asset consists of four pressures per layer (labeled the 'truth'), defined as:

$$\begin{aligned} p_{1,true} &= p_{injector} \\ p_{2,true} &= p_{1,true} - \Delta p_{12,true} \\ p_{3,true} &= p_{2,true} - \Delta p_{23,true} \\ p_{4,true} &= p_{3,true} - \Delta p_{34,true} \end{aligned} \tag{4.1.1}$$

While (4.1.1) holds for each layer, in reality there is only one injector and producer. However, the virtual asset requires as many injectors/producers as there are layers, since choke valve models are not included in MRST's options. The pressure supplied to each wellbore pair of the virtual asset hence will be $p_{2,true}$ and $p_{3,true}$.

The pressure drops $\Delta p_{12,true}$ and $\Delta p_{34,true}$ are given by Δp_{chl} and Δp_{chr} as defined in section 3.2. For $\Delta p_{23,true}$, however, no formula is available. Therefore, pressures $p_{2,true}$ and $p_{3,true}$ are obtained by solving minimization problem (3.3.33) for $q_{t,j}$, with the total pressure drop of a layer given by:

$$\Delta p^j_{true} = \frac{\rho_w}{2}\frac{(q_t^j)^2}{A^2_{chl,j}}\frac{1}{C_d} + p^j_{2,true}(q_t^j) - p^j_{3,true}(q_t^j) + \frac{(f_{w,j}\rho_w + f_{o,j}\rho_o)}{2}\frac{(q_t^j)^2}{A^2_{chr,j}}\frac{1}{C_d} \tag{4.1.2}$$

However, as a measurement is rarely 100% accurate, an error is added to each of the true pressures of (4.1.1). Error vector ε^j is assumed to be Gaussian white noise, hence the the j^{th} layer measured are:

$$p^j_{meas} = p^j_{true} + \varepsilon^j, \quad \text{with } \varepsilon^j \sim N(0, P_y) \tag{4.1.3}$$

where for p^j_{true} is a row vector containing $p^j_{1,true}$ up to $p^j_{4,true}$ and P_y the covariance matrix of layer *j*. The variance of each p_{true} is assumed to be equal, i.e. P_y is a constant times the identity matrix.

4.1.2 Data assimilation

Next, the measured pressures are used to update the predicted pressures of the analytical models by estimating for each layer the permeability and the flowrate of the preceding time step. Additionally, the Net Present Value (see section 4.1.3) is updated from the predicted value to an estimated value based on the newly updated analytical models.

Since the reservoir considered exists of two layers, there are only four parameters to be estimated. Such a small number of parameters can be efficiently estimated with Matlab's *fmincon* routine, hence there is no need for intricate data assimilation techniques. At the end of time step *n*, the parameters can be found by minimizing for each layer:

$$\min_{k,q_t} J^n$$
$$J^n = (d^n - y^n)^T P_y^{-1} (d^n - y^n) + (k^n - k^0)^T P_k^{-1} (k^n - k^0) \tag{4.1.4}$$

The vectors d^n and y^n in expression (4.1.4) are respectively the measured and estimated pressures, whereas P_y is the covariance matrix from expression (4.1.3) that describes the uncertainty in the measured pressures. Parameters k and k^0 are the current and initial permeability estimate, while P_k is the variance matrix describing the uncertainty in the initial permeability estimate of a layer.

4.1.3 Net Present Value maximization

The last pillar of CLRM concerns maximizing the profit, i.e. maximizing the Net Present Value (NPV). NPV is defined as the sum of all (discounted) future cash flows, i.e. the NPV of a reservoir is today's value of future money.

The NPV depends on the monetary value of oil (r_o^p), the cost of water injection and production (r_w^i, r_w^p), and on the flowrates in each producer and injector (q_o^p, q_w^i and q_w^p). Since no gas resides in the reservoir oil, the oil volume at reservoir conditions is approximately equal to the volume at surface conditions, hence the oil formation volume factor ($B_o = V_{o,res} / V_{o,surf}$) is taken equal to one. The size of a time step (Δt_n) as well as the discount factor influence the NPV. The discount factor depends on the discount rate (*b*), i.e. the rate with which the value of money changes over a reference time period, and on the time factor $\tau_n = \sum_{k=1}^{n} \Delta t_k / \tau_{ref}$ (with τ_{ref} the reference time period of *b*).

The *estimated* Net Present Value at the end of time step *n* can be expressed as

$$J^n_{est} = J^{n-1}_{est} + \frac{\sum_i r_w^i (q^i_{w,est})_{n-1} + \sum_p r_o^p (q^p_{o,est})_{n-1} + r_w^p (q^p_{w,est})_{n-1}}{\left(1 + \frac{b}{100}\right)^{\tau_{n-1}}} \Delta t_{n-1} \tag{4.1.5}$$

Therefore, at the *start* of time step *n* (with $1 \le n \le N$), the *predicted* Net Present Value at the end of the *final* time step (*N*) can be expressed as:

$$J^N_{pred} = J^{n-1}_{est} + \sum_{m=n-1}^{N-1} \frac{\sum_i r_w^i (q^i_{w,pred})_m + \sum_p r_o^p (q^p_{o,pred})_m + r_w^p (q^p_{w,pred})_m}{\left(1 + \frac{b}{100}\right)^{\tau_m}} \Delta t_m \tag{4.1.6}$$

Note that due to incompressible flow and one injector-producer pair per layer (j) it is possible to write $q_w^i = q_o^p + q_w^p = q_w^j$. Also assuming constant time step sizes ($\Delta t_m = \Delta t$), reduces (4.1.6) to:

$$J_{pred}^{N} = J_{est}^{n-1} + \sum_{m=n-1}^{N-1} \sum_{j=1}^{N_{layers}} \frac{r_o \cdot (q_{o,pred}^{j})_m + r_w (q_{w,pred}^{j})_m}{\left(1+\frac{b}{100}\right)^{\tau_m}} \Delta t \tag{4.1.7}$$

where $r_o = r_o^p + r_w^i$ is the net oil revenue, $r_w = r_w^p + r_w^i$ is the net water cost, $\tau_m = m \cdot \Delta t / \tau_{ref}$, and q_o and q_w are the producer flowrates.

Moreover, maximizing (4.1.7) for the remaining $N - (n-1)$ time steps is equivalent to minimizing

$$J_{pred}^{n} = -\sum_{m=n-1}^{N-1} \sum_{j=1}^{N_{layers}} \frac{r_o (q_{o,pred}^{j})_m + r_w (q_{w,pred}^{j})_m}{\left(1+\frac{b}{100}\right)^{\tau_m}} \Delta t \tag{4.1.8}$$

In order to minimize expression (4.1.8), the choice once again falls to Matlab's *fmincon* routine, as the number of variables is relatively small. If, however, multiple injector and producer wells are used to produce a reservoir or if the reservoir consists of a large number of layers, the routine can easily become computationally intensive. Hence other methods to minimize (4.1.8) will then need to be considered, such as gradient-based optimization methods (e.g. adjoint-based gradient computation). For example, Suwartadi (2012) applied gradient-based optimization to address output constraint problems (e.g. limiting water production), whereas Brouwer (2004) used gradient-based optimization to, among other, optimize the NPV of a reservoir operated by an array of injectors and producers that could be switched on and off at any time.

Minimizing (4.1.8) is achieved by maximizing the total flowrate of each layer ($q_t^j = q_o^j + q_w^j$), which in turn is accomplished by fully opening the injector and producer inflow control valves (i.e. the choke valves) and, if adjustable, setting the producer pressure to the lowest possible value. After breakthrough, the inflow control valves can be used to reduce a layer's production until it is no longer profitable and a layer should be closed off (i.e. as soon as $r_o q_{o,pred}^j \leq |r_w| q_{w,pred}^j$ or $r_o q_{o,est}^j \leq |r_w| q_{w,est}^j$).

Note that *if* there is a restriction on the maximum flowrate ($q_t = \sum q_t^j \leq q_{t,\max}$), then expression (4.1.8) should be used to maximize the NPV. On the other hand, when there is no restriction on q_t, the aforementioned considerations imply that (4.1.8) can be further reduced to

$$J_{pred}^{n} = -\sum_{j=1}^{N_{layers}} \frac{r_o (q_o^j)_n + r_w (q_w^j)_n}{\left(1+\frac{b}{100}\right)^{\tau_n}} \Delta t \tag{4.1.9}$$

Maximizing the NPV by controlling the flowrates of each layer as described above is known as *predictive* (or proactive) control. An alternative approach is *reactive* control, which entails a simple on-off approach to oil production: the entire producer is shut down once the economic threshold is exceeded (i.e. $r_o \sum_j q_{o,est}^j \leq |r_w| \sum_j q_{w,est}^j$ as there are no ICV's).

While reactive control may be reasonably effective for a reservoir being operated by multiple injector and producer wells, it is not the best strategy for the reservoir under consideration. The reason is that it can lead to a situation where it is still profitable to continue the production process, while the economic threshold has already been reached in some layers. Consequentially, potential profit is lost since either all layers are continued to be produced from (including the no longer profitable ones) or production is completely halted.

4.2 Virtual asset simulations

Supplying a constant injector/producer pressure and constant choke valve settings to the virtual asset, this section investigates the behavior of the resulting (true) pressures. The (rectangular) reservoir is being operated by either horizontal or vertical wells.

4.2.1 Horizontal wells

The reservoir consists of two layers positioned next to one another along the width of the reservoir, implying a horizontal injector/producer pair (see Table 4.1 for parameters). As each layer is located at a depth of 3000m, resulting in an injector pressure of 30MPa. The producer pressure is set at 20MPa, resulting in the Δp^{ref} of 10MPa. The standard deviation of the (white Gaussian) measurement noise (see (4.1.3)) for each of the true pressures is set at 5% of the injector pressure, i.e. 1.5MPa.

Although Table 4.1 includes the number of Legendre-Gauss abscissas, this section does not consider data assimilation and NPV optimization. Moreover, as there are only two grid cells in the *y*-direction and the reservoir is 500m wide, each layer contains one grid cell in the y direction with width 250m.

General parameters			
Parameter	*Symbol*	*Value*	*Unit*
Water density	ρ_w	1014	kg m^{-3}
Oil density	ρ_o	859	kg m^{-3}
Initial water saturation	S_{wi}	0.25	-
Residual oil saturation	S_{or}	0.1	-
End-point water rel perm	$k_{rw,0}$	0.5	-
End-point oil rel perm	$k_{ro,0}$	0.9	-
Permeability	k	[600;300]	mD
Corey exponent water	n_w	3	-
Corey exponent oil	n_o	3	-
Viscosity water	μ_w	0.35	cp
Viscosity oil	μ_o	1.9	cp
Reservoir length	l	1000	m
Reservoir width	w	500	m
Reservoir height	h	10	m
Porosity	ϕ	0.25	-
Time step size	dt	10	days
Total time	t	1000	days
Pressure drop model specific parameters			
# Legendre-Gauss abscissas	-	100	-
MRST specific parameters			
Number of grid cells in *x*-direction	nx	100	-
Number of grid cells in *y*-dimension	ny	2	-
Number of grid cells in *z*-dimension	nz	1	-
Choke parameters			
Discharge coefficient	C_d	0.7	-
Left choke throat area	$A_{chl,j}$	$\pi(0.01/2)^2$	m^2
Right choke throat area	$A_{chr,j}$	$\pi(0.01/2)^2$	m^2
fmincon **conditions**			
Pressure drop reference	Δp^{ref}	10	MPa

Maximum total injection rate	$q_{t,\max}$	2000	m^3/day
Minimum injection rate layer j	$q_{t,\min}^{j}$	0	m^3/day
Measurements			
Noise mean	μ_i^j	0	MPa
Noise standard deviation	σ_i^j	1.5	MPa

Table 4.1 - Virtual asset simulation for horizontal wells: parameters

Figure 4.1 below shows for each layer both the resulting producer flowrates and the reservoir total flowrate, as well as the (theoretical) maximum layer and reservoir flowrate. The flowrates are almost linear with exception of water breakthrough and initial moments. At breakthrough, water and oil production rates suddenly in- and decrease respectively and can even be detected in the reservoir total rate (a sudden yet small decrease). However, the more layers there are in reservoir, the smaller the impact of a single breakthrough on the reservoir total rate.

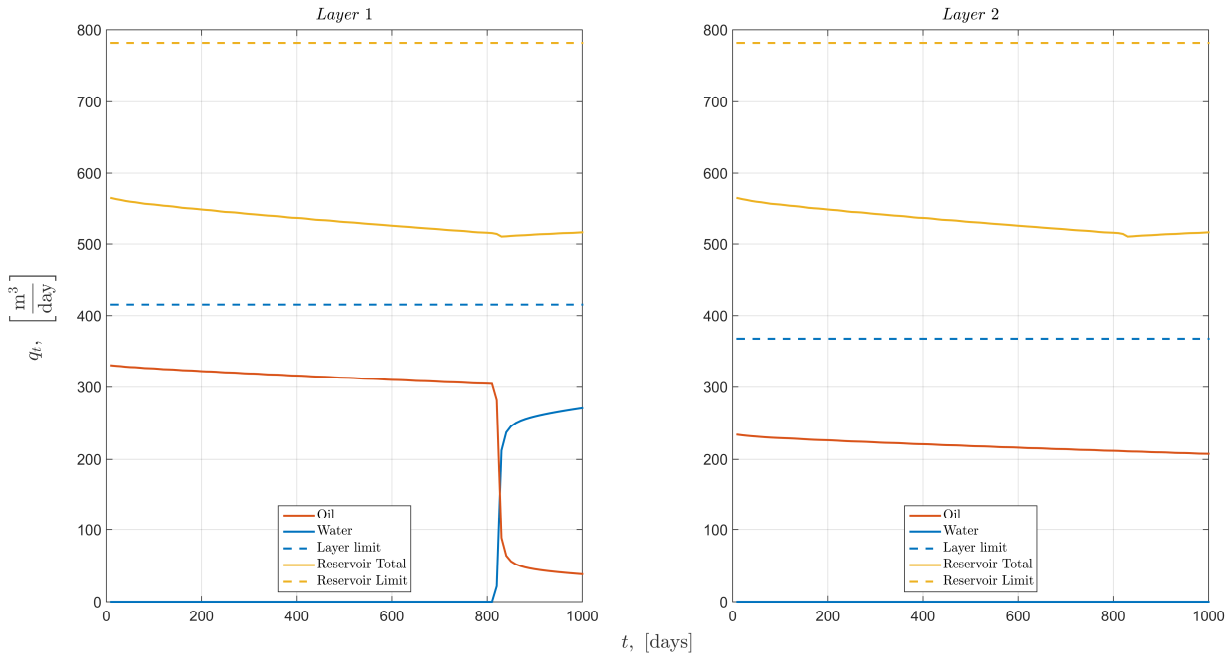

Figure 4.1 - Horizontal wells: flowrates

Both true and measured pressures corresponding to the above flowrates are shown in Figure 4.2. As the maximum flowrate is not reached, the reference pressure drop of 10MPa is easily maintained, meaning $p_{4,true}$ stays equal to 20MPa. While pressure $p_{3,true}$ behaves similar to the flowrates, $p_{2,true}$ does the exact opposite: with the exception of initial and water breakthrough moments, it increases linearly up to the point of breakthrough and decreases again afterwards.

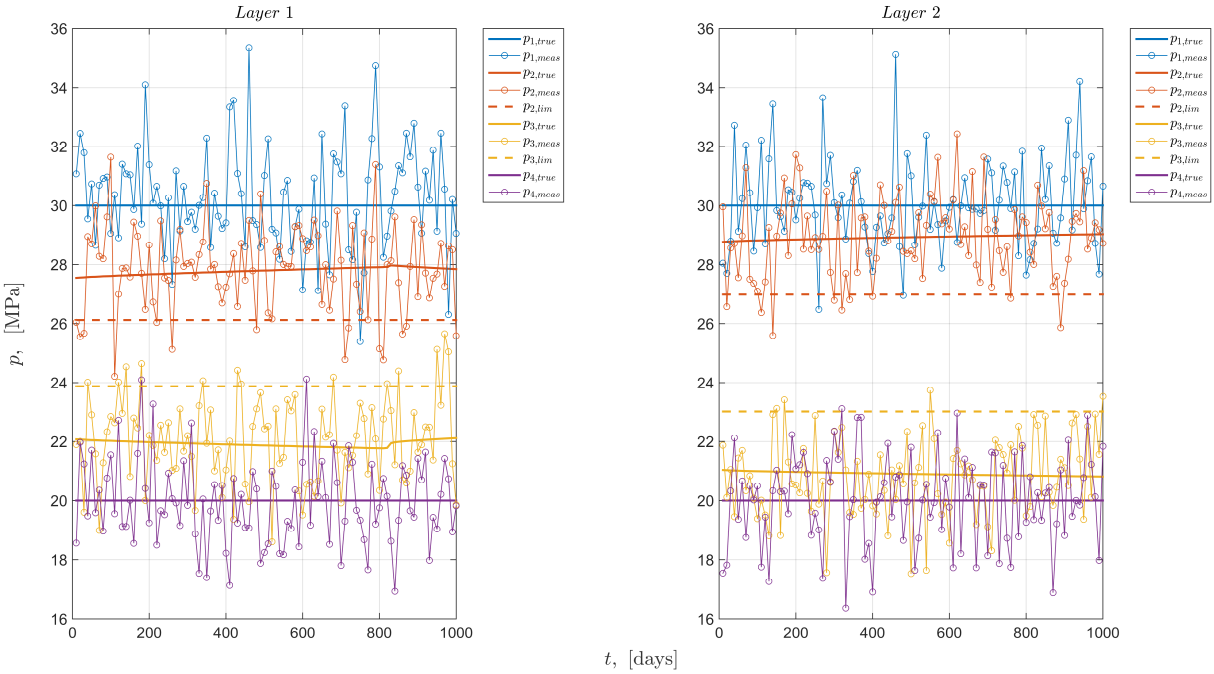

Figure 4.2 - Horizontal wells: *true* & *measured* pressures

The definition of the true pressures (see (4.1.1)) always ensures that $p_{1,true} \geq p_{2,true} \geq p_{3,true} \geq p_{4,true}$. Contrarily, as there are no conditions on the measurement noise, there are multiple occurrences where the measured pressures are inconsistent with one another (e.g. $p_{1,meas} \leq p_{2,meas}$ and/or $p_{3,meas} \leq p_{4,meas}$ while also $p_{2,meas} \geq p_{3,meas}$). These inconsistencies are more likely to occur in low permeability layers (see Figure 4.2). Considering the total pressure drop expression (4.1.2), one can explain this: compared to a high permeability layer with an identical reference pressure, a lower permeability layer should experience lower flowrates (Figure 4.1) and a higher reservoir pressure drop (due to the choke valve expressions). This in turn causes pressures $p_{1,true}$ and $p_{2,true}$ as well as $p_{3,true}$ and $p_{4,true}$ to be closer to one another, making it likelier for inconsistencies to occur once the measurement error is added.

Reaching maximum total flowrate

In order to understand the behavior of flowrates and pressures under maximum flowrate conditions, the maximum flowrate is adjusted (based on Figure 4.1) such it is already reached in the early production stage (see Table 4.2). Note that the theoretical flowrate limits do not change.

fmincon **conditions**			
Maximum total injection rate	$q_{t,max}$	550	m^3/day

Table 4.2 - Attaining maximum flowrate (horizontal wells): adjusted parameters

Figure 4.3 below shows the resulting flowrates and it is immediately clear that the reservoir total flowrate is equal to the maximum flowrate of 550m^3/day. Simultaneously, the production rate during this stage is nearly constant per layer. After 200 days the maximum flowrate is no longer attained and the flowrates are similar to those in Figure 4.1. Comparing Figure 4.1 with Figure 4.3 even reveals that there is hardly any difference between the moment of water breakthrough because of the small difference in the production rate.

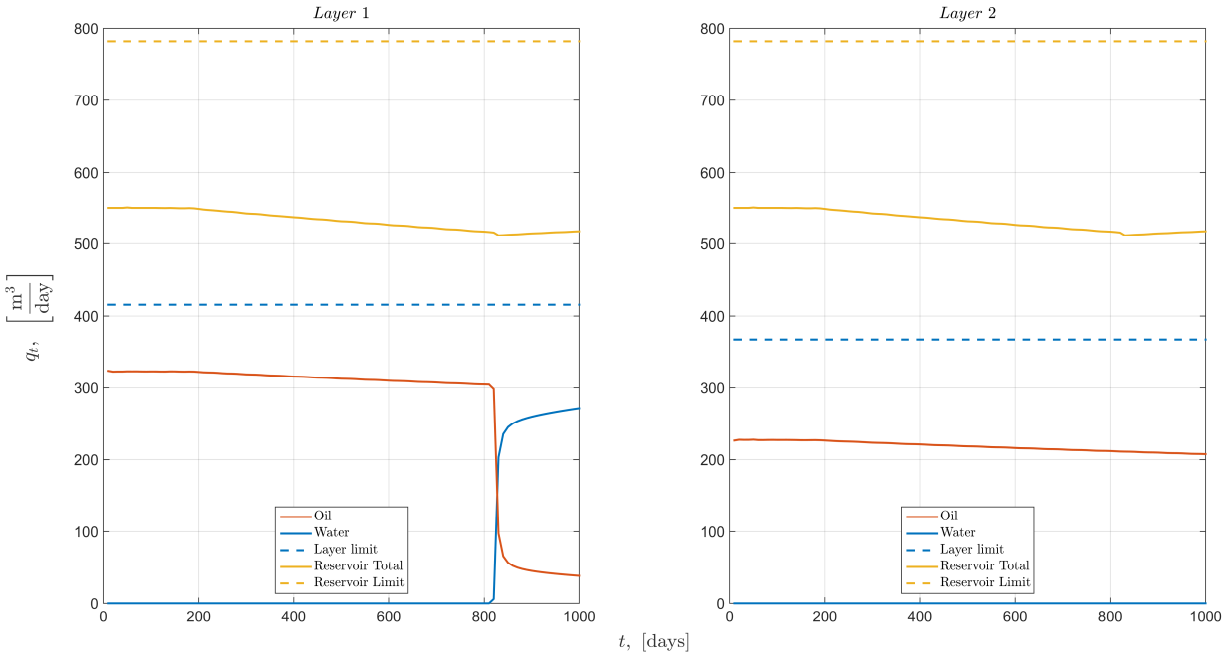

Figure 4.3 - Attaining maximum flowrate (horizontal wells): flowrates

Due to the way the pressures are calculated (expression (4.1.1)), the pressure $p_{1,true}$ always equals its prescribed value of 30MPa. Additionally, pressure $p_{2,true}$ of each layer is initially constant due to the constant total flowrate of each layer. Pressures $p_{3,true}$ and $p_{4,true}$, however, start off at a higher value than their counterparts in Figure 4.2 due to having reached the flowrate limit. The constant flowrates result in a constant choke valve pressure drop, causing $p_{3,true}$ and $p_{4,true}$ to differ only by a constant. Consequently, pressures $p_{4,true}$ can not maintain their preset value of 20MPa. Once the flowrates drop below maximum, however, the pressure profiles are again similar to those in Figure 4.2.

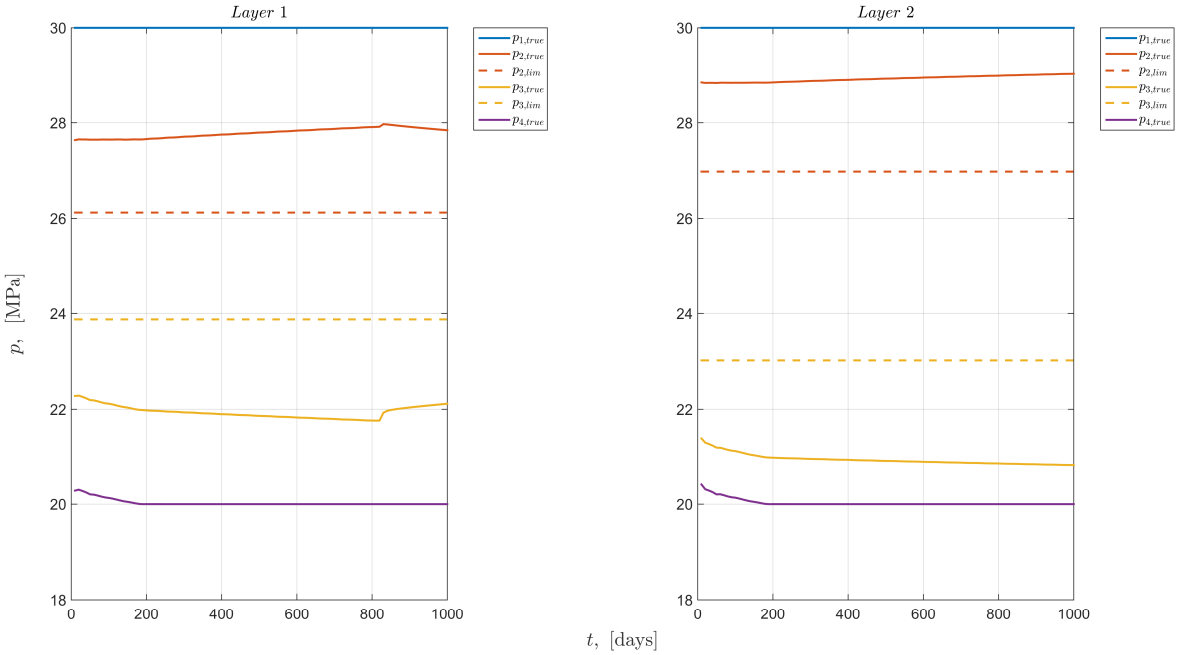

Figure 4.4 - Attaining maximum flowrate (horizontal wells): *true* pressures

4.2.2 Vertical wells

The other configuration (Figure 3.1) consists of layers on top of one another (separated by a horizontal impermeable layer). Hence, the wells in the reservoir are now *vertical* and located at *x*,*y*,*z*-coordinates

(0, *w*/2, *z*) and (*l*, *w*/2, *z*). Realistically, such a situation allows two-dimensional flow to occur within each layer (in the *x* and *y* direction) and requires a change in the virtual asset's parameters. Those parameters that need to be adapted are displayed below, while all others are as in Table 4.1.

General parameters			
Parameter	*Symbol*	*Value*	*Unit*
Reservoir length	*l*	500	m
Reservoir width	*w*	210	m
Reservoir height	*h*	20	m
MRST specific parameters			
Number of grid cells in *x*-direction	*nx*	50	-
Number of grid cells in *y*-dimension	*ny*	21	-
Number of grid cells in *z*-dimension	*nz*	2	-

Table 4.3 - Virtual asset simulation for vertical wells: parameters

Another change is that the pressure boundary conditions, $p_{1,true}$ and $p_{4,true}$ of each layer, are no longer necessarily equal nor constant. First of all, the height difference of layers increases the pressure $p_{1,true}$ of all layers below the top one. Accounting for the changing fluid composition, the same principal can be applied to the pressures $p_{4,true}$, yielding for layer *j* the true pressures:

$$p_{1,true}^{j} = p_{inj} + g \cdot \rho_w \cdot \sum_{k=1}^{j-1} dz(k) \qquad \text{and} \qquad p_{4,true}^{j} = p_{pro} + g \cdot \sum_{k=1}^{j-1} \rho_m^k \cdot dz(k) \tag{4.1.10}$$

where p_{inj} and p_{pro} are the top layer's injector and producer pressure, $\rho_m^k = f_w^k \rho_w + (1 - f_w^k)\rho_o$ the water-oil mixture density of layer *k*, *g* is the gravitational constant, and *dz*(*k*) is the height of layer *k*.

The pressure drop in layer *j* is still given by $\Delta p_{true}^{j} = \Delta p_{12,true}^{j} + \Delta p_{23,true}^{j} + \Delta p_{34,true}^{j}$, but from expression (4.1.10) it also follows that

$$\begin{aligned} \Delta p_{true}^{j} &= p_{1,true}^{j} - p_{4,true}^{j} \\ &= p_{inj} + g \cdot \rho_w \cdot \sum_{k=1}^{j-1} dz(k) - \left(p_{pro} + g \cdot \sum_{k=1}^{j-1} \rho_m^k \cdot dz(k) \right) \end{aligned} \tag{4.1.11}$$

However, due to the adjusted pressure boundary conditions the difference between two layers' pressure drop is no longer zero:

$$\Delta p_{true}^{j} - \Delta p_{true}^{j-1} = g \cdot (\rho_w - \rho_m^{j-1}) \cdot dz(j-1) \tag{4.1.12}$$

Therefore, minimization problem (3.3.33) changes to

$$\begin{aligned} &\min_{q_{t,j}} \sqrt{\sum_{j=1}^{n} \left(\Delta p_{true}^{j} - \Delta p_{true}^{j-1} - g \cdot (\rho_w - \rho_m^{j-1}) \cdot dz(j-1) \right)^2} \\ &\textit{with} \quad \sum_{j=1}^{n} q_{t,j} \le q_{t,\max} \\ &\textit{and} \quad q_{t,j} \ge 0 \ \forall j \end{aligned} \tag{4.1.13}$$

with $\Delta p_{true}^{0} = \Delta p^{ref} = p_{inj} - p_{pro}$, $\Delta p_{true}^{j} = \Delta p_{12,true}^{j} + \Delta p_{23,true}^{j} + \Delta p_{34,true}^{j}$ and *dz*(0) = 0.

In Figure 4.5 the resulting flowrates are shown. The new well orientation and reservoir configuration result in a brief nonlinear increase of the flowrates, though they soon start decreasing as seen in

previous simulations. The two-dimensional flow inside each layer, however, results in more significant and less sudden flowrates changes in the oil, water and reservoir flowrates.

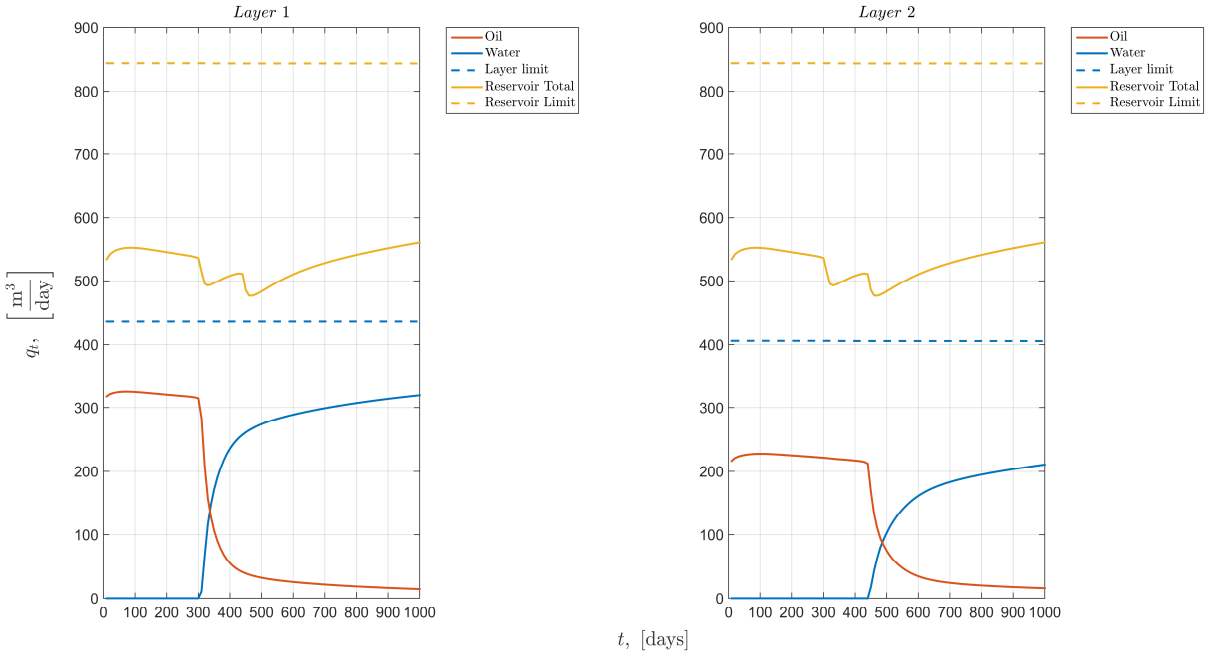

Figure 4.5 - Vertical wells: flowrates

The true pressures consequently also show slightly different results (see Figure 4.6). The new well orientation and reservoir configuration (allowing two-dimensional flow) results in a more significant and less sudden change in pressure once breakthrough occurs. Additionally, after breakthrough, the pressures $p_{2,true}$ and $p_{3,true}$ respectively de- and increase nonlinearly (in contrast to in Figure 4.2).

The new pressure boundary conditions for layer 2 can be seen in $p_{1,true}$ and $p_{4,true}$, but are negligible as for this layer the added pressure to $p_{1,true}$ is $\Delta p_{1,true} = g \cdot \rho_w \cdot 10 \approx 0.099\text{MPA}$ and for $p_{4,true}$ the value is given by: $0.0843\text{MPA} \leq g \cdot \rho_m \cdot 10 \leq \Delta p_{4,true} \leq g \cdot \rho_w \cdot 10 \approx 0.099\text{MPA}$.

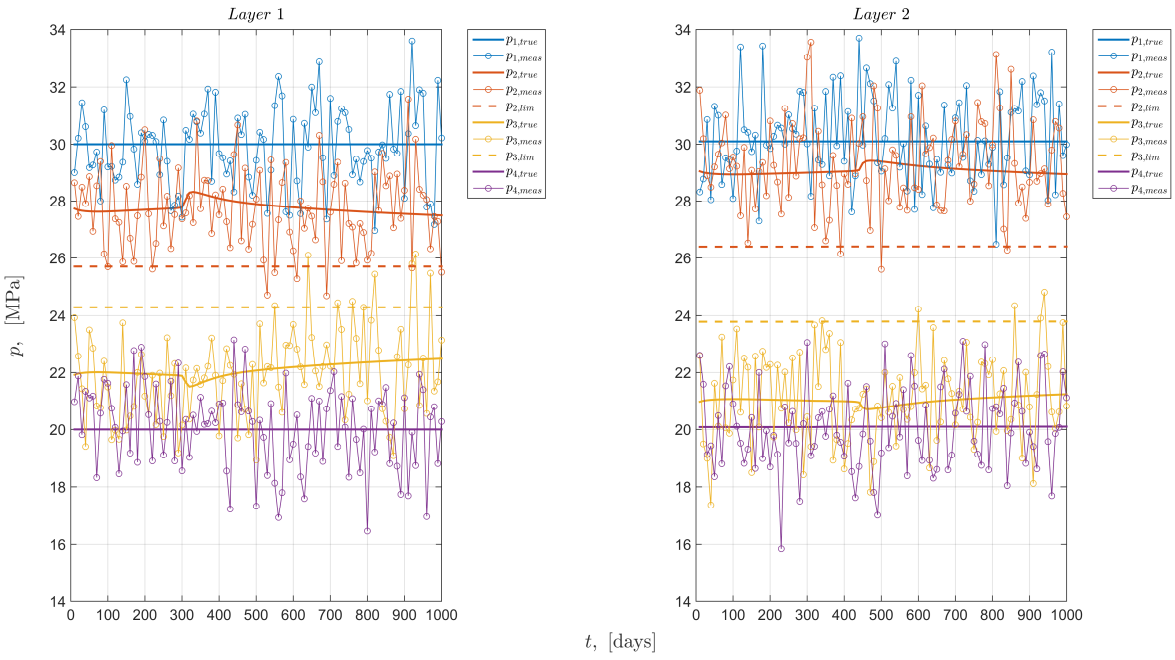

Figure 4.6 - Vertical wells: *true* & *measured* pressures

Reaching maximum total flowrate

In the simulation above the maximum total flowrate was again not reached. The maximum flowrate is therefore again lowered, such that the two-dimensional flow aspects under maximum flowrate conditions can be understood. However, this time the maximum flowrate is set so low that it almost always is at maximum flowrate conditions (see Table 4.4).

fmincon **conditions**			
Maximum total injection rate	$q_{t,max}$	500	m^3/day

Table 4.4 - Attaining maximum flowrate (vertical wells): adjusted parameters

Just as in the previous section's maximum flowrate investigation, the theoretical flowrate limit of each layer as well as the reservoir flowrate limit do net change. Just as before (and as intended), the maximum total flowrate limit is never violated. Moreover, only two times does the flowrate drop below the maximum value: both times just after a water breakthrough has occurred.

Additionally, the total flowrate of each layer barely changes as can be concluded from the near constant oil flowrates before any breakthrough has happened. More interestingly, however, are the breakthrough moments: breakthrough in one layer leads to a sudden increase in the (oil and/or water) flowrate of the other layer.

The resulting pressures behave correspondingly, as can be seen in Figure 4.8. First of all, pressures $p_{1,true}$ always equals the prescribed value by definition. In the pre-breakthrough phase, pressures $p_{2,true}$ are again constant due to constant flowrates, whereas pressures $p_{4,true}$ and $p_{4,true}$ follow the actual flowrate behavior. Due to attaining maximum flowrate, however, $p_{4,true}$ can not attain their prescribed value.

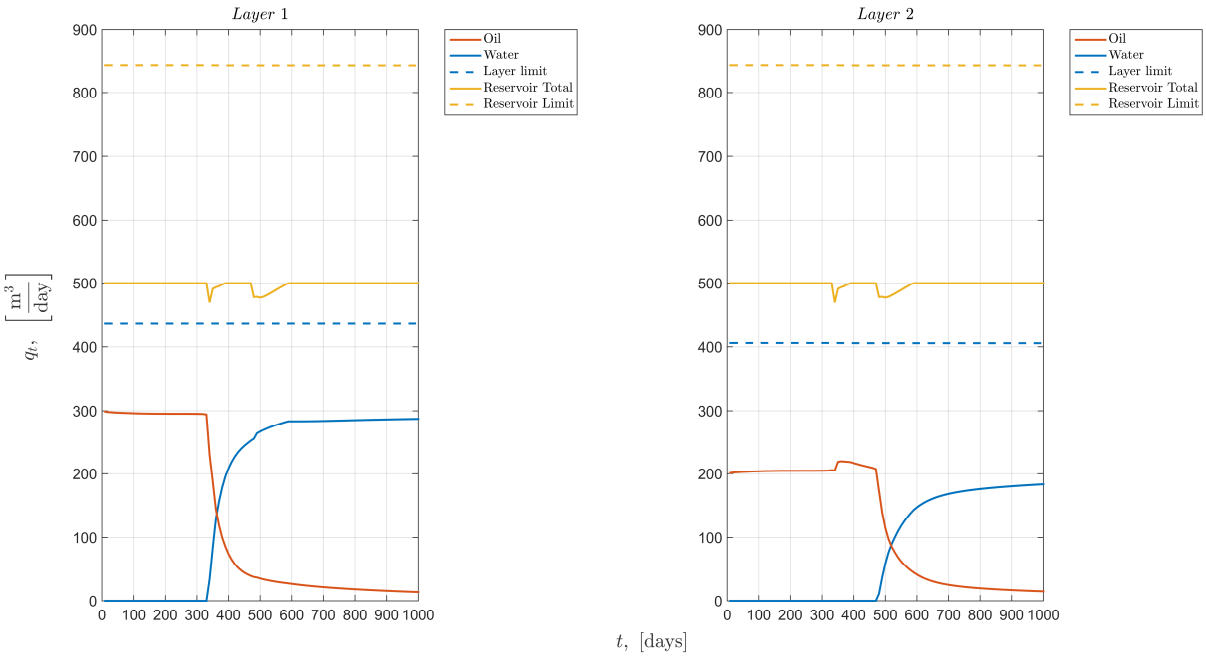

Figure 4.7 - Attaining maximum flowrate (vertical wells): flowrates

When breakthrough occurs in a layer however, its total flowrate decreases and causes an increase of $p_{2,true}$ whereas $p_{3,true}$ and $p_{4,true}$ decrease. Meanwhile, the other layer experiences a decrease in pressures $p_{2,true}$, $p_{3,true}$ and $p_{4,true}$ because its flowrate has increased. Additionally, Figure 4.8 shows that after both

breakthroughs the pressures $p_{2,true}$ go back to initial levels (e.g. see layer 1 as $p_{2,true}$ coincides with the 28MPA gridline).

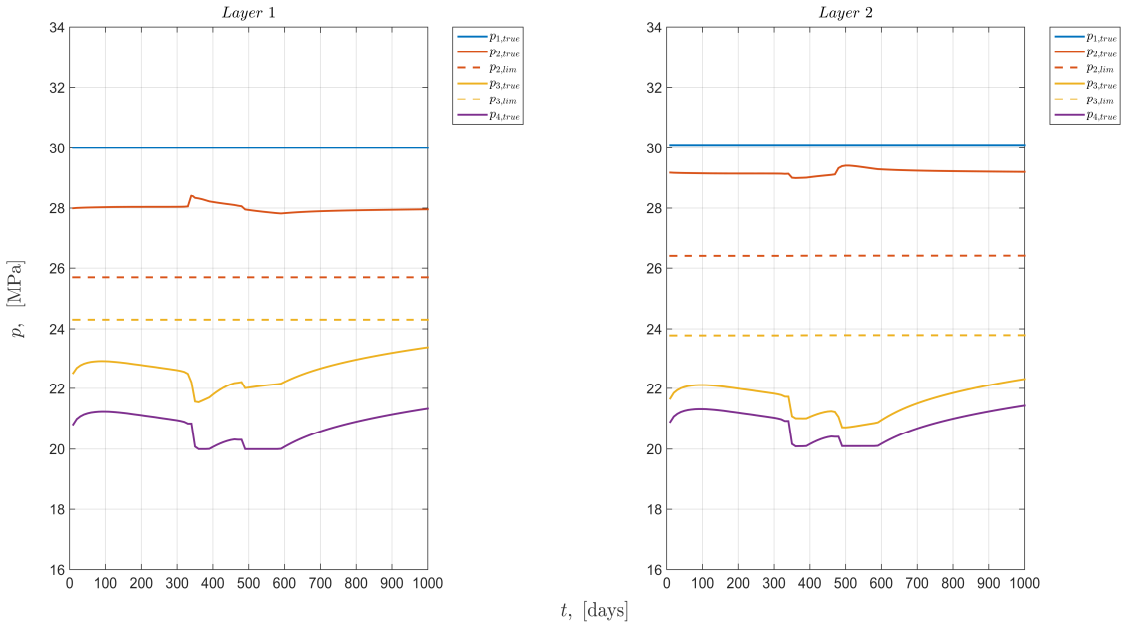

Figure 4.8 - Attaining maximum flowrate (vertical wells): *true* pressures

4.3 Horizontal well - Linear flow

From here on out the entire process of CLRM is considered. The first scenario considers horizontal wells with linear displacement and pressure drop (i.e. expressions (2.1.40) and (3.3.6)) for which all parameters are displayed below in Table 4.5. For the NPV optimization the choke area is no longer constant (as in Table 4.1) because it changes whenever the diameter, maximally 50mm, is altered.

Additionally, the discount rate is set at 15% per reference time of 365 days. Because there is only one injector and producer per layer and because the maximum flowrate is set at a high rate (1500m^3/day), the discount rate will have no influence on determining the optimal choke valve settings and therefore no influence on the resulting flowrates. Of course, the NPV will be different when compared to a 0% discount rate.

General parameters			
Parameter	*Symbol*	*Value*	*Unit*
Water density	ρ_w	1014	kg m^{-3}
Oil density	ρ_o	859	kg m^{-3}
Initial water saturation	S_{wi}	0.25	-
Residual oil saturation	S_{or}	0.1	-
End-point water rel perm	$k_{rw,0}$	0.5	-
End-point oil rel perm	$k_{ro,0}$	0.9	-
Permeability	k	[600;300]	mD
Corey exponent water	n_w	3	-
Corey exponent oil	n_o	3	-
Viscosity water	μ_w	0.35	cp
Viscosity oil	μ_o	1.9	cp
Reservoir length	l	1000	m
Reservoir width	w	500	m

Reservoir height	h	10	m
Porosity	ϕ	0.25	-
Time step size	dt	10	days
Total time	t	1000	days
Pressure drop model specific parameters			
# Legendre-Gauss abscissas	-	100	-
MRST specific parameters			
Number of grid cells in *x*-direction	nx	100	-
Number of grid cells in *y*-dimension	ny	2	-
Number of grid cells in *z*-dimension	nz	1	-
***fmincon* conditions**			
Maximum total injection rate	$q_{t,\max}$	2000	m^3/day
Minimum injection rate layer *j*	$q_{t,\min}^{j}$	0	m^3/day
Virtual asset specific parameters			
Meas. noise mean	μ_i^j	0	MPa
Meas. noise standard deviation	σ_{meas}	$0.05 \cdot P_{inj}$	MPa
Data assimilation specific parameters			
Initial permeability estimate	k^0	[600;300]	mD
Permeability sensitivity	P_k	$(0.05 \cdot k^0)^2$	mD
Measurement sensitivity	P_y	$(\sigma_{meas})^2$	MPa
NPV optimization parameters			
Choke valve discharge coefficient	C_d	0.7	-
Left choke maximum diameter	$d_{chl,j}$	50	mm
Right choke maximum diameter	$d_{chr,j}$	50	mm
Minimum producer pressure	P_{pro}	20	MPa
Net oil revenue	r_o	45	$/$m^3$
Net water cost	r_w	-5	$/$m^3$
Discount rate	b	15	%
Reference time	t_{ref}	365	Days

Table 4.5 - CLRM parameters (horizontal wells, linear model)

Figure 4.9b depicts the true (virtual asset) and estimated (data assimilation) results for the CLRM for a reservoir operated by horizontal wells, whereas measurements of the pressures (Figure 4.9b) have been left out for clarity.

Considering that maximum flowrate of 1500m^3/day is not achieved within the simulated time, the choke valve diameters remain at their maximum value just as could be expected. Only when it becomes uneconomical to stay fully them open, are the diameters reduced to zero to close off the layer (e.g. layer 1 at approximately 650 days). A noteworthy observation is that the closing of choke valve diameters is gradual and not instantaneous: as the NPV is updated at each time step, new diameters can be found such that the (predicted) flowrates still lead to an increase in the NPV (even if it is just a dollar, or less).

Since the choke valve diameters are fully open, the choke valve pressure drops are virtually nonexistent, which results in $p_{2,true}$ coinciding with $p_{1,true}$ and $p_{4,true}$ coinciding with $p_{3,true}$. The exception, of course, is when layer 1 is gradually being closed off and $p_{2,true}$ drops towards $p_{3,true}$.

The estimated pressure $p_{1,est}$ is per definition equal to $p_{1,true}$. As the flowrate estimates (Figure 4.9c) seem accurate, $p_{2,est}$ is close to $p_{2,true}$ and the small choke valve pressure drop explains why $p_{4,est}$ lies close to $p_{3,est}$. Due to the measurement error, however, the flowrate estimate is not perfect and this is reflected in pressure $p_{3,est}$: in general an overestimation of flowrates causes an overestimation in the reservoir pressure drop (see expression (3.3.6)) and results in underestimation of $p_{3,true}$.

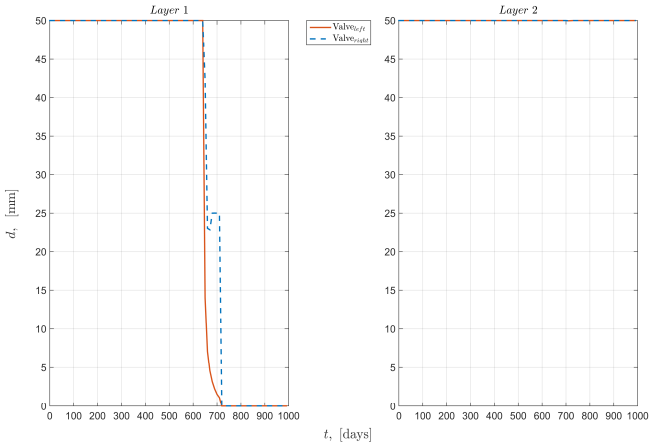

a) Choke valve diameter

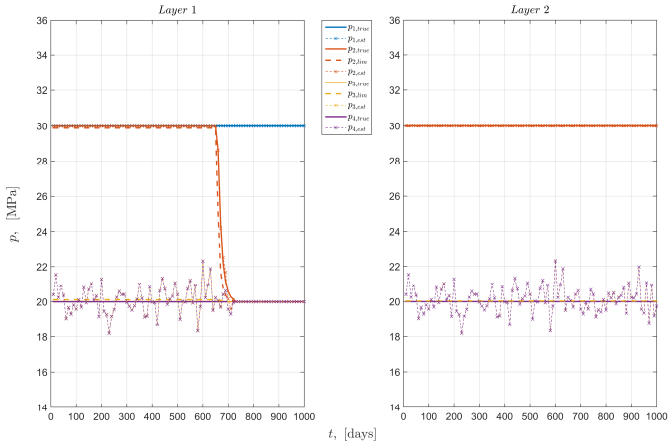

b) Pressures - true and estimated

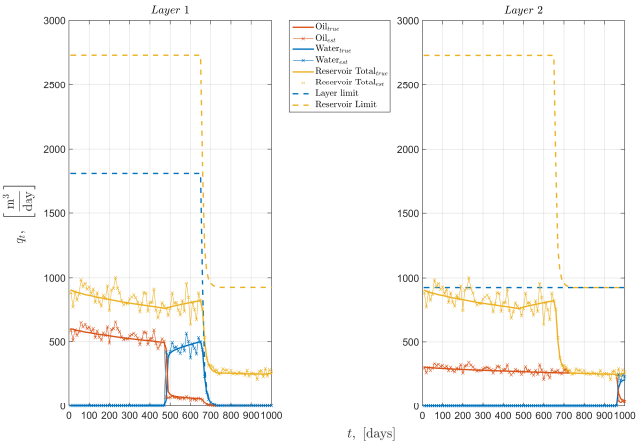

c) Producer flowrates - true and estimated

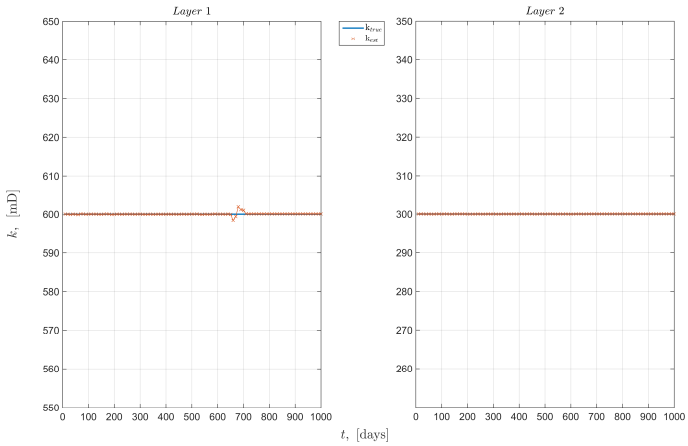

d) Permeability - true and estimated

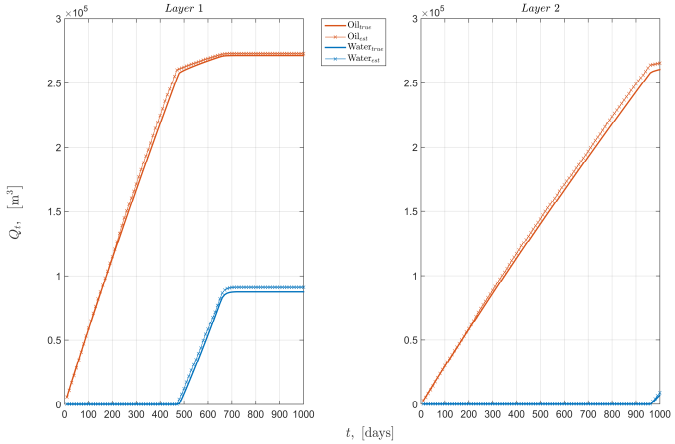

e) Cumulative production - true and estimated

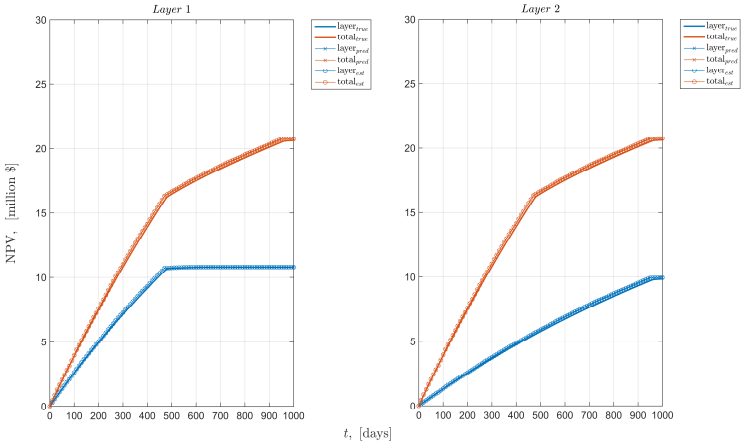

f) NPV development - true and estimated

Figure 4.9 - CLRM results (horizontal wells, linear model) - 15% discount

Although the flowrate estimates are not perfect (see Figure 4.9c), they are fairly close the true rates and even the moment of breakthrough in layer 1 is almost perfectly captured. Additionally, also the

permeability estimates are spot on (except for the moment of closing layer 1), in part thanks to the perfect initial guess k^0. Therefore, the (one-dimensional) linear propagation and pressure model are appropriate models for flow between two horizontal wells that fully penetrate the reservoir's opposing sides. Due to the seemingly accurately estimated flow rates, also the cumulative production and the NPV (Figure 4.9e,f) yield predictions and estimations close to the true values.

Though this section considers a discount factor of 15%, the results are similar when a discount factor of 0% is used. The reason is that the maximum flowrate is not reached in the simulation above, which means that choke valves will be fully opened (except for closing off moments). Fully open choke valves in turn lead to identical true pressures, flowrates, and cumulative production. Consequently, this results in similar estimations of the aforementioned (see Appendix A for the results). The estimated NPV values for both the discounted and non-discounted scenarios are summarized in the table below.

NPV (million $)	Layer 1	Layer 2	Cumulative
15% discount	10.7	10.0	20.7
0% discount	11.9	11.8	23.7
Difference	-10.1%	-15.3%	-12.7%

Table 4.6 - Estimated NPV: discounted versus non-discounted (horizontal wells, linear model)

Lastly, verifying that the estimates are indeed accurate means considering the error between estimated and true flowrates (i.e. the true flowrate estimation error), as well as between estimated and predicted flowrates (model flowrate estimation error). Figure 4.10 below shows that (on average) the true flowrates are slightly overestimated, whereas the estimated flowrates are slightly lower than predicted. Additionally, in each layer the two errors exhibit a strong positive correlation (qualitatively speaking), indicating the appropriateness of the model. Moreover, as the conditions of the layers are identical (except for the permeability), there is also a positive correlation (qualitatively speaking) between the layers' flowrate errors. Hence, the model flowrate estimation error as well as its change over time could possibly be used to reduce the true flowrate estimation error.

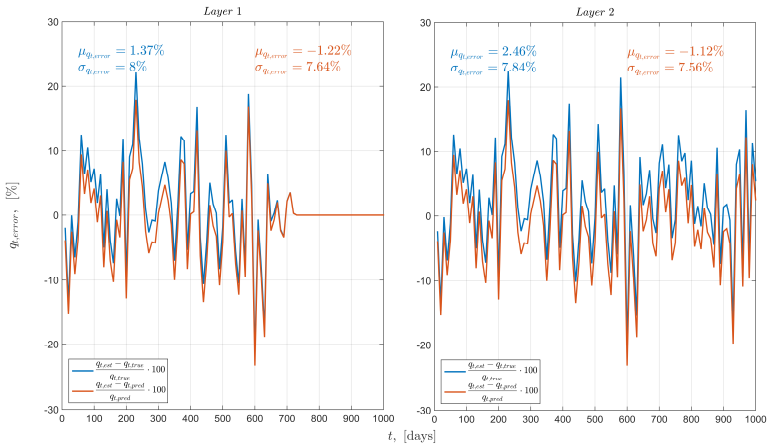

Figure 4.10 - CLRM results (horizontal wells, linear model) - Flowrate errors

4.4 Vertical well - Linear flow

In this section two simulations are carried out using the same (linear) model as in the previous section. However, the reservoir is now operated by vertical wells meaning there is two-dimensional flow within each layer. The first simulation shows that the model still yields accurate estimates for reservoirs of small width, whereas the second one shows that for a realistic width the model fails to produce accurate estimates.

Further more, from hereon out all parameters are equal to those in Table 4.5 and only the ones that are different will be specified. The parameters that change due to the vertical wells scenario are:

General parameters			
Parameter	*Symbol*	*Value*	*Unit*
Reservoir length	l	500	m
Reservoir width	w	210	m
Reservoir height	h	20	m
MRST specific parameters			
Number of grid cells in x-direction	nx	50	-
Number of grid cells in y-dimension	ny	21	-
Number of grid cells in z-dimension	nz	2	-

Table 4.7 - CLRM parameters (vertical wells)

4.4.1 Small width

This section considers a reservoir of small width, for which the width is reduced by a factor 30 from 210m to 7. The number of grid cells in the y-dimension is also reduced, from 21 to 7 (see the table below) and for accurate results the number of grid cells in the x-direction is increased to 500, resulting in grid cell dimensions of 1x1x10m (x,y,z).

General parameters			
Parameter	*Symbol*	*Value*	*Unit*
Reservoir width	w	7	m
MRST specific parameters			
Number of grid cells in x-direction	nx	500	-
Number of grid cells in y-dimension	ny	7	-

Table 4.8 - CLRM (small width) parameters (vertical wells, linear model)

The purpose of this simulation is to show that the linear model is still accurate for a reservoir with the aforementioned properties. The resulting choke valve diameters, (true and estimated) pressures, flowrates and permeability, and the flowrate errors are depicted in Figure 4.11. Note that the cumulative production and NPV are left out as they are of no interest at the moment.

The results are (visually) similar to those in Figure 4.9, although the flowrates are smaller because of the smaller width. Additionally, some deviating behavior can be seen (e.g. choke valves and pressures of layer 2) around the closing off moment of layer 1. More importantly, the average flowrate errors and the standard deviation of the flowrate errors are again similar (just as in section 4.3 (Figure 4.10)), meaning the linear model is indeed accurate for a reservoir with small width.

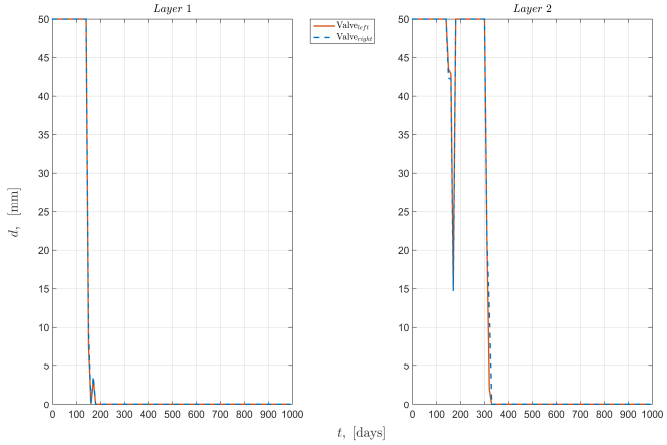

a) Choke valve diameter

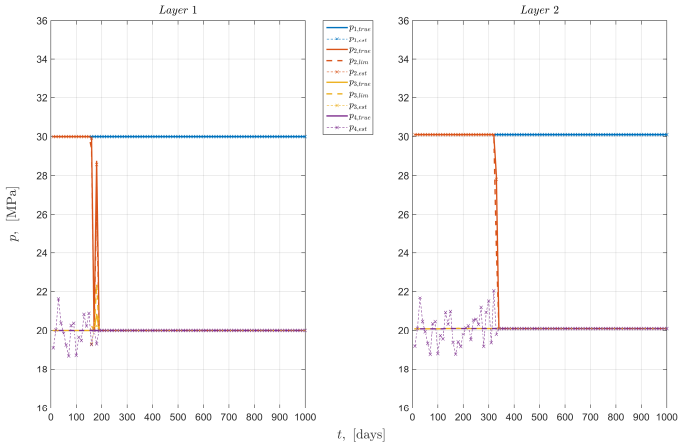

b) Pressures - true and estimated

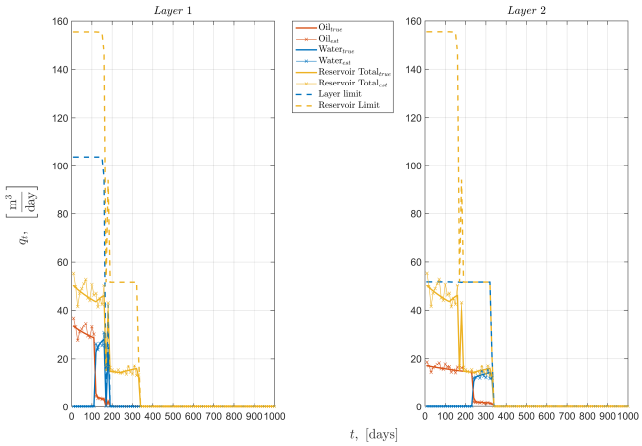

c) Producer flowrates - true and estimated

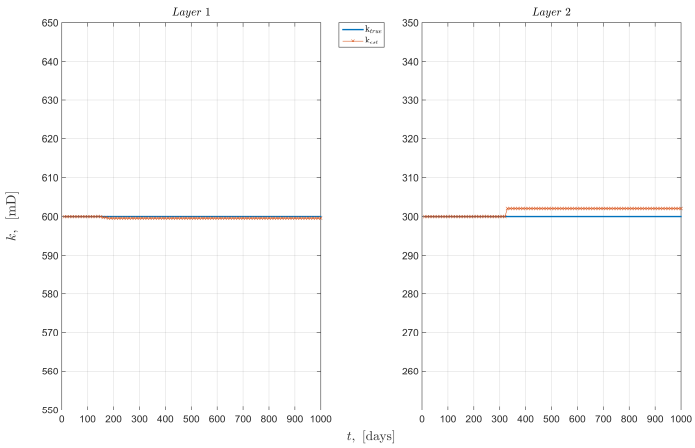

d) Permeability - true and estimated

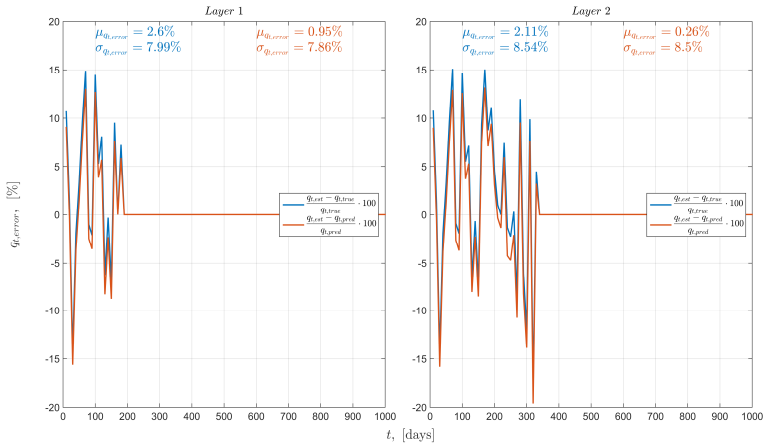

e) Flowrate errors

Figure 4.11 - CLRM results (vertical wells, linear model) - small width

4.4.2 Realistic width

This section investigates the use of the linear model for the vertical wells case, using the parameters given in Table 4.5. The reservoir parameters, however, are given in Table 4.7.

First of all, no deviating behavior (compared to Figure 4.9) is detected with respect to the choke valve diameters, estimated permeability and estimated pressures other than that the closure occurs for both layers at earlier times. The cause for the (earlier) closure of both layers is the overestimation of the flowrates as can be seen in Figure 4.12c.

The flowrate errors (see Figure 4.13) indeed show that there is a significant overestimation of the flowrates, with an average of approximately 60%. Consequently, the cumulative production (Figure 4.12e) estimates are completely wrong: in truth no water breakthrough has occurred in either layer, but the model estimates a large amount of water has already been produced. From the moment the model estimates water is being produced, the oil production drops and mitigates its overestimation only partly.

The overestimation of oil production obviously results in an overestimation of the NPV. In the early stage before (estimated) breakthrough (i.e. the first 100 days), the estimated and true NPV respectively are approximately 6.3 and 3.7 million dollars. This difference of approximately 70% is close to the mean flowrate error for the first 100 days (Figure 4.13). After 100 days, however, the water that is estimated to be produced reduces the increase in estimated NPV while the true NPV continues to increase at a constant rate. Hence, the overestimation in NPV at the end of the simulated time is significantly lower than the 60% average flowrate overestimation (see Table 4.9). Moreover, the vast overestimation of flowrates implies that the NPV can be significantly increased due to the fact that oil can still be produced without producing any water.

NPV (million $)	Layer 1	Layer 2	Cumulative
Estimated	4.6	4.7	9.3
True	4.0	3.9	7.9
Estimation error	15%	20.5%	17.7%

Table 4.9 - True and estimated NPV (vertical wells, linear model) - 15% discount

Additionally, the flowrate errors within each layer are no longer close to one another, meaning that the model flowrate error no longer is a good indication of the true flowrate error (even though there still seems to be some (positive) correlation between flowrate errors). Therefore, the model flowrate estimation error can hardly reduce the true flowrate error. In other words, the linear model can not accurately describe this type of reservoir flow.

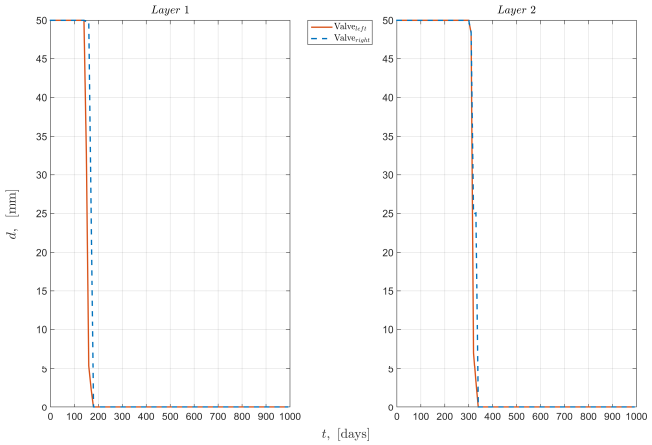

a) Choke valve diameter

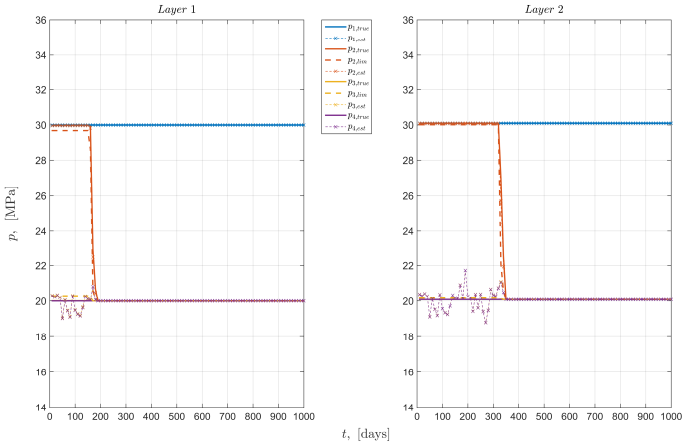

b) Pressures - true and estimated

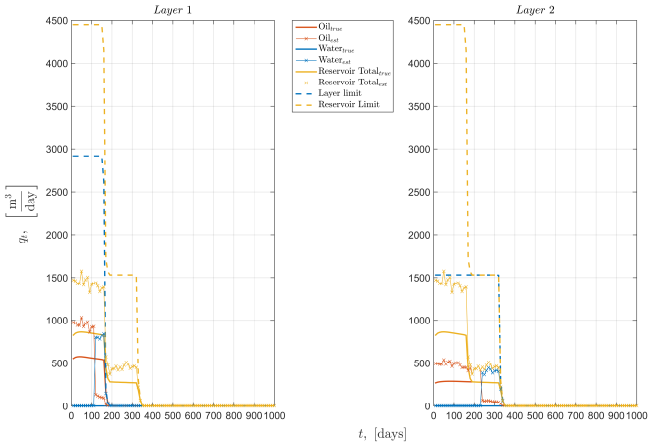

c) Producer flowrates - true and estimated

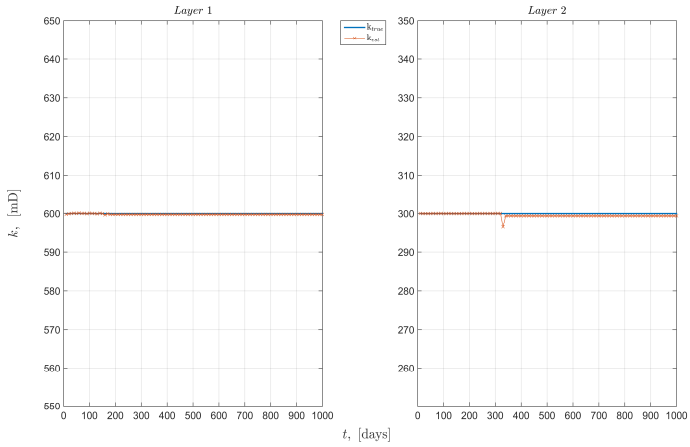

d) Permeability - true and estimated

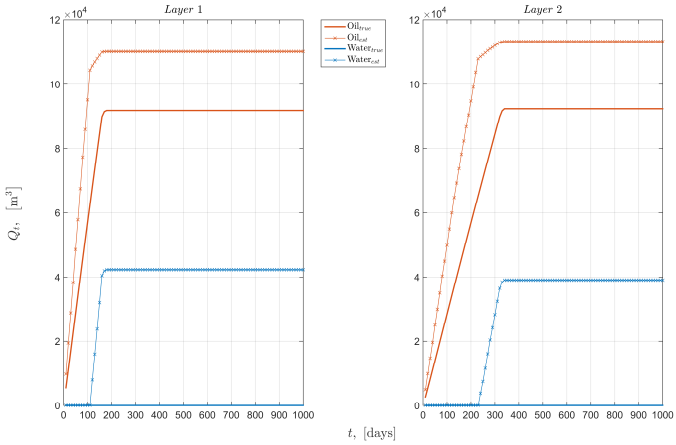

e) Cumulative production - true and estimated

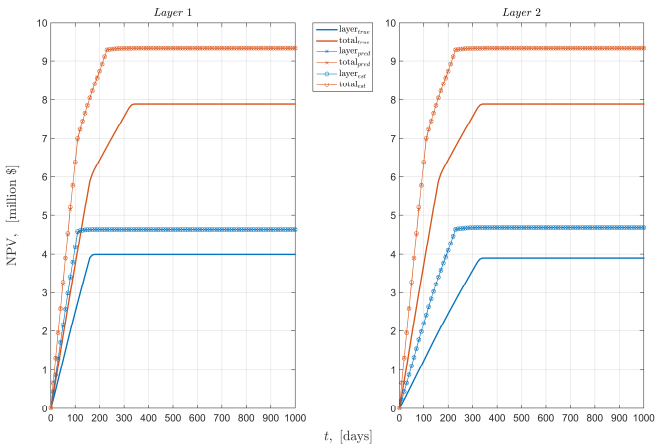

f) NPV development - true and estimated

Figure 4.12 - CLRM results (vertical wells, linear model) - 15% discount

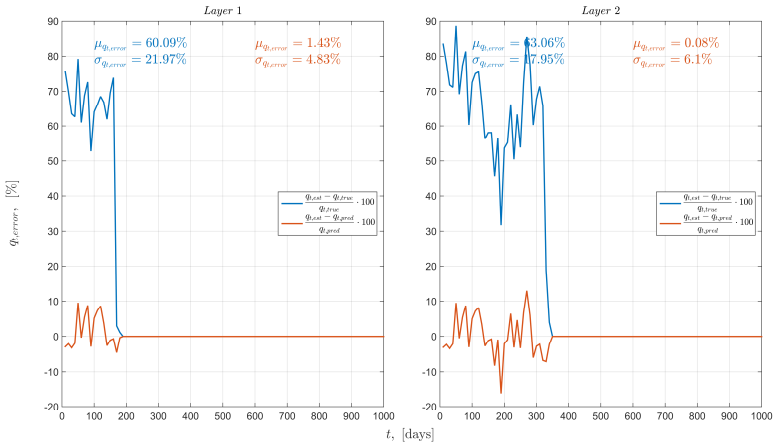

Figure 4.13 - CLRM results (vertical wells, linear model): Flowrate errors

4.5 Vertical well - Radial-Linear-Radial flow

The previous section showed that the linear model can not accurately describe two-dimensional two-phase flow in a bounded reservoir. Therefore, the RaLiRa model (expressions (2.1.54) up to (2.1.56), and (3.3.13)) is considered in this section, with all parameters again as in Table 4.5 and Table 4.7.

Figure 4.14 below shows the simulation results for the RaLiRa model, of which the choke valve diameters, true and estimated pressures, and permeability estimates all behave as expected from earlier simulations. The choke valves remain fully open until it is no longer economical to produce from a layer, resulting in small choke valve pressure drops and therefore pressures are mainly governed by the reservoir pressure drop from $p_{2,true}$ and $p_{3,true}$. At the same time permeabilities are estimated accurately, though there is a small deviation from the true value when a layer is being closed off.

More importantly, the flowrate estimates have been improved upon significantly (Figure 4.14c and Figure 4.15) as the average flowrate error has been reduced to about 19%. Subsequently, the estimated moment of water breakthrough, even though still too early, is better approximated by the RaLiRa model. Of course the improvement in the flowrate estimates also results in more accurate cumulative production and NPV values.

The overestimation in water production (Figure 4.14e) reduces the estimated NPV and results in a small estimation error (see Table 4.10). However, due to the flowrate overestimation and therefore the water production overestimation, the NPV can still be improved upon further.

The RaLiRa model (qualitatively speaking) also leads to a strong positive correlation between the true and model flowrate estimation errors, i.e. the change over time in the model flowrate estimation error is indicative of the true flowrate estimation error's change over time. Additionally, the true flowrate estimation error of each layer spikes from the moment of water breakthrough (until the layer is closed off), while the model flowrate estimation error does not. This indicates that the model is not able to accurately capture the true flowrates after breakthrough.

NPV (million $)	Layer 1	Layer 2	Cumulative
Estimated	4.5	4.4	8.9
True	4.6	4.5	9.1
Estimation error	-2.2%	-2.2%	-2.2%

Table 4.10 - True and estimated NPV (vertical wells, RaLiRa model) - 15% discount

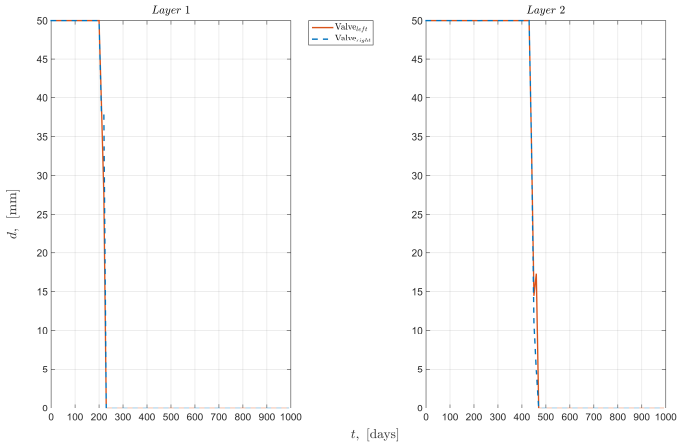

a) Choke valve diameter

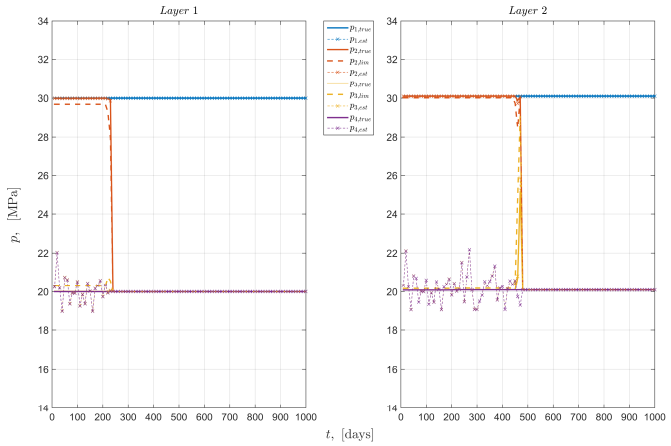

b) Pressures - true and estimated

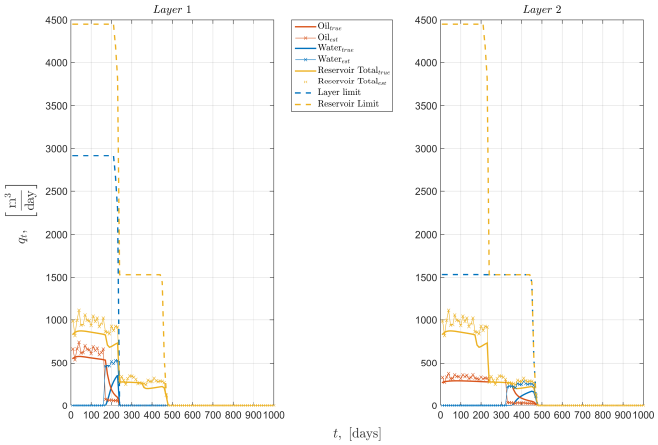

c) Producer flowrates - true and estimated

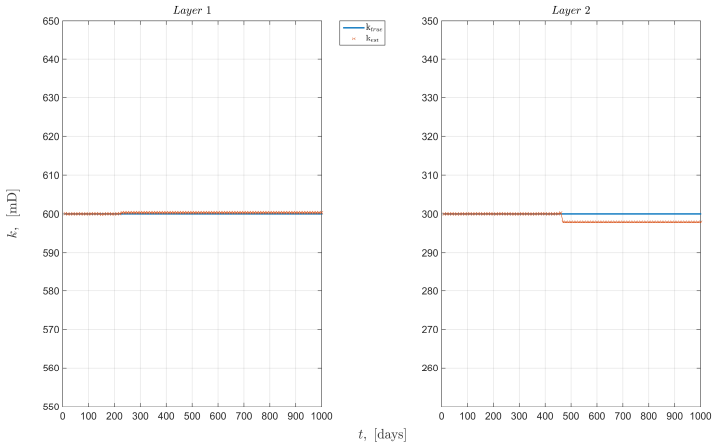

d) Permeability - true and estimated

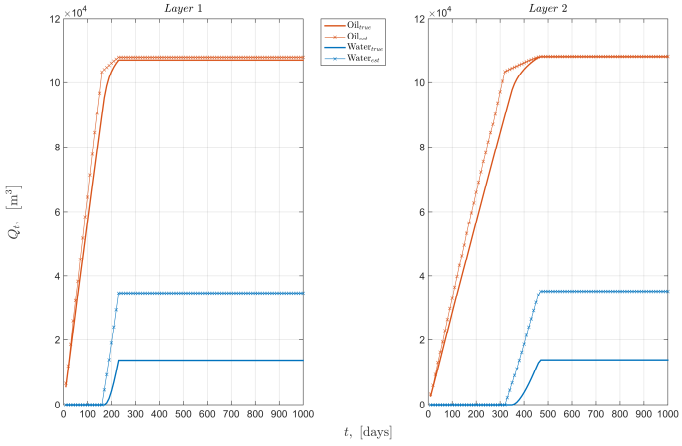

e) Cumulative production - true and estimated

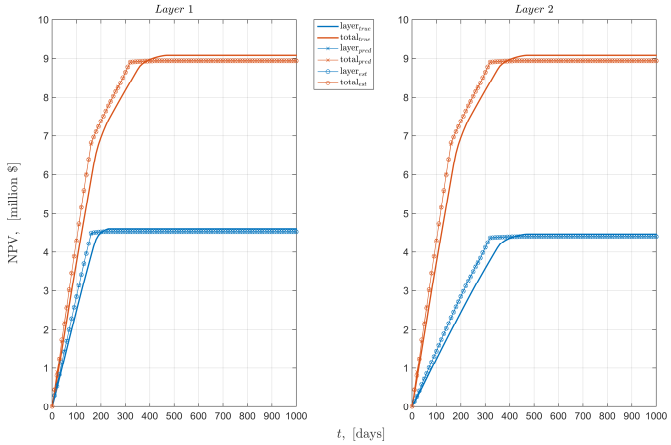

f) NPV development - true and estimated

Figure 4.14 - CLRM results (vertical wells, RaLiRa model) - 15% discount

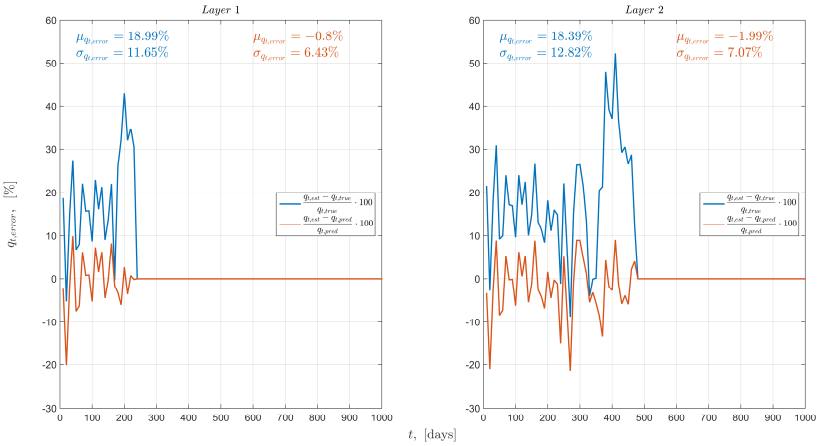

Figure 4.15 - CLRM results (vertical wells, RaLiRa model): Flowrate errors

4.6 Vertical well - Linear flow & Bounded Reservoir Pressure

While the RaLiRa model of the previous section definitely improved upon the flowrate errors (compared to the linear model, i.e. Figure 4.13), further improvement is still possible by considering the pressure drop model for two-dimensional two-phase flow in a bounded reservoir (see section 3.3.3, expression (3.3.19)). Therefore, the linear displacement model is combined with the bounded reservoir pressure drop model, abbreviated to 'the linear bounded reservoir pressure model' (Li-BoReP). Once again the parameters describing the reservoir in question can be found in Table 4.5 and Table 4.7.

The choke valve diameters, the true and estimated pressures, as well as the estimated permeabilities yield no new results with respect to the previous section except for a slight delay in the closure of each layer (see Figure 4.16 below).

Comparing Figure 4.16c&e with their counterparts in Figure 4.12 and Figure 4.14 immediately reveals that the flowrate estimate has been significantly improved upon by the Li-BoReP model. Subsequently the estimated cumulative production and NPV (see Table 4.11 below) have been improved as well (although the true NPV is only 0.1 million dollars higher than in Table 4.10).

The moment of breakthrough, on the other hand, is now exceeded and coincides with the moment that the true water and oil production rates are equal. However, if the breakthrough moment is precisely estimated, the overestimation of the cumulative water production will be worse.

NPV (million $)	Layer 1	Layer 2	Cumulative
Estimated	4.8	4.7	9.5
True	4.7	4.5	9.2
Estimation error	2.1%	4.4%	3.3%

Table 4.11 - True and estimated NPV (vertical wells, Li-BoReP model) - 15% discount

Already revealed by Figure 4.16e, the new pressure model has decreased the error between the estimated and true flowrate significantly. Figure 4.17 shows that this error is reduced to below the approximate range of 7%-8%, while the standard deviation is of the same order of magnitude as in the previous simulation. Moreover, the flowrate errors once again have a strong positive correlation (qualitatively speaking). However, the spike at time of breakthrough still exists, which means that flowrates are still overestimated and further improvement is still possible.

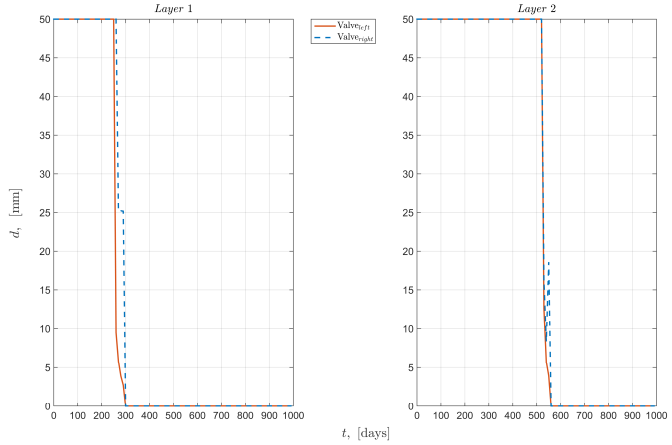

a) Choke valve diameter

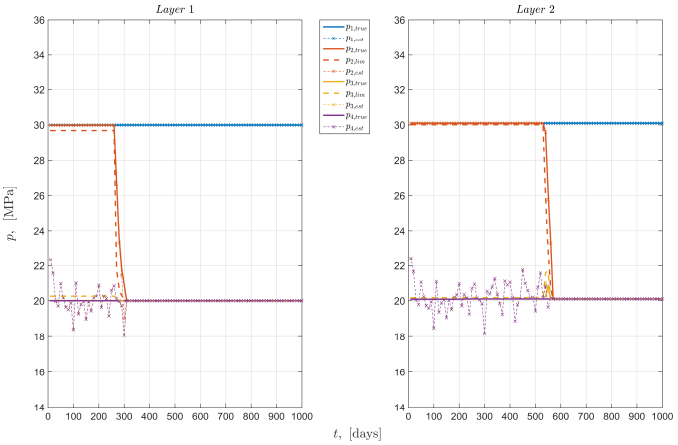

b) Pressures - true and estimated

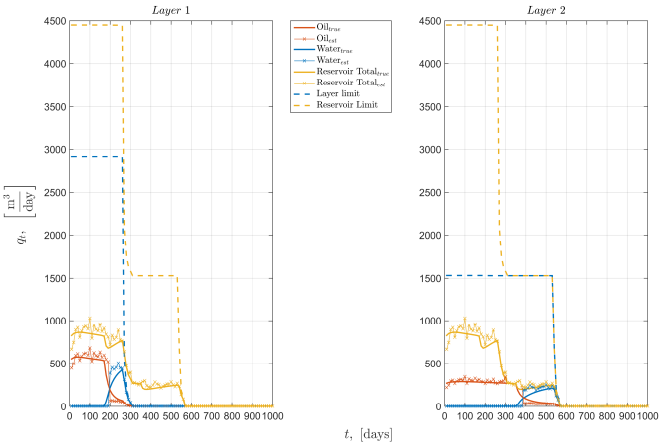

c) Producer flowrates - true and estimated

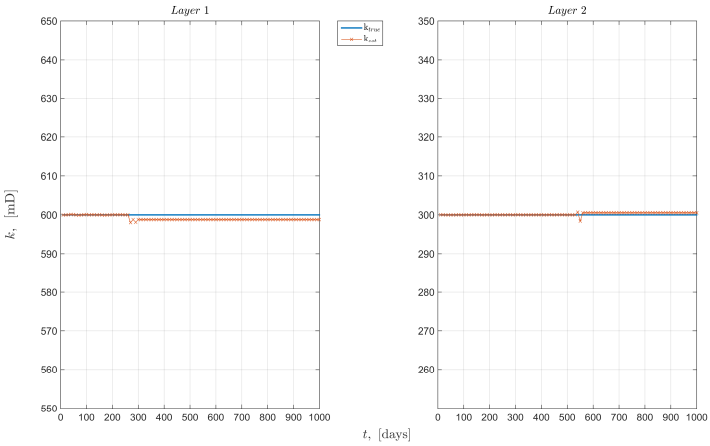

d) Permeability - true and estimated

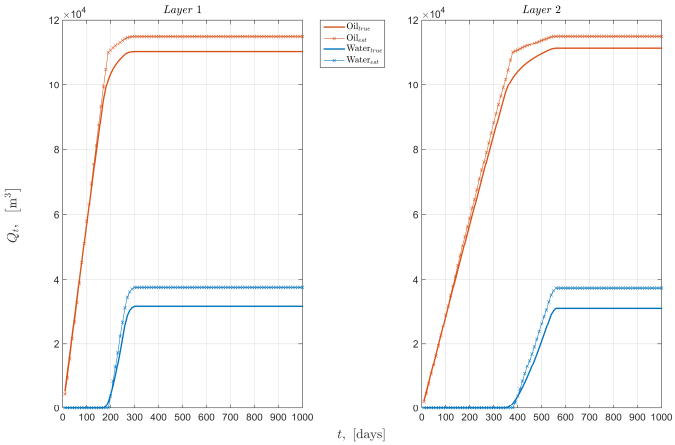

e) Cumulative production - true and estimated

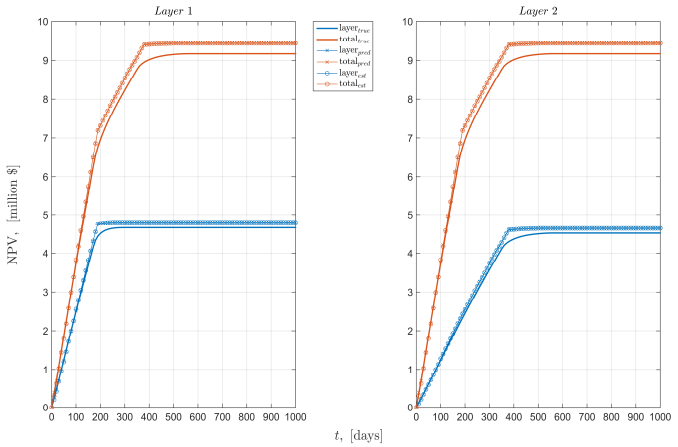

f) NPV development - true and estimated

Figure 4.16 - CLRM results (vertical wells, Li-BoReP model) - 15% discount

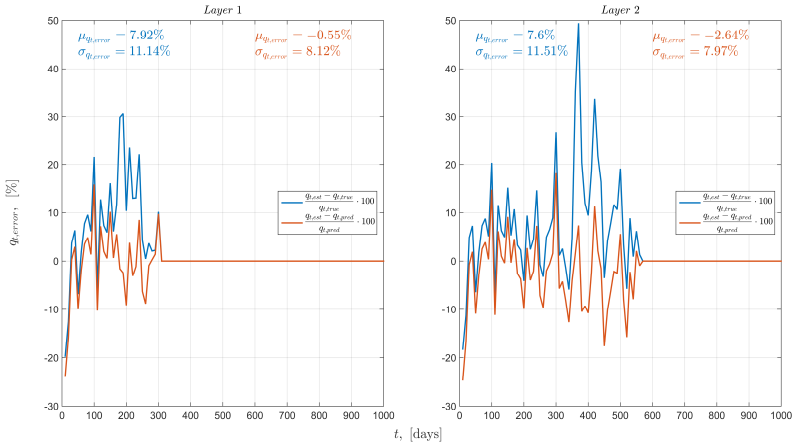

Figure 4.17 - CLRM results (vertical wells, Li-BoReP model): Flowrate errors

4.7 Vertical well - Radial-Linear-Radial flow & Bounded Reservoir Pressure

While the previous section used the linear displacement model, it is already known that the RaLiRa displacement model better estimates the moment of breakthrough (see section 4.5). Therefore, the next simulation considers the bounded reservoir pressure drop model in combination with the RaLiRa displacement model (abbreviated to 'RaLiRa-BoReP model'). Note that the all parameters don't change (see Table 4.5 and Table 4.7).

The results are shown in Figure 4.18 below and as before the choke valve diameters, the true and estimated pressures, and the estimated permeabilities are generally similar to those in Figure 4.16. The other three figures are of greater interest, as these show among other that the moment of breakthrough is almost perfectly estimated. Consequently, the estimated cumulative water production is worse than for the Li-BoReP model (Figure 4.16) because the water production is estimated to start earlier and the displacement model only accounts for flow along the inter-well axis. Another consequence of the near perfect breakthrough estimate is that the cumulative oil production is estimated more accurately than in the Li-BoReP model.

As the RaLiRa-BoReP model uses the same displacement model as the RaLiRa model (section 4.5), it is no surprise that in both cases the simulation ends at the same estimated level of cumulative produced oil and water. Additionally, the flowrate estimates in the RaLiRa-BoReP are lower than those of the RaLiRa model (compare for instance the true flowrate estimation errors of Figure 4.15 and Figure 4.19). Consequently, the RaLiRa-BoReP model finishes the production process (slightly) later than the RaLiRa model, yet this delay barely effects the estimated and true NPV (see Table 4.12).

NPV (million $)	Layer 1	Layer 2	Cumulative
Estimated	4.5	4.4	8.9
True	4.6	4.5	9.1
Estimation error	-2.2%	-2.2%	-2.2%

Table 4.12 - True and estimated NPV (vertical wells, RaLiRa-BoReP model) - 15% discount

While the Li-BoReP model better estimates cumulative water production and the RaLiRa-BoReP model better estimates cumulative oil production, the true NPV of both models only differs by 0.1 million dollars. Moreover, the flowrate errors (Figure 4.19) again show (qualitatively speaking) a strong positive correlation. However, Figure 4.19 indicates that the Li-BoReP model is slightly better at estimating true flowrates, as its mean flowrate estimation errors are lower. On the other hand, the

standard deviations of the RaLiRa-BoReP model's true and model flowrate estimation errors are of the same order of magnitude as those of the Li-BoReP model. A possible extension is to use those models conjointly in order to more accurately predict both water and oil cumulative productions. However, this option is not investigated in this thesis.

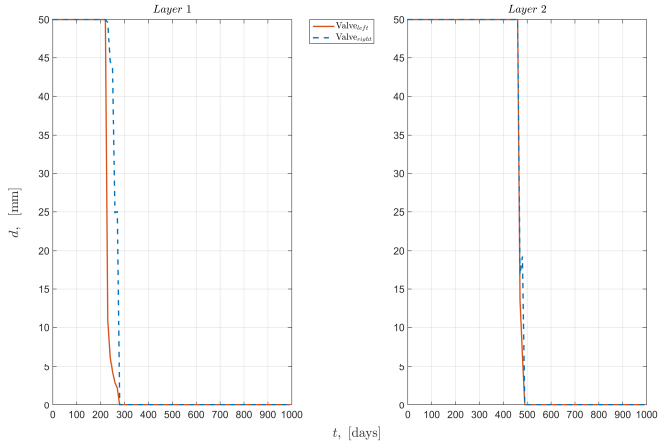

a) Choke valve diameter

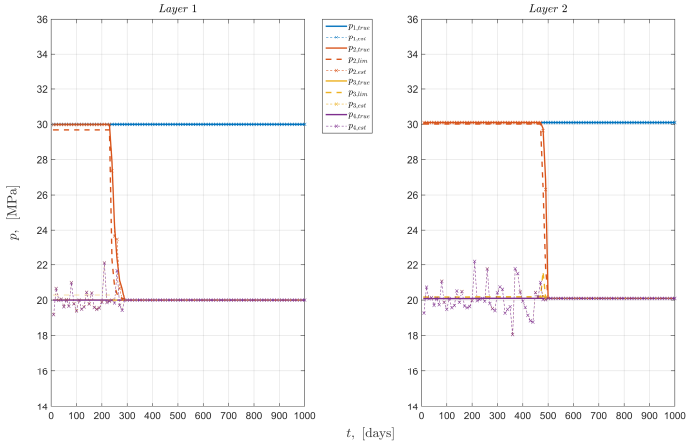

b) Pressures - true and estimated

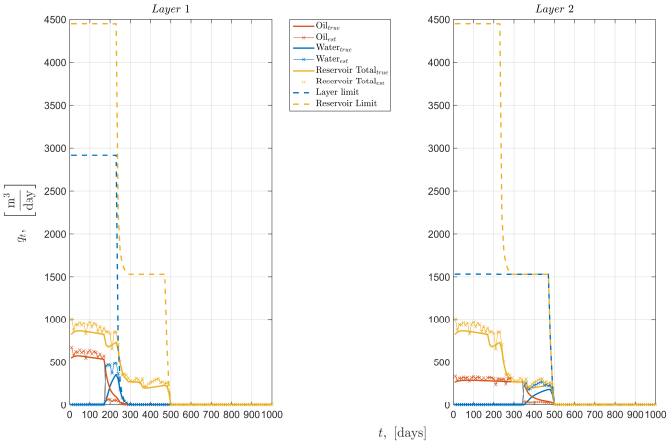

c) Producer flowrates - true and estimated

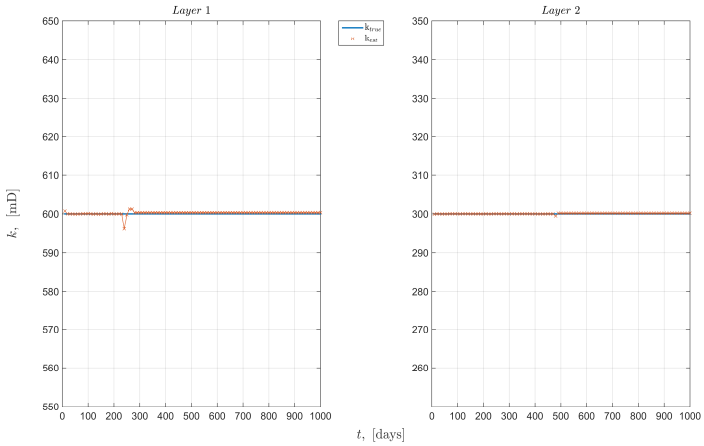

d) Permeability - true and estimated

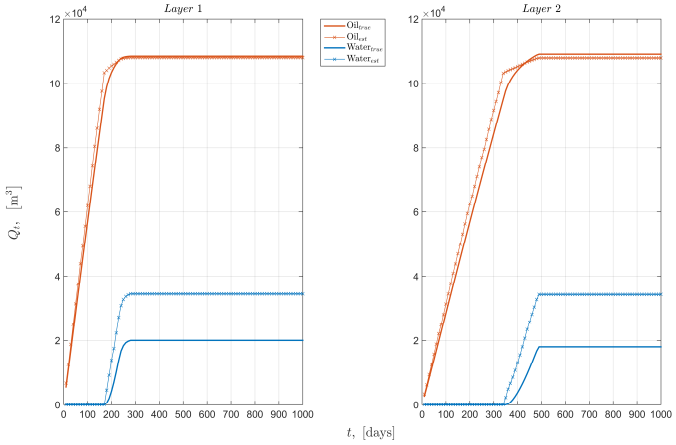

e) Cumulative production - true and estimated

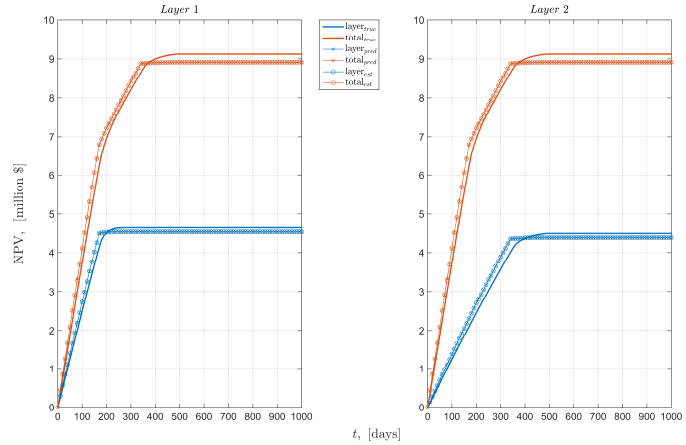

f) NPV development - true and estimated

Figure 4.18 - CLRM results (vertical wells, RaLiRa-BoReP model) - 15% discount

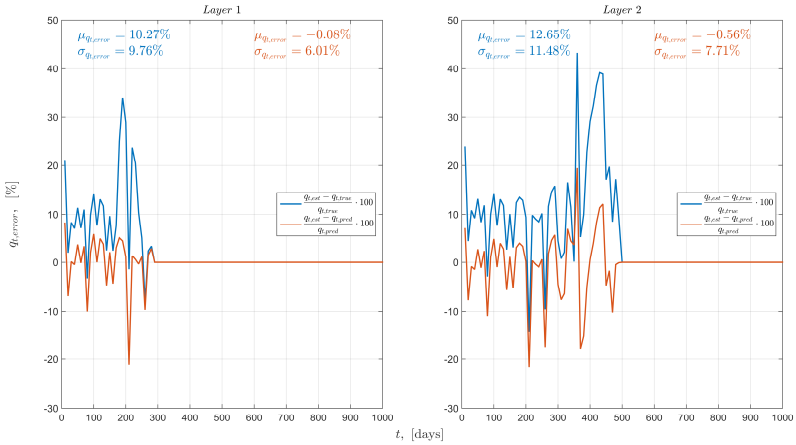

Figure 4.19 - CLRM results (vertical wells, RaLiRa-BoReP model): Flowrate errors

4.8 Computation time

As mentioned in the introduction of this thesis, the required computational effort of analytical models is low compared to that of numerical simulators. Although not the main focus of this thesis, a brief mentioning of approximate computation times should give an idea of the power of the analytical models under consideration. The table below lists these approximate computation times.

CLRM phase / Analytical Model	Virtual Asset	Data Assimilation	NPV Optimization	Cumulative time
Linear (vertical wells)	316s	116s	404s	836s
RaLiRa	363s	130s	518s	1011s
Li-BoReP	374s	209s	467s	1050s
RaLiRa-BoReP	420s	166s	390s	976s

Table 4.13 - Approximate computation times

The cumulative computation times listed above encompass the entire simulation. The total simulation times and time step size is equal for all cases and mentioned in each case's table in earlier sections. Important to mention is that whenever a layer is closed off, it no longer contributes to the computation time. Moreover, no clear statistics are drawn from the above table, although it is clear that data assimilation (i.e. matching estimated and measured pressures by estimating flowrates with the analytical model) is always faster than the virtual asset (i.e. the numerical model).

For all analytical models, the NPV optimization computation time is small (on average less than two seconds per time step) if neither maximum flowrate nor layer closure time has been reached (i.e. if choke valves can remain open). If this does occur, however, the computation time easily increases to approximately seventy seconds, which could be further improved upon by supplying gradients to the algorithm.

Similarly, data assimilation computation times for the analytical models are small (on average also less than two seconds per time step) unless a layer is at the moment of water breakthrough or at the closing off moment. However, data assimilation computation time can take approximately fifty seconds for breakthrough moments and could also possibly be improved upon by supplying gradients.

5
Conclusion and discussion

In this chapter, conclusions are drawn based on the results obtained in the previous chapters and are subsequently discussed. First the linear model for the horizontal well setup is treated, after which the focus shifts to the models for the vertical well case. Lastly, a conclusion is given with respect to the main research objective.

The (one-dimensional) linear model has been of interest first and foremost because of its simplicity and analytic nature. Its limitations were tested early on for a horizontal well setup (section 3.3.5), which revealed that the model (without incorporating choke valves) is unable to provide control over the flow in a multi-layered reservoir when there is flow occurring from one layer into another. Therefore, the linear model (without choke valves) is unsuitable for most heterogeneous reservoirs. On the other hand, if each layer of a reservoir is homogeneous and produced by horizontal wells, then the model works adequately as evidenced by the near identical flowrate estimation errors (Figure 4.10).

Even though the homogeneous requirement is a limitation, this model can possibly also be suitable for a heterogeneous reservoir where the permeability only varies perpendicular to the well direction (i.e. in the flow direction, x). The reason is that its one-dimensional displacement description (expression (2.1.40)) does not depend on the permeability and the pressure drop is only evaluated along the x-direction.

Unfortunately, the linear model is no longer appropriate in case of vertical wells and two-dimensional flow within each (still homogeneous) layer as indicated by the large true flowrate estimation error (Figure 4.13). The RaLiRa model, describing flow along the inter-well axis of two vertical wells as a Radial-Linear-Radial type of displacement, was subsequently introduced to better handle the two-dimensional flow aspects. This was definitively a step in the right direction, as the cumulative oil production was estimated almost perfectly. However, the water production still could be improved upon. More importantly, the mean true flowrate estimation error (Figure 4.15) and its standard deviation were greatly reduced. However, a spike occurred in the errors around and after water breakthrough, meaning flowrates were being significantly overestimated.

After improving the displacement description, the next step to further reduce the mean and standard deviation of the true flowrate estimation error was to improve the pressure description. This new description (section 3.3.3) was subsequently combined with both the Linear and RaLiRa displacements, which resulted in the Li-BoReP and RaLiRa-BoReP models. While the results of the models were mostly similar, the average true flowrate error was found to be smaller for the Li-BoReP model and this could be considered an advantage over the other model. On the other hand, if one's interest lies in accurately estimating the moment of water breakthrough, the RaLiRa-BoReP model is definitely the better choice.

Interestingly, the RaLiRa-BoReP model estimated the cumulative oil production adequately, while the Li-BoReP model estimated the cumulative water production more accurately. However, the standard deviation was hardly reduced by either model because the flowrates were still significantly overestimated once breakthrough had occurred. Therefore, it is hard to draw a conclusion with respect to which of the two models is better and the model choice consequently depends on the user's end-goal.

For the accurately predicted horizontal well case (with an average true flowrate estimation error of approximately 2%), there was no spike after breakthrough and yet the standard deviation was still approximately 8%. Therefore the margin of improvement of the standard deviation of the true flowrate estimation error for the Li-BoReP and RaLiRa-BoReP models is most likely small.

The spike occurring in the flowrate estimation error is caused by the simplicity of both the displacement models: once breakthrough occurred, the model's estimate of the water saturation at the producer is at least equal to the shock front saturation level because the models only consider the streamline along the inter-well axis. In truth, the saturation level at the producer is lower as it takes longer for the water to arrive at the wellbore via all other streamlines (Figure 2.7b). This spike, however, could likely be reduced by improving the flowrate estimates. Improving flowrate estimates after breakthrough, is most likely to be achieved by deriving an (accurate) two-dimensional description of Buckley-Leverett flow in a bounded reservoir. However, a two-dimensional flow description of the Buckley-Leverett solution (other than the radial form) is not known to exist yet, let alone for a bounded reservoir.

Indications of the required computation times were given at the end of chapter 4 where each of the simulations in Table 4.13 consisted of 100 time steps, 2100 grid cells for the virtual asset, and 2 layers for the analytical model. The table seems to indicate a lack of large computational efforts for the analytical model, especially considering that no gradients and the like were supplied to the NPV and data assimilation algorithms which could speed up computations. Moreover, improvements of the analytical models' code might also be possible to reduce their computation times as well.

In conclusion: with respect to the research objective it is concluded that the analytical models considered in this thesis can yield reasonably accurate estimates of the true reservoir flow, especially when incorporating the bounded reservoir pressure model.

6 Recommendations

Main results have been summarized and discussed in the previous chapters and already lead to some considerations for future research within the topic of analytical descriptions for subsurface reservoir flow in a Closed-Loop Reservoir Management setting. A number of recommendations for future research are listed in this chapter.

1. First of all, both displacement models are limited in their usefulness due to the necessity of (near perfect) homogeneous absolute permeability. However, for the linear model, this necessity can be slightly weakened as its displacement and pressure formulae allow for incorporating a non-constant permeability in direction perpendicular to the well orientation (i.e. in the x-direction). In order to facilitate easy and accurate permeability estimations, accurate initial permeability estimates are recommended to be obtained beforehand.

2. A different addition to the permeability model could be to include a skin factor that accounts for formation damage (e.g. a near well-bore reduction in permeability), which for example can occur during drilling and production processes.

3. With respect to the Li-BoReP and RaLiRa-BoReP models considered in this thesis, one could consider to combine both models to accurately estimate both the breakthrough moment as well as cumulative productions.

4. Also interesting could be the introduction of a gas phase to the subsurface reservoir flow and usage of an analytical three-phase description for one-dimensional flow. With respect to NPV optimization, addition of such a third phase also necessitates the incorporation of formation volume factors in order to account for gas that is retained within the oil.

5. Yet another alternative is to attempt to incorporate gravitational effects (e.g. resulting from a pitch in the reservoir) or capillary pressure effects in the analytical model description.

6. Especially interesting and useful would be to derive and incorporate a two-dimensional analytical Buckley-Leverett flow description, as this does not yet exist.

7. In addition to such a two-dimensional flow model one could then try to incorporate multiple injectors and producers inside each layer, as is already possible for single phase flow (e.g. potential flow theory). This additionally leads to more complex and interesting NPV optimization, as wells will no longer necessarily be fully opened until an economic threshold is reached.

8. Lastly, Model Predictive Control could possibly be applied to further reduce flowrate errors.

7 References

Bear, J., 1972: *Dynamics of fluids in porous media*, Elsevier, New York.

Brooks, R.H., and Corey, A.T., 1966. Properties of porous media affecting fluid flow. *Journal of Irrigation and Drainage Division* **92**, 61 - 68**.**

Brouwer, D.R., 2004. Dynamic water flood optimization with smart wells using optimal control theory, PhD Dissertation.

Buckley, S.E. and Leverett, M.C., 1942. Mechanisms of fluid displacement in sands. *Petroleum Transactions AIME* **146**, 107-116. doi: http://dx.doi.org/10.2118/942107-G

Burdine, N.T., 1953. Relative permeability calculations from pore size distribution data. *Society of Petroleum Engineers* **5** (03): 71 - 78. doi: http://dx.doi.org/10.2118/225-G

Davis, P.J., and Rabinowitz, P., 1975: *Methods of Numerical Integration*, Academic Press, New York, San Francisco, London.

Hildebrand, F.B., 1987: *Introduction to numerical analysis (2nd ed.)*, Dover Publications, New York.

Jansen, J.D., 2013: *A Systems description of flow through porous media* - author version 1d.

Jansen, J.D., 2016: *Nodal Analysis of Oil and Gas Wells* - author version 4d, May.

Li, K., 2004a. Theoretical development of the Brooks–Corey capillary pressure model from fractal modeling of porous media. *Proceedings of the SPE/DOE Fourteenth Symposium on Improved Oil Recovery held in Tulsa, Oklahoma, April 17-21, 2004*. SPE 89429-MS. doi: http://dx.doi.org/10.2118/89429-MS

Li, K., 2004b. Generalized capillary pressure and relative permeability model inferred from fractal characterization of porous media. *Proceedings of the SPE Annual Technical Conference and Exhibition, Houston, Texas, September 26-29, 2004*. SPE 89874-MS. doi: http://dx.doi.org/10.2118/89874-MS

Li, K., 2010. More general capillary pressure and relative permeability models from fractal geometry. *Journal of Contaminant Hydrology* **111**: 13 - 24. doi: http://dx.doi.org/10.1016/j.jconhyd.2009.10.005

Li, K., and Horne, R.N., 2001. An experimental and theoretical study of steam/water capillary pressure. *Society of Petroleum Engineers Reservoir Evaluation and Engineering* **4** (06): 477 - 482. SPE 75294-PA. doi: http://dx.doi.org/10.2118/75294-PA

Li, K., and Horne, R.N., 2006. Fractal modeling of capillary pressure curves for The Geysers rocks. *Geothermics* **35** (2): 198 - 207. doi: http://dx.doi.org/10.1016/j.geothermics.2006.02.001

Ling, K., 2015. Fractional flow in radial systems: a study for peripheral waterflood. *Journal of Petroleum Exploration and Production Technology* **6** (3): 441 - 500. doi: http://dx.doi.org/10.1007/s13202-015-0197-3

Matthews, C.S. and Russell, D.G. 1967. *Pressure Buildup and Flow Tests in Wells*, Vol. 1. Richardson, Texas: Monograph Series, SPE.

Szego, G., 1967: *Orthogonal Polynomials (3rd ed.)*, American Mathematical Society, Providence, Rhode Island.

Suwartadi, E., 2012. Gradient-based methods for production optimization of oil reservoirs, PhD dissertation.

Terwilliger, P.L., Wilsey, L.E., Hall, H.N., Bridges, P.M., and Morse, R.A., 1951. An experimental and theoretical investigation of gravity drainage performance. *Petroleum Transactions AIME* **192**: 285 - 296. doi: http://dx.doi.org/10.2118/951285-G

Weijermars, R., Van Harmelen, A., and Zuo, L., 2016. Controlling flood displacement fronts using parallel analytical streamline simulator. *Journal of Petroleum Science and Engineering* **139**: 23 - 42. doi: http://dx.doi.org/10.1016/j.petrol.2015.12.002

Welge, H.J., 1952. A simplified method for computing oil recovery by gas or water drive. *Petroleum Transactions AIME* **195**: 91 - 98. doi: http://dx.doi.org/10.2118/124-G

Appendix A
Additional figures

This appendix shows the results of the undiscounted horizontal well case which was briefly mentioned in Section 4.3. However, they are not discussed as they are similar to those of the discounted case.

A.1 Horizontal well - Linear flow 0% discount

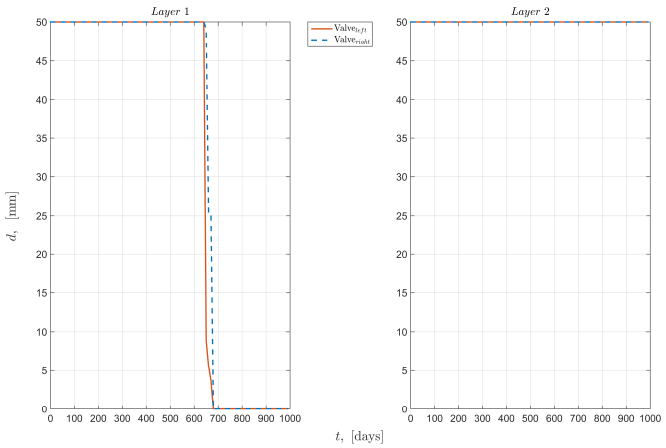

a) Choke valve diameter

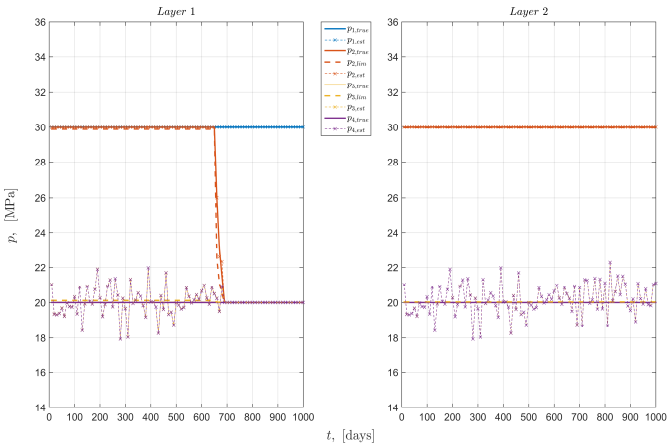

b) Pressures - true and estimated

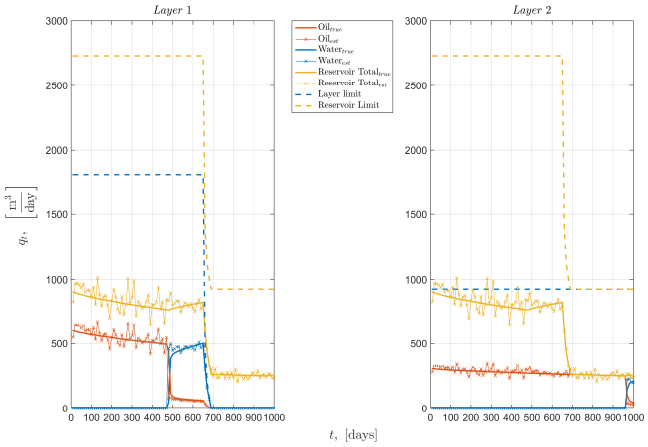

c) Producer flowrates - true and estimated

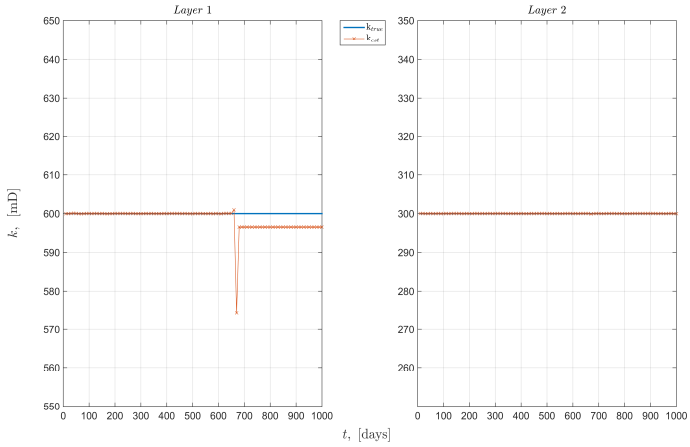

d) Permeability - true and estimated

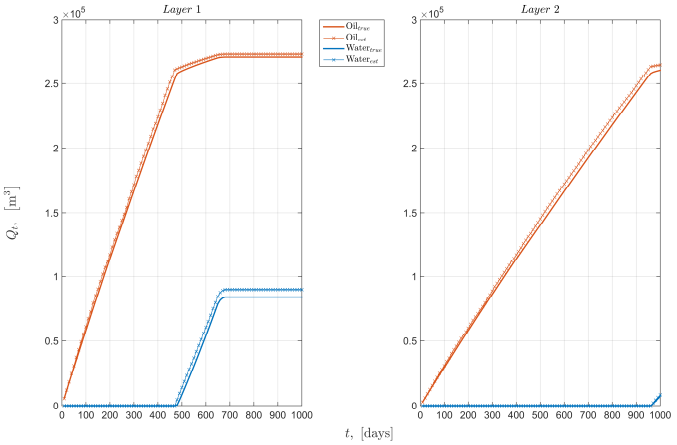

e) Cumulative production - true and estimated

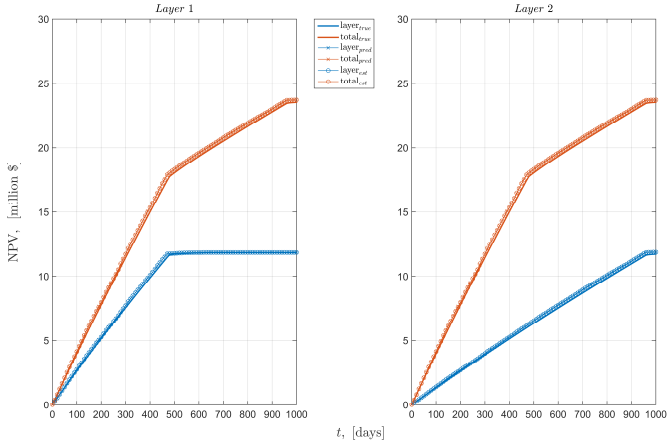

f) NPV development - true and estimated

Figure A.1 - CLRM results (horizontal wells, linear model) - 0% discount

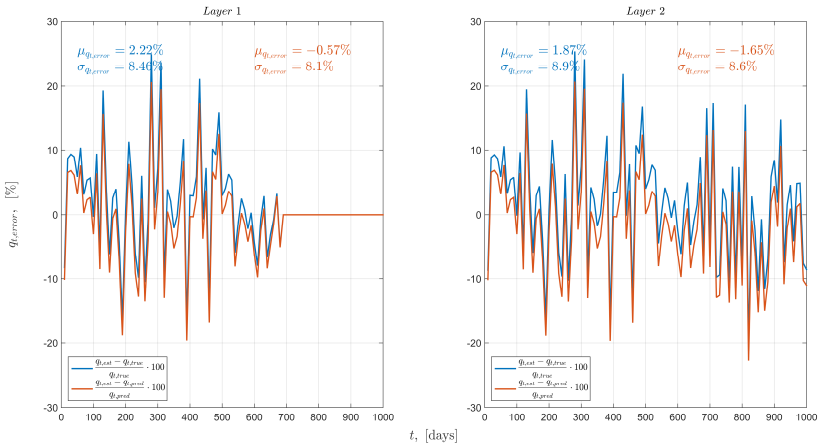

Figure A.2 - CLRM results (horizontal wells, linear model) - Flowrate errors

NPV (million $)	Layer 1	Layer 2	Cumulative
Estimated	11.8	11.9	23.7
True	11.8	11.7	23.5
Estimation error	0%	1.7%	0.9%

Table A.1 - True and estimated NPV (horizontal wells, linear model) - 0% discount

A.2 Vertical well - Radial-Linear-Radial flow 0% discount

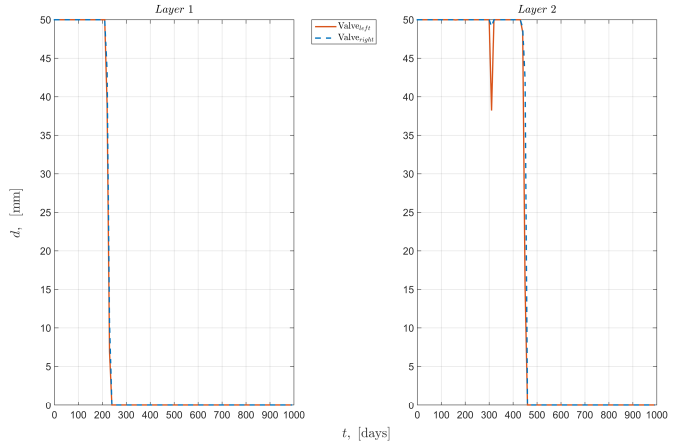

a) Choke valve diameter

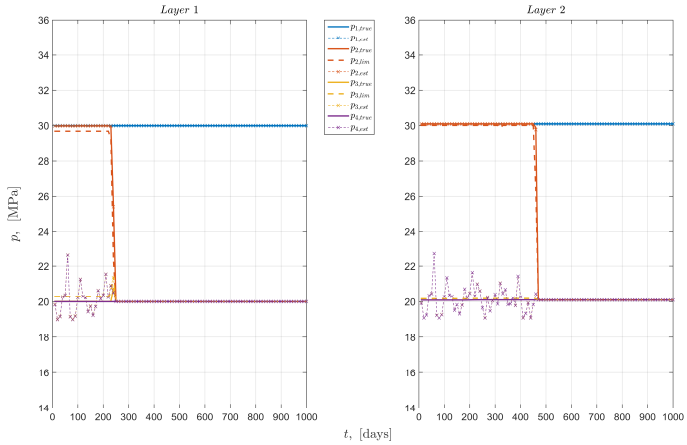

b) Pressures - true and estimated

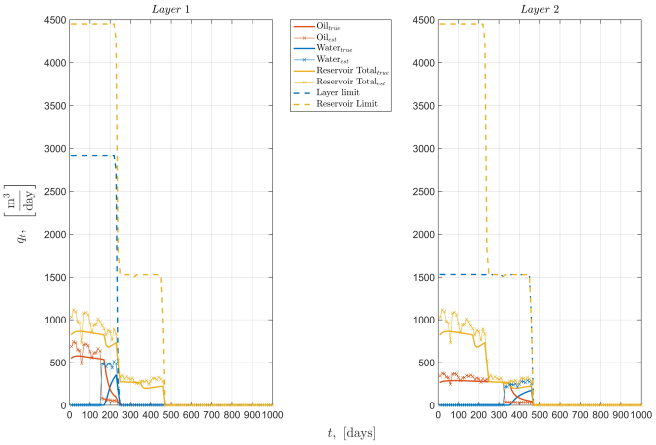

c) Producer flowrates - true and estimated

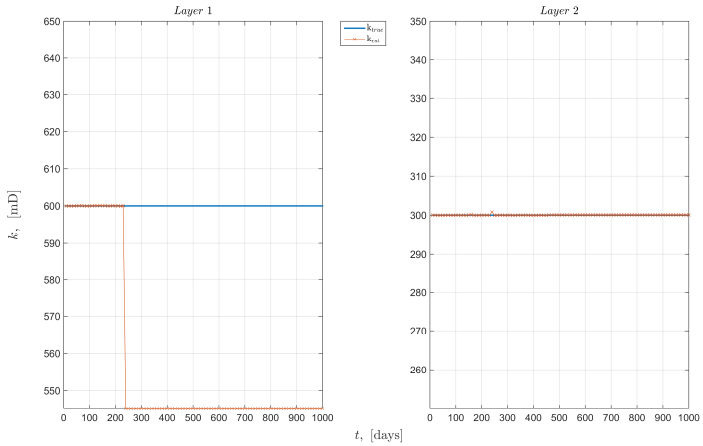

d) Permeability - true and estimated

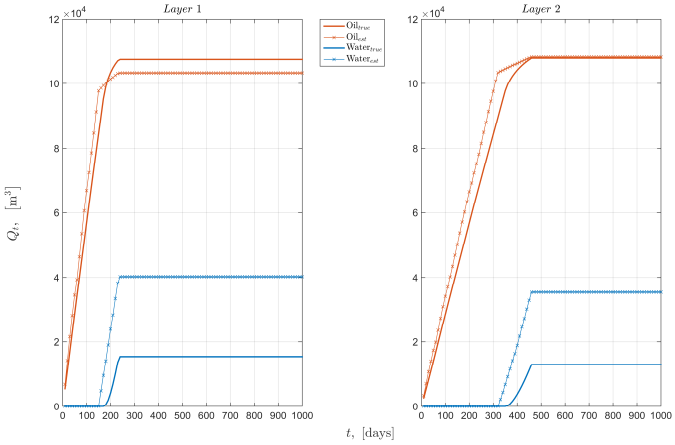

e) Cumulative production - true and estimated

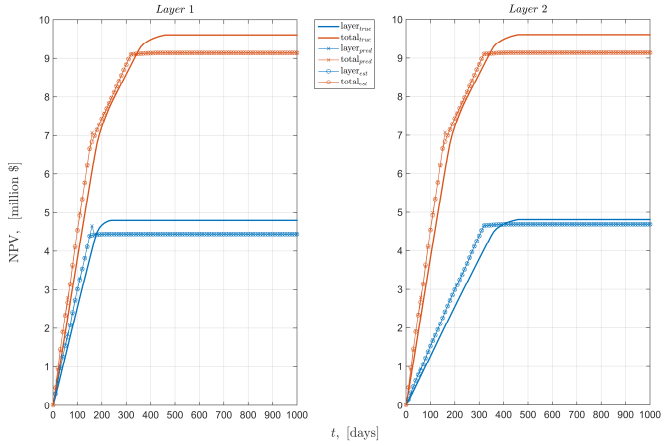

f) NPV development - true and estimated

Figure A.3 - CLRM results (vertical wells, RaLiRa model) - 0% discount

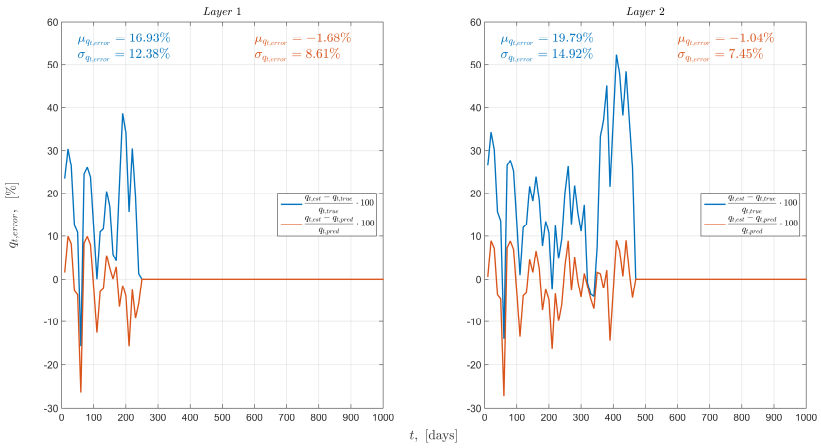

Figure A.4 - CLRM results (vertical wells, RaLiRa model) - Flowrate errors

NPV (million $)	Layer 1	Layer 2	Cumulative
Estimated	4.4	4.7	9.1
True	4.8	4.8	9.6
Estimation error	-8.3%	-2.1%	-5.2%

Table A.2 - True and estimated NPV (vertical wells, RaLiRa model) - 0% discount

A.3 Vertical well - Linear flow & Bounded Reservoir Pressure 0% discount

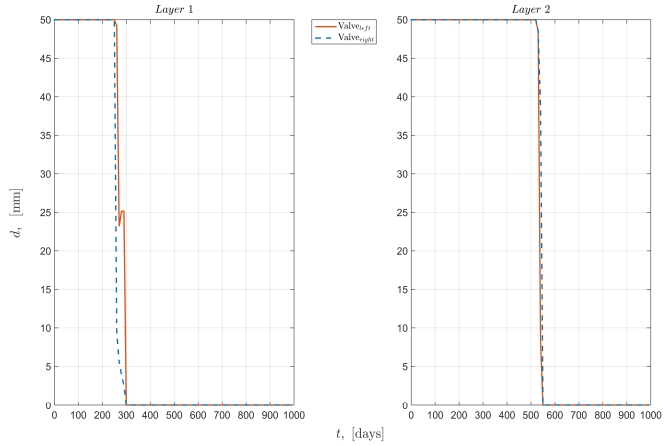

a) Choke valve diameter

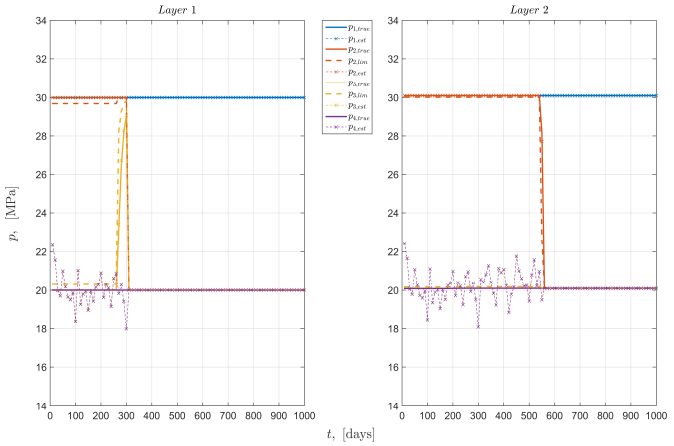

b) Pressures - true and estimated

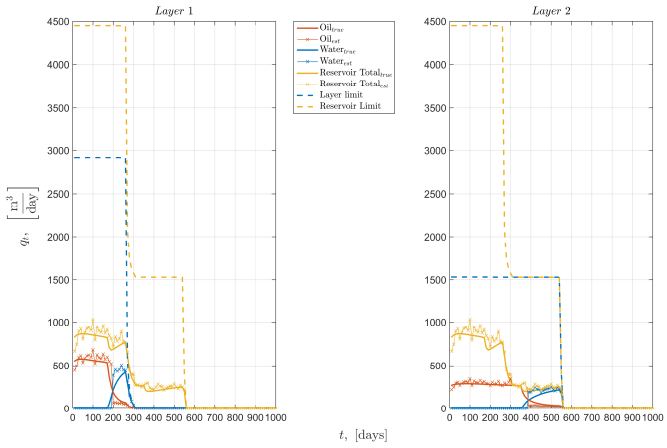

c) Producer flowrates - true and estimated

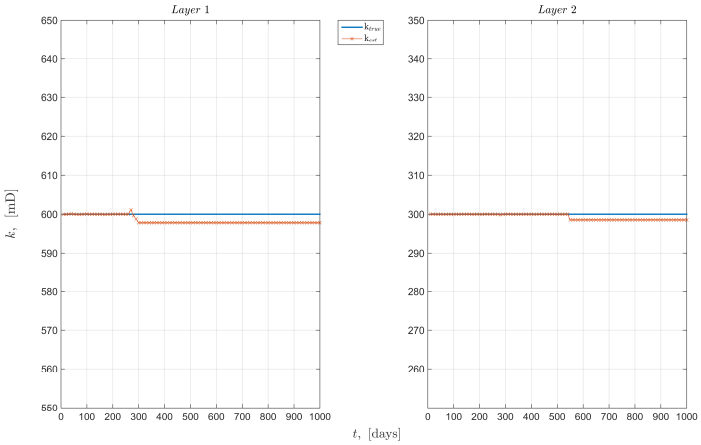

d) Permeability - true and estimated

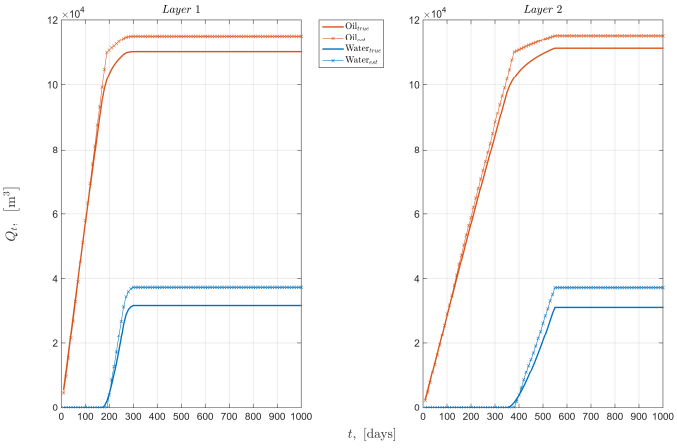

e) Cumulative production - true and estimated

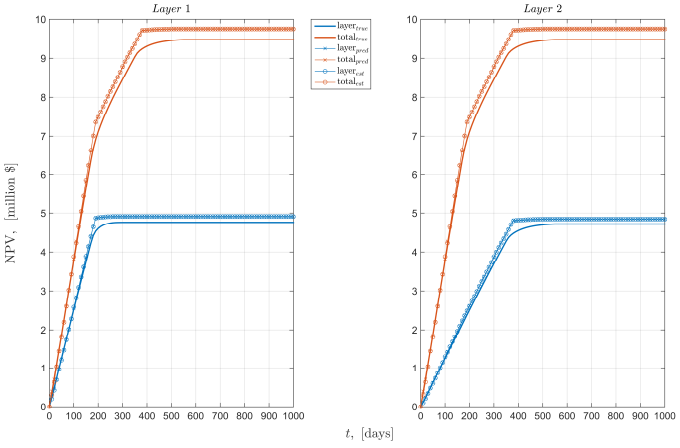

f) NPV development - true and estimated

Figure A.5 - CLRM results (vertical wells, Li-BoReP model) - 0% discount

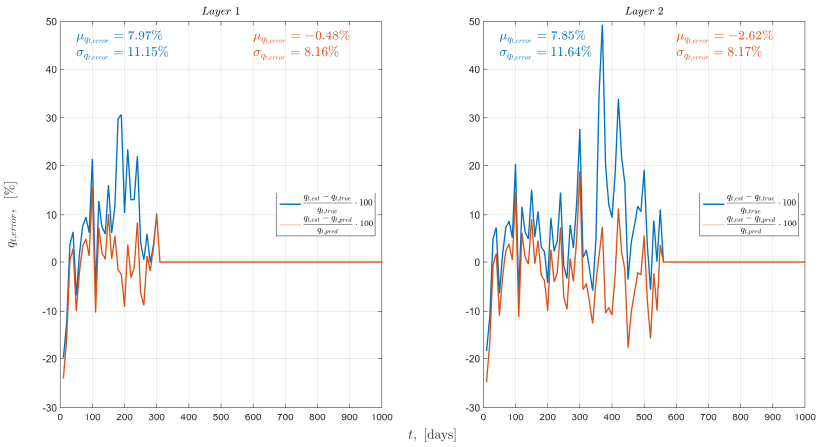

Figure A.6 - CLRM results (vertical wells, Li-BoRep model) - Flowrate errors

NPV (million $)	Layer 1	Layer 2	Cumulative
Estimated	4.9	4.8	9.7
True	4.8	4.7	9.5
Estimation error	2.1%	2.1%	2.1%

Table A.3 - True and estimated NPV (vertical wells, Li-BoReP model) - 0% discount

A.4 Vertical well - Radial-Linear-Radial flow & Bounded Reservoir Pressure 0% discount

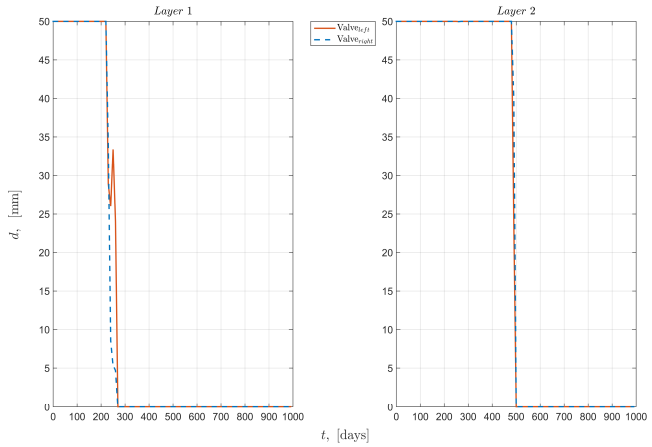

a) Choke valve diameter

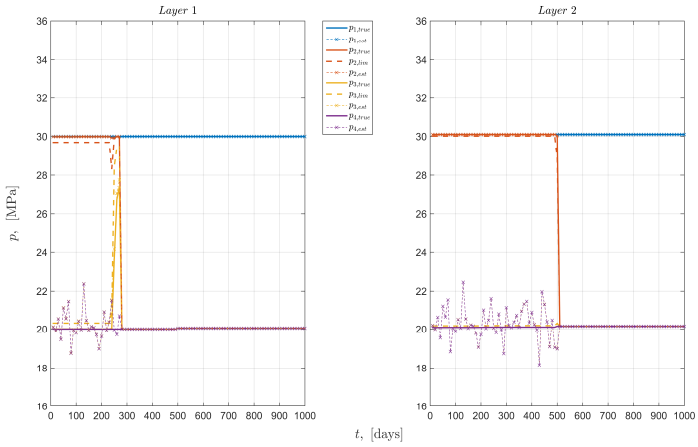

b) Pressures - true and estimated

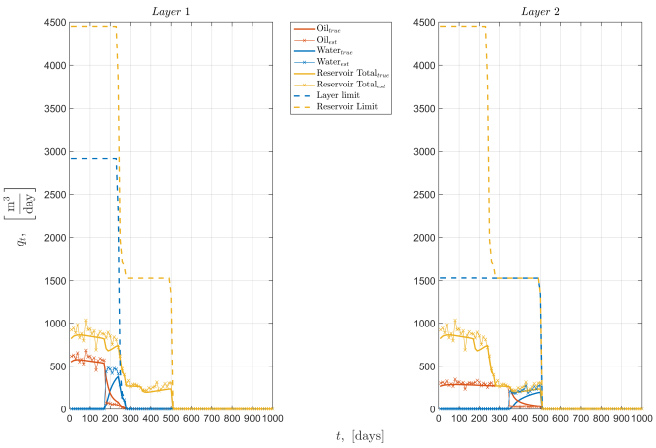

c) Producer flowrates - true and estimated

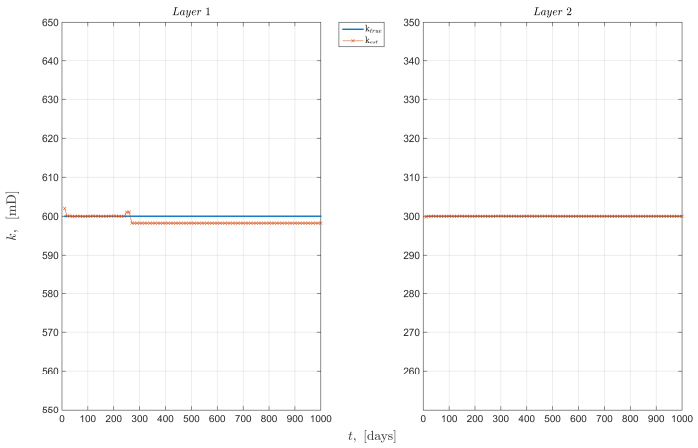

d) Permeability - true and estimated

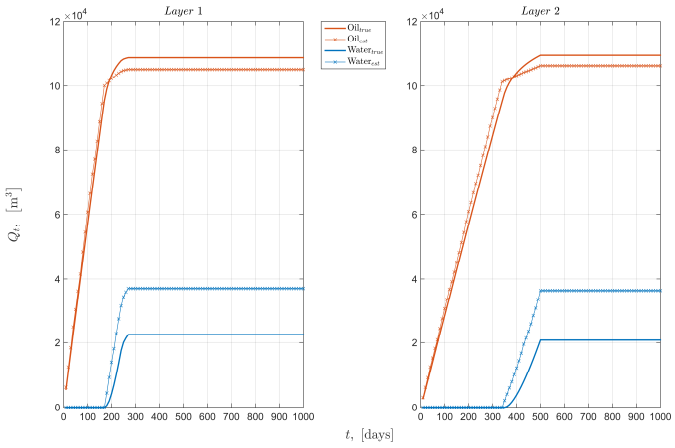

e) Cumulative production - true and estimated

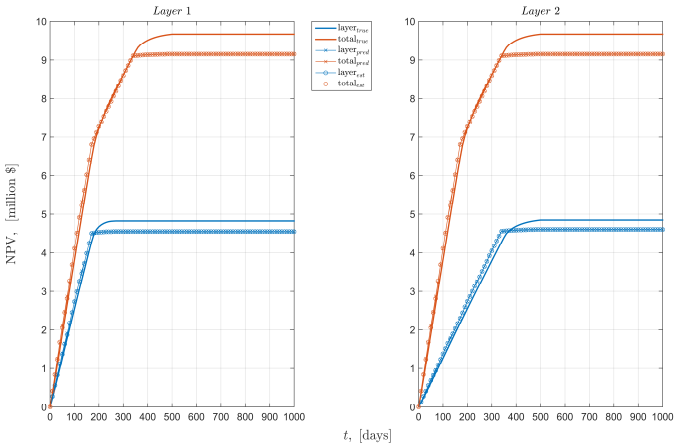

f) NPV development - true and estimated

Figure A.7 - CLRM results (vertical wells, RaLiRa-BoReP model) - 0% discount

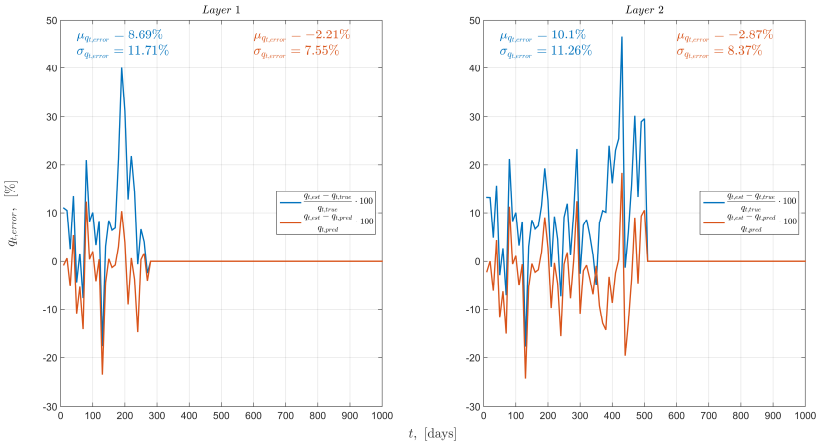

Figure A.8 - CLRM results (vertical wells, RaLiRa-BoReP model) - Flowrate errors

NPV (million $)	Layer 1	Layer 2	Cumulative
Estimated	4.6	4.6	9.2
True	4.8	4.8	9.6
Estimation error	-4.2%	-4.2%	-4.2%

Table A.4 - True and estimated NPV (vertical wells, RaLiRa-BoReP model) - 0% discount